



Review

Recent Progress in Chitosan-Containing Composite Materials for Sustainable Approaches to Adsorption and Catalysis

Linda Z. Nikoshvili ^{*}, Boris B. Tikhonov, Pavel E. Ivanov, Polina Y. Stadolnikova, Mikhail G. Sulman and Valentina G. Matveeva ^{*}

Department of Biotechnology, Chemistry and Standardization, Tver State Technical University, A. Nikitina Street 22, 170026 Tver, Russia

^{*} Correspondence: nlinda@science.tver.ru (L.Z.N.); matveeva@science.tver.ru (V.G.M.); Tel.: +7-904-005-7791 (L.Z.N.); +7-905-601-0144 (V.G.M.)

Abstract: In recent years, composite materials including organic–inorganic systems have drawn special attention due to their enhanced properties such as adsorbents and heterogeneous catalysts. At the same time, large-scale production of environmentally benign functionalized biopolymers, such as chitosan (CS), allows for constantly developing new materials, since CS reveals remarkable properties as a stabilizing agent for metal-containing compounds and enzymes and as an adsorbent of organic molecules. This review is focused on CS-based materials and on the composite systems including CS-oxide and CS-metal composites in particular for application as adsorbents and supports for catalytically active metal nanoparticles and enzymes.

Keywords: chitosan; biopolymer crosslinking; structured biopolymers; organic–inorganic composites; adsorbents; catalytic supports; immobilized enzymes



Citation: Nikoshvili, L.Z.; Tikhonov, B.B.; Ivanov, P.E.; Stadolnikova, P.Y.; Sulman, M.G.; Matveeva, V.G. Recent Progress in Chitosan-Containing Composite Materials for Sustainable Approaches to Adsorption and Catalysis. *Catalysts* **2023**, *13*, 367. <https://doi.org/10.3390/catal13020367>

Academic Editors: Jesús M. Requies, Victoria Laura Barrio Cagigal and Nerea Viar

Received: 16 January 2023

Revised: 2 February 2023

Accepted: 3 February 2023

Published: 7 February 2023



Copyright: © 2023 by the authors. Licensee MDPI, Basel, Switzerland. This article is an open access article distributed under the terms and conditions of the Creative Commons Attribution (CC BY) license (<https://creativecommons.org/licenses/by/4.0/>).

1. Introduction

Chitosan (CS) is a natural polysaccharide composed of 2-amino-2-deoxy-D-glucose residues connected via 1,4-glycosidic bonds, which is obtained by deacetylation of chitin (Figure 1)—the main component of the exoskeleton of crustaceans, insects and the cell walls of fungi [1–3].

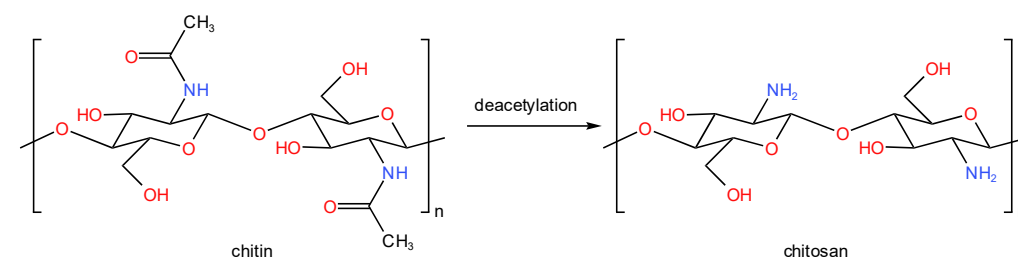


Figure 1. Deacetylation of chitin.

Deacetylation is carried out with concentrated aqueous solutions of NaOH (from 35% up to 50 wt.%) at temperatures of 100–180 °C for 0.5–10 days. To obtain highly deacetylated CS, an at least 10-fold molar excess of NaOH is required [4]. During the process of chitin deacetylation, the overall ordering of the molecule structure strongly decreases (the degree of crystallinity decreases to 40–50%). Deacetylation is also accompanied by hydrolysis of glycosidic bonds, which leads to the production of a polydisperse CS by molecular weight [5]. Deacetylation degree (DD), which is the ratio of the number of glucosamine units to the total number of monomer units in a polysaccharide molecule, is typically higher than 50% [6]. It is noteworthy that both chitin and CS are polysaccharides of variable composition representing a mixture of polymers that differ in molecular weight, the DD,

and the distribution of monomers units within the molecule [7]. The molecular weight of commercial CS varies in a wide range from 100 kDa up to 1200 kDa depending on the sources of raw materials and production method [1,8].

CS is a unique biopolymer that contains primary amines as well as hydroxyl groups and has exceptional properties and wide application. The high adsorption capacity of CS is used for the capture of cations, anions, organic dyes and pharmaceutical ingredients from wastewater. It is noteworthy that CS-based materials are also used as carriers for drug delivery. In addition, various CS-based metal-containing nanocomposite materials have been effectively used in catalytic reactions. CS can be also used for the development of promising inexpensive materials for the agricultural industry. The constant demand for effective adsorbents for the removal of pollutants can be met by fine-tuning the structural properties of CS using appropriate crosslinking agents or additives. Thus, the development of CS-based materials is a constantly growing field requiring continuous research [1,2,9], which also causes the corresponding growth of the CS market [10]. There is a large number of synthetic polyamines, such as polyaniline (PANI) [11–14], polyalkylamines [15,16], polylysine [17,18] and polyornithine [19], which can be applied in adsorption, catalysis or medicine. Synthetic materials reveal excellent antibacterial and adsorption properties. However, CS-based materials are still promising due to the low cost, biocompatibility and biodegradability.

Much research on chitin and CS is focused on the search for new and improved production methods. Key areas of interest include enzymatic conversion; chemical or physical modifications of polysaccharides to expand their applicability, investigation of the mechanisms of biological activity of these polymers and products of their physical, chemical or enzymatic degradation; as well as biochemical and molecular characteristics of chitosanolytic and chitinolytic enzymes [20].

CS can be divided into the following types: technical, industrial, food and medical. This division depends on the CS solubility in diluted solutions of organic acids (acetic, lactic and malic acids) and its characteristics such as viscosity, molecular weight and DD. The most valuable for practical use is CS with high DD, low molecular weight and high solubility, which make it a structure-forming agent and effective sorbent. Low molecular weight CS can be produced using variety of methods, among which are oxidative depolymerization, plasma process, ultrasound treatment, acid hydrolysis and enzymatic hydrolysis [21–27].

The pKa of CS' amino groups is 6.3–6.5; hence, below this value, amino groups are protonated, and CS is highly soluble. It is noteworthy that CS becomes soluble at about 50% protonation of amino groups [1,28]. CS solubility in low acidic aqueous solutions also depends on molecular weight, DD and on the ionic strength and distribution of acetyl groups along the CS chain [29]. CS oligomers are soluble at wide range of pH. On the contrary, CS samples with high molecular weight are soluble only in acidic aqueous media even at high DD (70–80%). The dependence of CS solubility on pH makes it possible to obtain capsules, films, membranes, gels, fibers, etc. However, insolubility at neutral and basic pH prevents the use of CS in some areas [30]; thus, a large number of CS derivatives have been synthesized. When $\text{pH} > 7$, the amino groups are deprotonated and exhibit nucleophilic properties. The lone electron pairing of nitrogen allows for the formation bonds with oppositely charged groups of different compounds, i.e., aldehydes, acids, acid anhydrides and epoxy resins. Thus, water-soluble CS derivatives can be obtained [31].

Despite the prominent properties of CS (biodegradability, biocompatibility, relatively high chemical stability, existence of different reactive groups, chelation capability of a large number of metals and their ions) there is a scarce number of CS-based composite materials used to catalytic reactions [32,33]. In this review, recent achievements in the development of CS-based adsorbents and catalytic materials, including metal containing catalysts and biocatalysts, will be considered with a focus on composite systems. However, before describing CS-based adsorbents and catalysts, the main approaches to CS' modifications and shaping should be provided in brief.

2. Chitosan Modifications

In protonated form CS is capable of interacting with negatively charged molecules, nanoparticles (NPs) and cells [9,34]. In general, CS is able to participate in four main types of interaction: ionic, hydrogen, hydrophobic and complex formation. This opens numerous methods of CS modification. The reactive groups of CS (primary amino groups, primary and secondary hydroxyl groups (C₆, C₃), glycosidic bonds and acetamide groups) and their possible modifications are presented in Figure 2 [1].

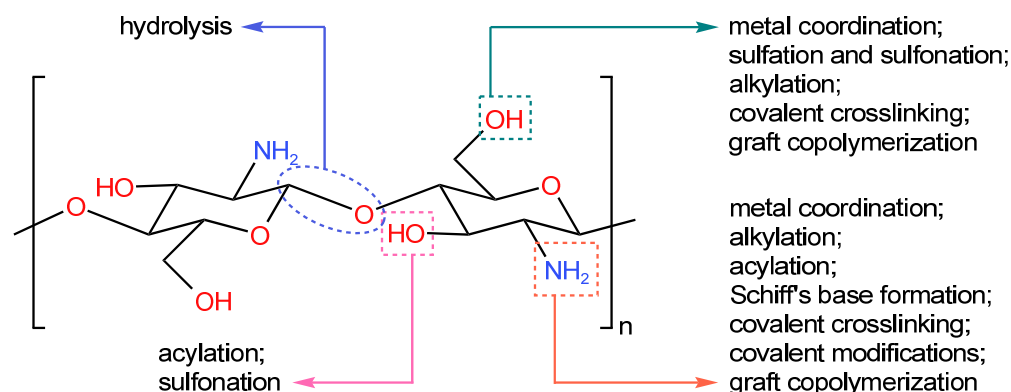


Figure 2. Functional groups of CS that can be chemically modified (based on Ref. [1]).

Chemical transformations of CS include the formation of ethers (methyl, ethyl, carboxymethyl, hydroxyethyl) and esters of both inorganic (nitrates, sulfates, xanthogenates) and organic (acetates) acids. Physical, chemical and mechanical properties of CS-based polymers can be significantly improved by mixing, inclusion of solid fillers, grafting (insertion of other functional groups), crosslinking and binding to other macromolecular chains, impregnation, interpenetration and ion imprinting methods [2].

2.1. Grafting of Functional Groups

Grafting of additional functional groups can noticeably increase the number of adsorption sites in a CS molecule and, consequently, its adsorption capacity [35]. Recently, Olshannikova et al. [36] synthesized 2-(4-acetamido-2-sulfanilamide) chitosan (Figure 3a)—water soluble derivatives with molecular weights of 200, 350 and 600 kDa. 2-(4-Acetamido-2-sulfanilamide)-CS was synthesized with high yield (75–83%) through the reaction of CS with 4-acetylsulfanilchloride in DMSO medium. A synthesized CS derivative was used for the successful immobilization of different cysteine proteases: ficin, papain and bromelain.

The formation of Schiff's bases is widely used in the modification of amines, allowing for better complexation with metal ions. Recently, Suresh et al. [37] synthesized Schiff's base of carboxymethyl CS/p-dimethylaminobenzaldehyde (Figure 3b) for complexation with Co, Ni and Zn for further biomedical application. Moreover, the obtained Zn complexes were shown to reveal promising catalytic properties in the oxidation of cyclohexane to cyclohexanol, allowing >70% of cyclohexanol yield for 12 h.

In addition to functional groups, other polymers can be grafted to CS as well. For example, Rostami et al. [38] grafted cellulose to CS using EDTA (Figure 4). The CS-EDTA-cellulose network contained both acidic and basic sites on the surface and was used as a multifunctional organocatalyst for the synthesis of 2-amino-4H-pyran derivatives with high yields (85–96%) at room temperature via a one-pot reaction between ethyl acetoacetate aromatic aldehydes and malononitrile in EtOH as a green solvent. The CS-EDTA-cellulose nanocatalyst was easily recovered from the reaction mixture by using filtration and reused at least five times without any significant decrease in its catalytic activity.

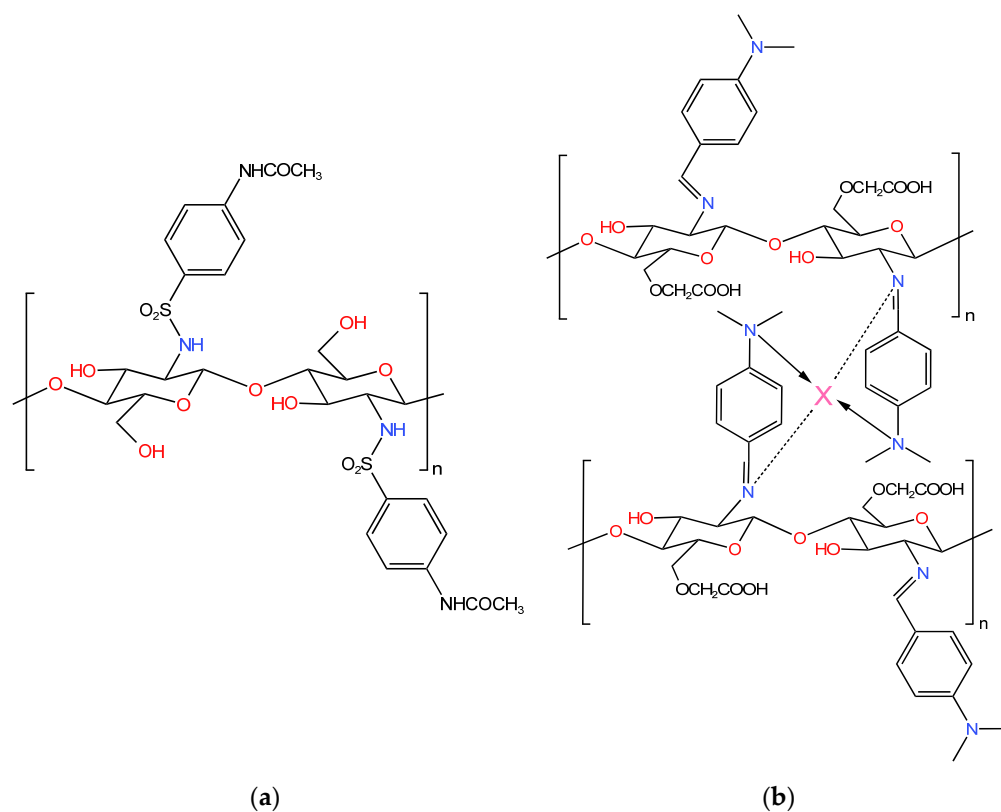


Figure 3. Structure of 2-(4-acetamido-2-sulfanilamide)chitosan (a) [36] and carboxymethyl CS/p-dimethylaminobenzaldehyde metal complex (b) [37].

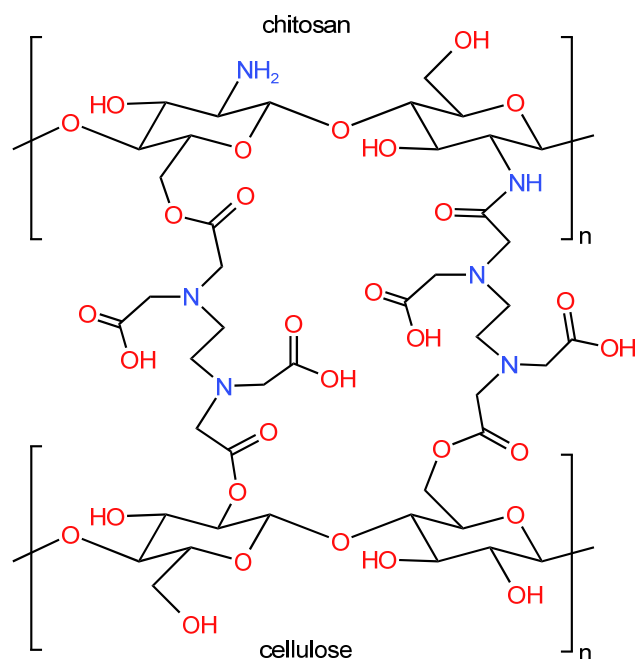


Figure 4. Structure of CS-EDTA-cellulose [38].

Thiolated CS (TCS) is prospective generation of mucoadhesive polymers [39–41]. TCS exhibits better mucoadhesive properties than native CS, which is due to the formation of covalent disulfide bonds between thiol groups and mucus glycoproteins. Compared to CS, TCS has several advantageous features such as improved permeability and mucoadhesive properties. The higher the concentration of thiol groups on the CS surface, the better

the mucoadhesive properties. In addition, soluble TCS exhibits gel-forming properties at physiological pH values. There is a large variety of TCS, some of which are presented in Figure 5 [39–43].

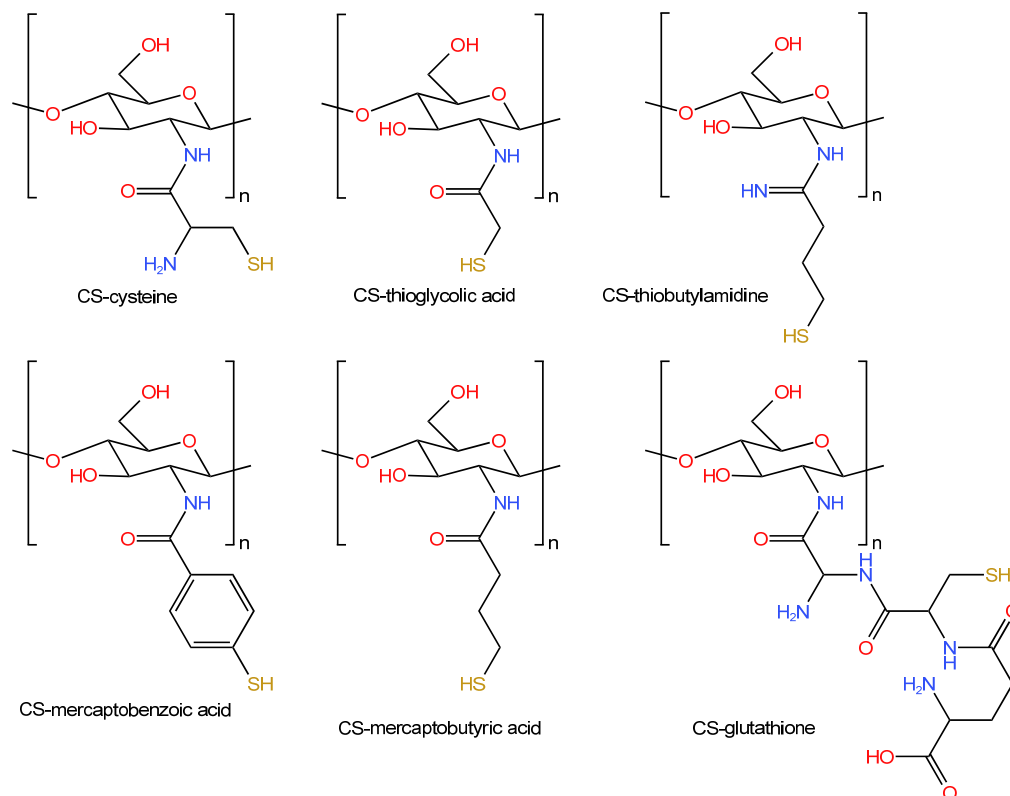


Figure 5. Examples of TCS structures.

2.2. Gelation

Gelation is one of the most widely used methods of CS modification [44]. Polymer hydrogels are hydrophilically crosslinked macromolecular systems capable of retaining significant amounts of water, while preserving the properties inherent in solids (certain shape, mechanical properties of the material during tensile and shear deformations). This combination of properties determines a wide range of their applications: sorbents, gas separation and ion-exchange membranes, structure-forming agents for food industry, drug carriers, artificial tissues and materials for soft and intraocular lenses [45,46].

In order to meet certain requirements for hydrogels, CS-based polymeric networks should meet two conditions:

- (i) Interactions between polysaccharide chains must be strong enough to form a molecular network;
- (ii) The network must be permeable to water molecules.

Gels that meet these requirements can be obtained through physical interactions, which include electrostatic, hydrogen and van der Waals bonds arising between polymer chains [47–49].

CS-based gels can be obtained by simply mixing the gel components under appropriate conditions. The disadvantage of these gels is their short lifetime, during which the gel retains its physicochemical properties. Gelation of CS can occur via its interaction with negatively charged particles (e.g., sulfates, citrates, phosphates) or metal ions. The properties of formed hydrogels depend on the charge density, CS concentration, DD of CS, and the nature of the crosslinking agent. It is noteworthy that CS hydrogels have low compressive strength [50]. Therefore, the combination of CS with other materials is

usually used to produce hydrogels. Some methods of hydrogel synthesis include radiation cross-linking technology, freezing-thawing, dissolution/lyophilization, etc. [51].

In this case, where the strengthening of interpolymer CS hydrogels is necessary, complexation processes are supplemented by covalent binding. Typically, low-molecular crosslinking agents, such as glutaraldehyde (GA) (Figure 6) and epichlorohydrin (ECH) (Figure 7) are used for CS crosslinking [2].

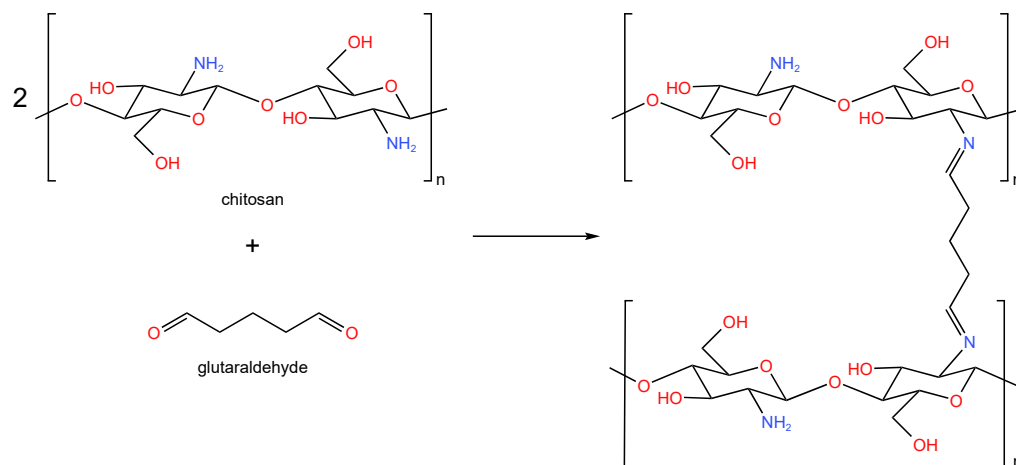


Figure 6. Crosslinking of CS with GA [2].

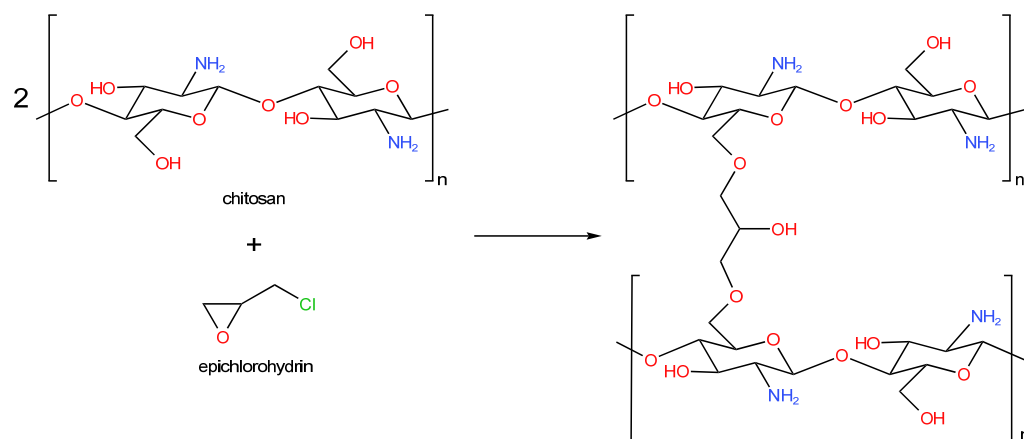


Figure 7. Crosslinking of CS with ECH [2].

The covalent binding of interpolymer hydrogels hardens their structure, which provides significant advantages in terms of mechanical and chemical stability, as well as the ability to form stable films and microparticles [52]. At the same time, the disadvantage of covalent crosslinking is the loss of functional groups of the polymer as a result of their reaction with the crosslinking agent. Moreover, the release of crosslinking agent from the gel with the destruction of its structure may result in toxic effects.

In recent years, the attention of researchers has been increasingly attracted by so-called “smart polymer gels”, capable of reversibly responding to changes in environmental properties (pH, temperature, ionic strength, the presence of certain substances, irradiation, electric field) [53–56]. An important class of smart gels is thermo-responsive CS-based materials [57–60]. Such gels can be obtained via the interaction between CS and low-molecular weight compounds (glycerophosphate) as well as with polymers (poly(N-isopropylacrylamide)). Thermo-responsive gels can be used for the targeted delivery of drugs, peptides and proteins to cells. Preliminary mixing of these components with CS solutions at room temperature, their injection into the affected tissues and subsequent formation of hydrogel leads to the controlled release of the active drug at body temperature.

There is a wide range of hydrogels obtained via formation of polyelectrolyte (PE) complexes between CS and other natural/synthetic polymers [61,62]. Such complexes have higher stability and do not require additional crosslinking agents. The stability of these complexes depends on the charge density, the nature of the solvent, ionic strength, pH and temperature [61].

In general, the interaction of CS with other polymers allows for an increase in molecular weight, decrease in crystallinity and an increase in the plasticity and elasticity of CS-based materials. There are several routes for such modifications:

- Reactions of polymer–analogous transformations [63];
- Grafted and block copolymerization reactions with synthetic monomers [64–66];
- Preparation of mixtures with natural/synthetic polymers.

In addition to the covalent binding of polymers, after hydrogel formation is completed, a two-stage process for the formation of the crosslinked structure is also possible. At the first stage, one of the polymeric components, the macromolecule that contains reactive functional groups, is formed. At the second stage, monomers are introduced into the reaction medium, forming a second polymer that covalently binds to the first one. This group of methods includes the formation of grafted polymers, block copolymers and co-networks [67].

2.3. Formation of Nanoparticles

It has been proven that CS derivatives are especially effective while in the form of NPs [68]. NPs are used as a method of integration and storage of active substances and consist of macromolecular and/or molecular structures in which active substances (drugs, enzymes, metal ions) are dissolved, stored, encapsulated or even adsorbed, or maintained at the outer interface [50]. The method for producing CS NPs was described for the first time by Ohya et al. in 1994 [69].

The processes used to produce CS NPs can be divided into several categories:

- (i) Physicochemical, in which NPs are formed by emulsification following solvent evaporation, solvent displacement, diffusion or salting out [70];
- (ii) The in situ chemical synthesis of macromolecules, resulting in polymerization or interphase polycondensation;
- (iii) Mechanical processes using high-energy devices, such as high-pressure homogenizers, ultrasonic devices or high-energy wet grinding.

Methods of CS NP synthesis include ionotropic gelation, emulsification and cross-linking, complexation with PE, self-assembly and drying processes. Below are some peculiarities of these methods:

- (i) Ionotropic gelation:

Ionotropic gelation is one of the most widespread methods of CS-based NP synthesis. Since CS is a cationic polysaccharide, its interaction with polyanions such as tripolyphosphate (TPP) results in gelation (Figure 8) [71].

In an acidic medium, CS can spontaneously turn into submicron-sized particles. The TPP solution is added dropwise to the CS solution under constant stirring until an opaque suspension is formed, which indicates the formation of NPs, the mean diameter of which is controlled by the CS/TPP molar ratio [72]. The mechanism of CS NP formation, the internal structure of resulting particles and the topology of their surface are determined by the following parameters: DD, molecular weight of CS, intrinsic viscosity, concentration and molar ratio NH_3^+/TPP [73]. At $\text{pH} > 7$, deprotonation of CS occurs, which reduces the crosslinking degree [74]. Moreover, pH of TPP solution controls the swelling behavior of the resulting gels: CS modified by ionotropic crosslinking (at a pH of about 3) with TPP revealed higher swelling ability [2,74] in comparison with gels formed at alkaline pH values of the TPP solution.

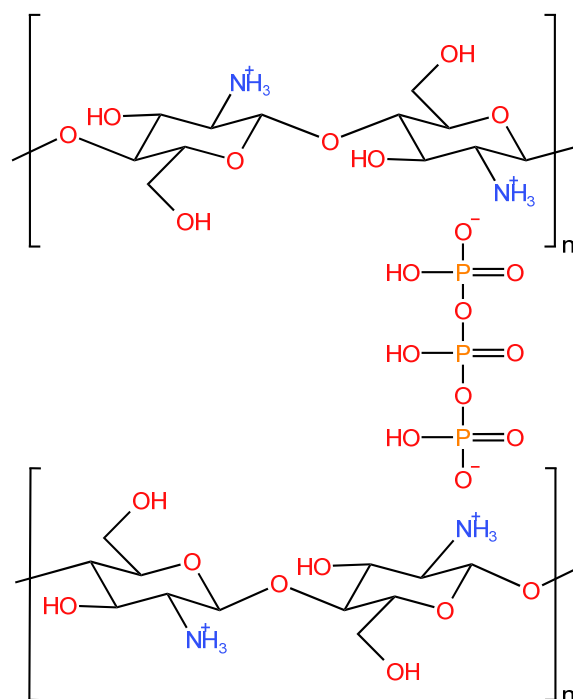


Figure 8. CS crosslinked with TPP via ionotropic gelation [71].

Other factors such as temperature and stirring rate may also affect CS NP size and polydispersity. After synthesis, smaller particles can be separated from larger ones by using filtration and ultracentrifugation [75]. The resulting CS NPs allow for capturing small hydrophobic and hydrophilic molecules, and also peptides, proteins and nucleic acids. Electrostatic interactions are considered to be the main mechanism for retaining biologically active compounds inside the CS NPs.

In addition to TPP, other polyanions can be used for ion gelation, e.g., adenosine triphosphate, fucoidan and sodium metabisulfite ($\text{Na}_2\text{S}_2\text{O}_5$) [76].

Molecules containing catechol, such as hydrocaffeic acid, have demonstrated the ability to increase the mucoadhesion of various polymers, including CS. Thus, hybrid microflowers were obtained from CS and calcium pyrophosphate, which were effectively used for the removal of dyes and in enzymatic catalysis [77].

(ii) Complexation with PEs:

The mechanism of CS NP formation in PE is based on the ionic interactions between CS and negatively charged polymers (the same principle is used for hydrogel formation [78]). Stability of PE complexes is based on several factors including the degree of ionization of each PE; charge density; concentration and proportion of PEs in the mixture; sequence of PE mixing; nature; and location of charged groups. The stability of PE complexes also correlates with the molecular weight of PEs, flexibility of polymer chains, process temperature, ionic resistance and pH of the reaction medium [79].

When the excess charges of PEs (positive or negative) are consolidated, a nonstoichiometric complex is formed. A stoichiometric PE complex contains equal amounts of each opposite charge. In the case of CS, various PE complexes can be formed when the positively charged CS surface interacts with anionic biopolymers such as sodium alginate (SA), pectin, carboxymethylcellulose, chondroitin sulfate, dextran sulfate, etc. [80].

(iii) Drying:

Spray-drying and supercritical drying are often used for the production of CS particles. These methods are relatively fast, simple and reproducible, allowing for highly stable CS particles of various sizes to be obtained [81]. Spray-drying is a comprehensive, convenient, one-step method for producing CS micro-/NPs loaded with heat-sensitive substances

such as pigments, medicines, essential oils, flavorings and proteins [82]. CS particles produced while using spray-drying have a smooth surface, spherical shape and narrow size distribution; they also demonstrate the high stability of an immobilized drug [83]. The size of the resulting particles is affected by the rate of the sprayed flow, the degree of CS crosslinking and the air flow rate [84].

(iv) Emulsification:

CS NPs can be obtained using nanoemulsion. Emulsification processes usually require high mechanical energy to produce small droplets. The decrease in energy need is possible while using water–oil mixture with the addition of surfactants [85]. First, the dispersion of CS is prepared in a solution of glacial acetic. Then, a portion of hydrophobic solvent (e.g., cyclohexane, cyclohexanol, soybean oil, etc.) is added to the CS solution under continuous stirring. The resulting mixture is treated with a surfactant, e.g., Triton X-100 or Tween, at stirring until the mixture becomes translucent, indicating the formation of an emulsion containing NPs [86]. Another option is to premix the surfactant with one of the solutions. The use of an ultrasound and an increase in reaction temperature may contribute to the process of NP/nanocapsule formation. Gel-forming agents such as chlorides, TPP or polycations can be also added to enhance CS NP formation [87].

NPs or nanocapsules formed using the emulsification method have high drug-loading efficiency and high bioavailability [88]. However, the mandatory use of strong crosslinking agents causes the issue of their incomplete removal [89].

(v) Self-assembly:

Self-assembled NPs can be formed in aqueous media from amphiphilic polymers [90]. Though CS is not an amphiphilic biopolymer, self-assembled CS NPs can be obtained through the structural modification of CS, allowing them to bind compounds such as fatty acids, phthaloyls, polyesters, cholesterol, etc., which causes CS' self-aggregation [91–93]. Quaternary CS derivatives are often used to produce self-assembled CS NPs [94] used as carriers for hydrophobic substances.

According to the most recent data, there are four main types of CS-containing NP structures (Figure 9) [95,96].

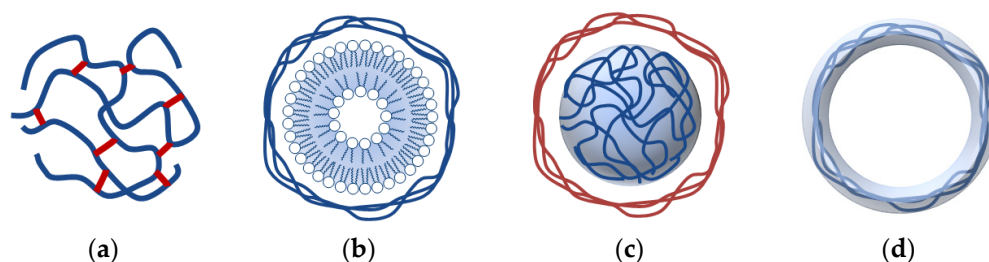


Figure 9. Types of CS-containing NPs: NP formed by crosslinking (a), liposome coated with CS (b), polymer-coated CS NP (c), CS nanocapsule (d) (based on Ref. [95]).

Thus, CS has many advantages for producing materials for adsorption and catalysis. However, the goal-oriented design and synthesis of chemically modified CS derivatives is a complex task. Depending on the type of functional moiety attached to the carbohydrate and also on the type of inorganic component, new adsorbents and catalysts with improved properties can be obtained, which requires further systematic effort.

3. Chitosan-Containing Materials and Composites as Adsorbents

CS is known to be an environment-friendly and cost-efficient adsorbent for dyes and inorganic ions from wastewater. However, CS has some drawbacks, including dissolution in an acidic environment and poor mechanical properties, resulting in unsatisfactory adsorption performances. Crosslinking allows for the enhancement of the mechanical properties and pH-stability of CS. At the same time, the grafting of CS with functional groups is an effective way of improving its adsorption performance [97].

In a work by Liu et al. [97], divinylbenzene (DVB) was selected as a crosslinking agent in a two-step, one pot method based on the acylation reaction between maleic anhydride and CS to prepare a series of DVB-crosslinked CS/maleic anhydride (MAH) polymers (CS/MAH-DVB), which was used to remove methylene blue (MB) from aqueous solutions. A simplified CS/MAH-DVB synthesis scheme is presented in Figure 10. Briefly, CS reacted with MAH in formamide medium in the presence of *p*-toluene sulfonic acid. Then, the modified CS reacted with DVB (vinyl groups were taken equimolar to MAH) in DMSO medium in the presence of 2,2'-azobisisobutyronitrile. As a result, three samples of CS/MAH-DVB polymers were prepared using 0.5, 1 and 2 CS/MAH molar ratios.

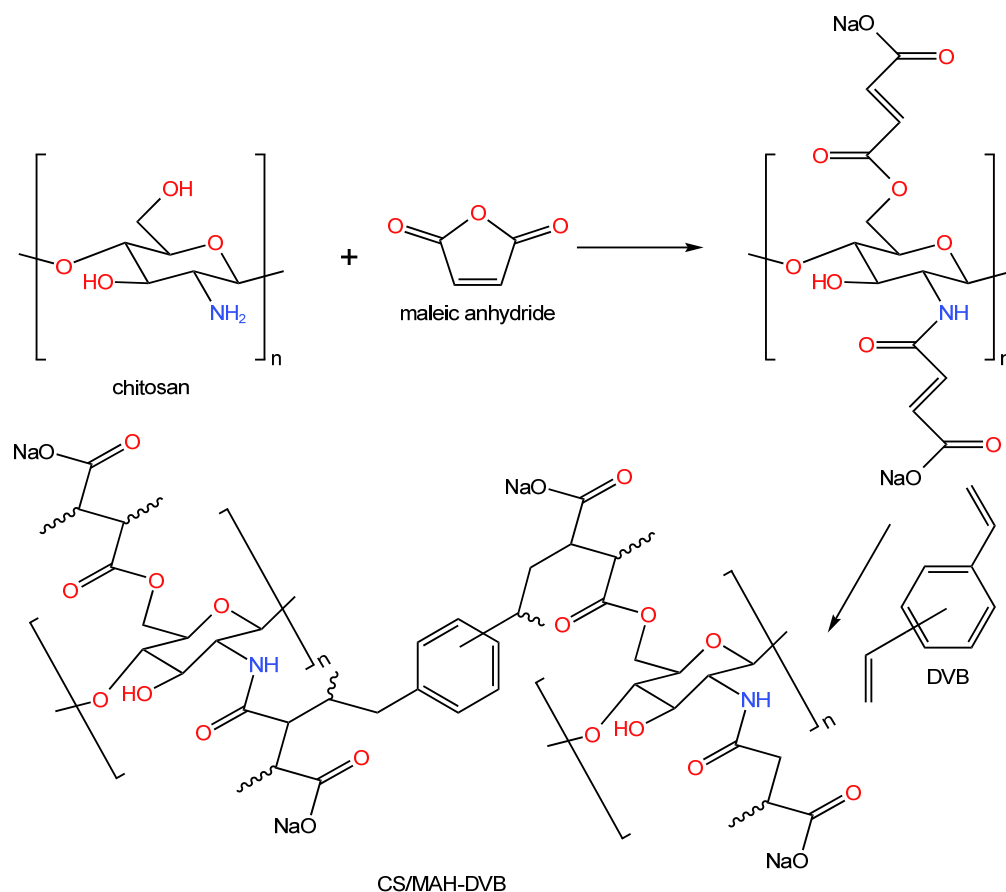


Figure 10. Synthesis of CS/MAH-DVB polymers [97].

The adsorption parameters (pH, contact time, initial concentration of dye and temperature) were varied, and the maximum adsorption capacities were 448 mg/g, 482 mg/g and 503 mg/g, respectively, for three CS/MAH-DVB polymers with different molar ratios at 298 K, which were superior to other reported bio-based adsorbents.

The adsorption mechanism was attributed to electrostatic interaction and π - π stacking interaction between MB and CS/MAH-DVB polymers. Furthermore, the CS/MAH-DVB polymers could easily be recycled by washing with acidic acetone, demonstrating excellent stability and favorable recyclability over five cycles [97].

Pyridine-modified CS was synthesized (Figure 11) and used for simultaneous adsorption of Cr(VI) and Cu(II) cations [98] at variation of concentration, contact time, and pH. The maximum adsorption capacities of pyridine-modified CS (at pH 4.5) in single and binary aqueous solutions were 1.84 mmol/g (at pH 5.5) and 1.13 mmol/g (at pH 4.5) for Cu(II) and 3.86 mmol/g (at pH 3.6) and 0.98 mmol/g (at pH 4.5) for Cr(VI), respectively. It was proposed that the imine and pyridine groups introduced on CS were able to adsorb oxyanions of Cr(VI) by the formation of outer-sphere complexes, while Cu(II) ions were adsorbed by the formation of inner-sphere complexes. The reuse of pyridine-modified CS

was studied. It was shown that Cu(II) ions were almost completely desorbed (~96%) and fully re-adsorbed (~100%), while the desorption of Cr(VI) was incomplete (~49%), resulting in lower re-adsorption (~36%). The thermodynamic parameters of adsorption revealed that the adsorption of both metal ions was enthalpically driven, but entropically unfavorable.

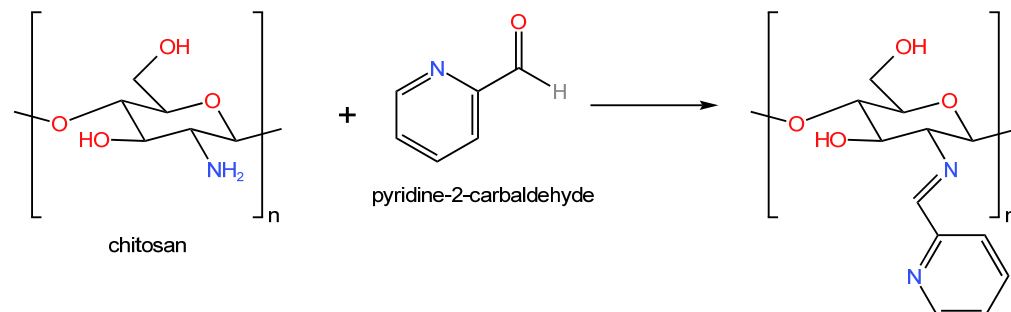


Figure 11. Modification of CS with pyridine-2-carbaldehyde [98].

In spite of numerous CS-based polymers with enhanced adsorption ability, structured CS-containing materials, e.g., in form of beads, exhibit good mechanical and fluid dynamic properties that are suitable for large-scale adsorption processes. Moreover, CS beads present remarkably enhanced adsorption capacity, mainly due to increased specific surface area and porosity [99].

3.1. Structured Chitosan Materials

The general method for preparation of CS beads consists of the dissolution of CS in acid medium and its subsequent dripping in alkaline medium. There are many beading parameters (CS molecular weight and concentration, acid concentration, NaOH concentration, temperature), which are the subject of optimization. Additionally, the subsequent crosslinking of CS beads with various agents allows for further increase in their permeability, stability and adsorption ability.

For example, Vakili et al. [99] studied CS beads crosslinked with 1,2,7,8-diepoxyoctane (DEO) in the adsorption of RR2 dye. A maximum adsorption capacity of 788.6 mg/g was achieved at a pH of 2. The satisfying performance of the CS beads (597.6 mg/g at pH 4), compared to that of CS flakes (487.23 mg/g), implied that beading is a promising process for enhancing CS effectiveness as an adsorbent. It was also proven that CS and crosslinked CS beads can be recycled (by washing with NaOH solution) at least five times before sensible performance loss.

DEO-crosslinked CS beads modified with spermine (SP) were synthesized (Figure 12) [100]. SP was chosen as an amination agent for the enhanced adsorption of Cr(VI) from aqueous solutions. As can be seen from Figure 12, DEO can interact with either $-\text{CH}_2\text{OH}$ or $-\text{NH}_2$ groups of CS; thus, free $-\text{CH}_2\text{OH}$ groups can further interact with ECH and then with SP. Optimal CS–DEO–SP beads were prepared using 1.5 mg/L of SP for 5 h at 50 °C. The prepared beads exhibited heterogeneous and porous surfaces. The obtained CS–DEO–SP beads were macroporous and had increased surface area, pore volume and pore size by 4.9, 7.1 and 1.4 times, respectively, in comparison with initial CS beads. The experimental data revealed that the adsorption of Cr(VI) ions on the CS–DEO–SP beads was extremely dependent on the solution's pH level. A maximum adsorption capacity of 352 mg/g was found at acidic condition (pH 2.0). Regeneration of CS–DEO–SP was successfully performed via treatment with NaOH solution (1.0 mol/L). Regenerated CS–DEO–SP beads allowed for the achievement of an adsorption capacity of 192.31 mg/g after five cycles of repeated use. Thus, high adsorption capacity, acid stability and reusability render the CS–DEO–SP beads a promising and effective adsorbent for eliminating Cr(VI) from metal plating wastewater.

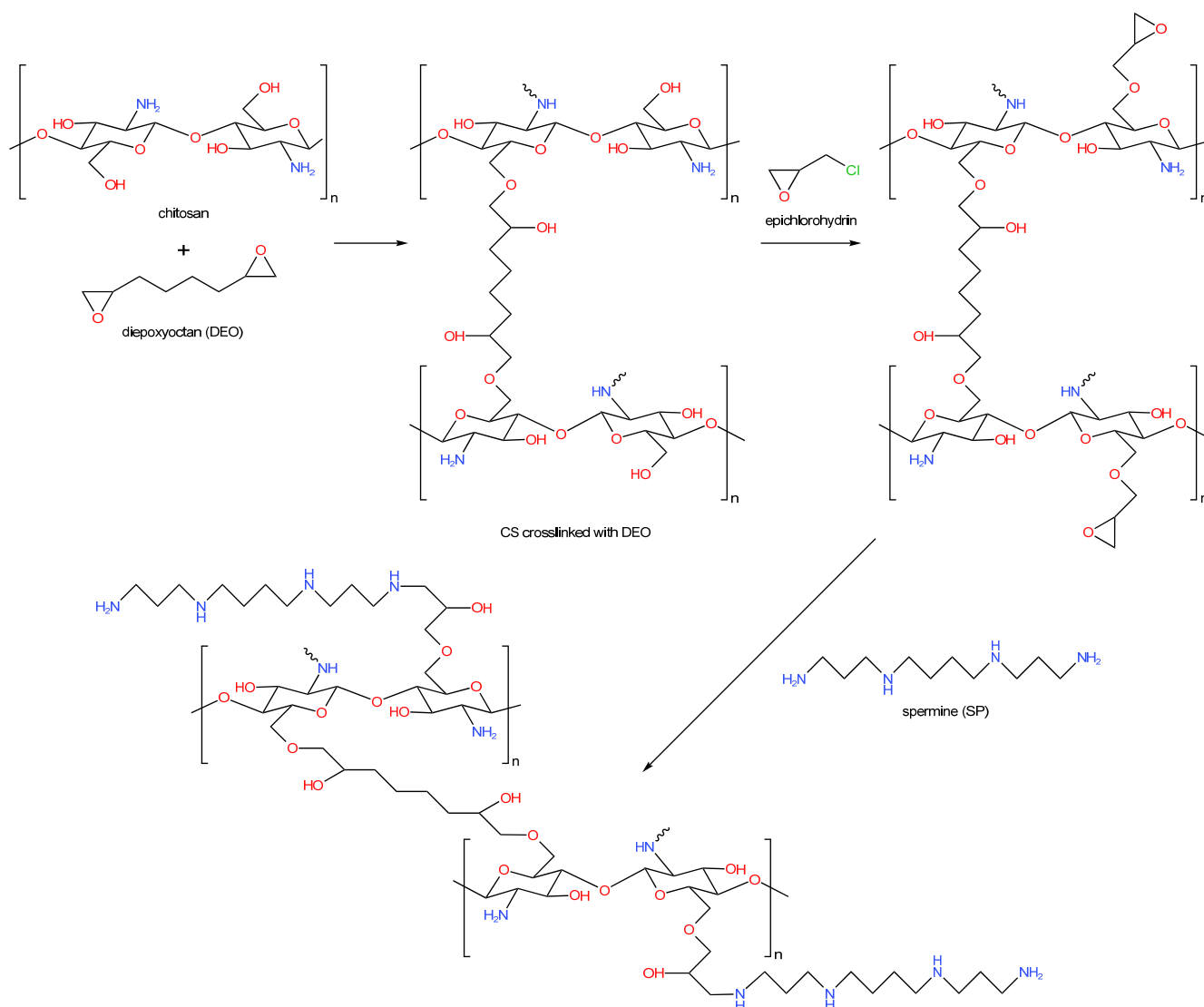


Figure 12. Synthesis of CS–DEO–SP beads [100].

Chanajaree et al. [101] synthesized CS beads crosslinked with GA for the removal of cationic (malachite green (MG)) and anionic (indigo carmine (IC)) dyes. For the synthesis of CS beads, high molecular weight (360,000 g/mol) CS was used. CS beads were formed using the common method, including the dissolution of CS in acetic acid and precipitation by dripping in NaOH solution with subsequent freeze drying. The removal of dyes was based on the soaking time at the same initial concentration (60 mg/L) at varying temperatures (30–40 °C). It was shown that crosslinked CS beads in freeze-dried form have a high adsorption capacity (714.29 mg/g) for MG, allowing quick removal of the dye in 30 min independent of the temperature, but they are not suitable for indigo carmine.

Farias et al. [102] studied the influence of crosslinking agent (GA or ECH) on the adsorption ability of CS spheres with respect to diesel oil at a concentration of 200–900 mg/L. It was found that the maximum amount of oil (1.82 mg/g) was adsorbed on CS crosslinked with GA. CS spheres crosslinked with ECH adsorb 1.642 mg/g of diesel oil. The difference in adsorption ability was explained by the modification of CS surface characteristics (porosity, roughness, etc.) after the crosslinking process.

A biofilm of crosslinked CS–ethylene glycol diglycidylether (CS–EGDE) with an average thickness of 4.24 μm was prepared by Jawad et al. [103] and used as a biosorbent for the following dyes: reactive red 120 (RR-120) and methyl orange (MO). The CS–EGDE

biofilm had low swelling index, good mechanical strength on glass plate and relatively high (64.4%) free amino group content. The maximum adsorption capacity of CS–EGDE at 303 K was 165.3 mg/g and 131.2 mg/g for RR-120 and MO, respectively. The mechanism of adsorption mainly included hydrogen bonding interaction, electrostatic attractions and $n-\pi$ stacking interaction.

Novel spherical adsorbents were synthesized by Lu et al. [104] via crosslinking of CS beads grafted by polyethylenimine (PEI) with GA (composite GACS@PEI) or ECH (composite EPCS@PEI, in which ECH is denoted as EP) (Figure 13).

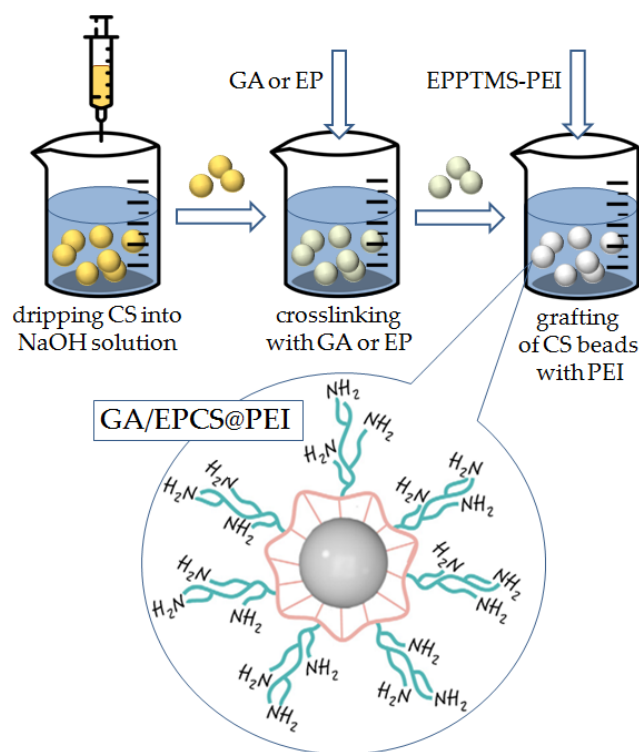


Figure 13. Preparation of GA/EPCS@PEI composites. Reproduced with permission from authors of [104], Elsevier, 2020.

CS beads were formed using the precipitation of drops of CS solution in glacial acetic acid with sodium hydroxide dissolved in a methanol–water mixture. CS beads were crosslinked with GA or ECH. In order to graft PEI to the surface of crosslinked CS beads, PEI was treated with 3-glycidyloxypropyltrimethoxysilane (EPPTMS). Such a treatment was shown to increase the number of adsorption sites of the resulting materials.

Synthesized composites of GA/EPCS@PEI were used to remove toxic contaminant—diclofenac sodium (DS)—from water. EPCS@PEI showed a maximum adsorption capacity of 253.32 mg/g and a removal efficiency of nearly 100% for the DS in the initial 50 mg/L solution. It was also shown that after the five repeated cycles of EPCS@PEI, the final removal rate is more than 80%, indicating excellent properties, where good adsorption capacities were retained over repeated cycles [104]. The adsorption capacity of EPCS@PEI was higher than for some other CS-containing composites, i.e., $\text{ZnFe}_2\text{O}_4/\text{CS}$ [105], which was only used at low DS concentrations and allowed for 75% of the adsorption removal rate.

Zhu et al. [106] synthesized an innovative adsorbent in the form of CS microspheres crosslinked with ECH and modified with PEI. In contrast to the majority of the described CS-based adsorbents, CS microspheres were obtained via inverted-phase emulsification crosslinking technique by using a one-pot method. Briefly, CS solution was added to liquid paraffin (oil phase) under mechanical agitation and addition of ethyl acetate and surfactant (span-80). Then, formaldehyde (FA) was added to protect the amino groups of the CS; after that, crosslinking was carried out at a pH of 8–10. After separation and drying, the resulting

crosslinked CS microspheres were modified with PEI using the surface grafting reaction (see Figure 14) by adding PEI solution to the suspension of microspheres at a pH of 10 (sample PEI-ECH-FA-CS MPs). Additionally, the carboxymethylation of PEI-ECH-FA-CS MPs was carried out (sample PEI-ECH-FA-CMCS MPs) by subsequent treatment with HCl solution in order to eliminate the protecting groups (sample PEI-ECH-CMCS MPs).

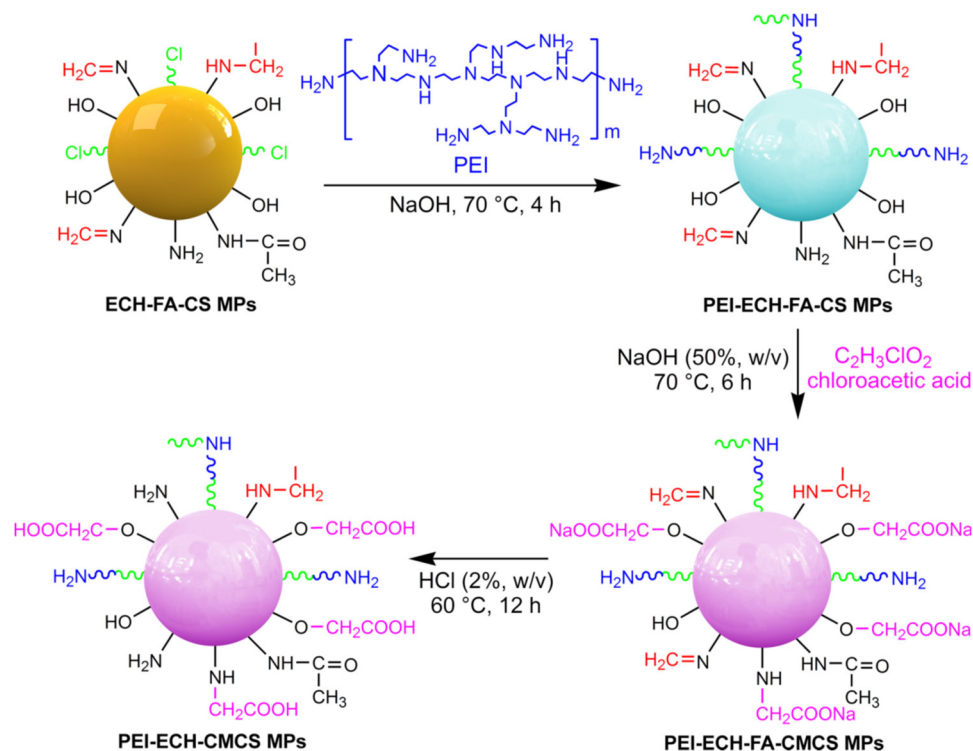


Figure 14. Chemical modifications to CS microspheres. Reproduced with permission from authors of [106], Elsevier, 2019.

As a result, the synthesized magnetic adsorbent (PEI-ECH-CMCS MPs) contained free amino- and carboxyl groups. The specific surface area of the PEI-ECH-CMCS MPs was about $29\text{ m}^2/\text{g}$, with porous 3D architectures, uniform spherical surfaces and narrow size distribution ($19\text{--}33\mu\text{m}$) [106].

PEI-ECH-CMCS MPs allowed for the capture of Cr(VI) and Pb(II) with a maximum adsorption capacity of 331.32 (at $\text{pH} = 3$) and 302.56 mg/g (at $\text{pH} = 5$), respectively, in batch experiments. Excellent reusability and feasibility were evidenced by an adsorption capacity loss $< 12.10\%$ and high removal efficiency for Cr(VI) (95.79%) and Pb(II) (91.40%) in synthetic effluents [106].

Sabarudin et al. [107] synthesized CS beads crosslinked with both TPP and ECH for the adsorption of MO. It was shown that TPP could act as a protecting agent for the amino groups of CS, while ECH reacted with the primary hydroxyl groups of the polymer. Various concentrations of TPP, ECH and immersion time in the TPP solution were studied. It was proposed that TPP prevents chemical binding between the NH_2 of CS and ECH, which reduced the adsorption capacity of CS beads. The effect of pH and the kinetics of adsorption were also investigated. As a result, $\text{pH} 3$, 10% (w/v) TPP, 5% (v/v) ECH and 12 h immersion time in TPP were selected as the optimum conditions for preparing CS beads. After removing the protective group from the beads, NH_2 groups of CS freely attracted the anionic dye MO, resulting in an adsorption capacity of 79.55 mg/g . Moreover, it was found that covalent crosslinking with ECH provided stability for CS in acidic conditions, whereas the concentration of TPP and immersion time controlled the pore size and morphology of the CS beads [107].

Interesting work was carried out by Urtasun et al. [108], who developed new, low-cost support material for multimodal chromatography using CS and Orange R–HE triazine dye. CS-based minispheres (CMS) with a mean diameter of 1.4 ± 0.2 mm were prepared using nonsolvent (acid-based) precipitation (dissolution of CS in acetic acid with subsequent dripping in NaOH solution) and crosslinked with ECH. Synthesized CMS were shown to be prospective sorbents for proteins, i.e., lactoferrin and lactoperoxidase—high value proteins found in diluted concentrations in sweet whey. Utilizing a simple operating process, these two proteins were adsorbed onto the CMS–Orange R–HE matrix, even though their concentrations were low in sweet whey (adsorption $\geq 90\%$). After adsorption, the differential elution process can be carried out, which results in two separate proteins with good yields and high purity.

CMS crosslinked with ECH at 60°C for 4 h and modified with sulfanilic acid (4-aminobenzenesulfonic acid) or glycidyl trimethylammonium chloride (GTMA) were synthesized (Figure 15) [109]. Crosslinked CMS modified with sulfanilic acid was used for the purification process of lactoferrin from cheese whey, while CMS treated with GTMA were designed for recovering whey protein isolate. The developed CMS allowed for 76.51% of lactoferrin adsorption for 4 h at a pH of 6.57. It is noteworthy that at the chosen pH of 6.57, the matrix and most of the proteins were charged negatively, while the target protein had the opposite charge, which allowed for high selectivity with respect to lactoferrin.

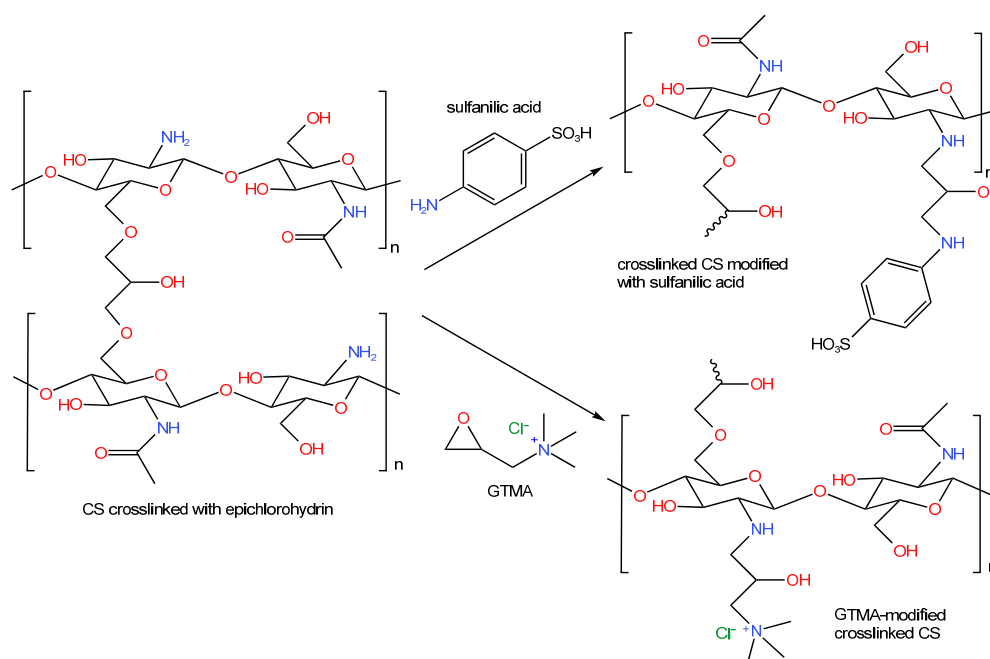


Figure 15. Simplified representation of modification of crosslinked CMS with sulfanilic acid or GTMA [109].

In the case of sequential purification of lactoferrin and whey protein isolate, a yield of 62.31% was obtained for lactoferrin, while for whey proteins about 52% of adsorption was achieved; that is, 2.71 mg of protein per mL of whey processed. The developed CMS allowed the cheese whey to be processed without any previous conditioning, to have good mechanic resistance, and to be easily recovered after the adsorption/washing and elution steps. Moreover, modified CMS can be used as new chromatographic matrices that can be applied to direct protein isolation [109].

Structured CS in the form of both beads and films is widely applied for the adsorption of inorganic anions [110] and cations [111,112].

For example, CS microspheres synthesized using the emulsification method and crosslinked with GA were used as an adsorbent for iodide anions [110]. The removal efficiency of CS microspheres was limited to 0.8792 mmol/g. Better adsorption efficiency

(>90% in 20 min with a maximum adsorption capacity of 1.5267 mmol/g) was achieved while using a modified CS-based sorbent, AgCl@CS, in a wide pH range (from pH 2 up to pH 10). For AgCl@CS, chemisorption from AgCl and physisorption from CS were responsible for I⁻ removal.

Recently, Zhang et al. [111] published a review on the application of CS and its derivatives for heavy metal removal from wastewater. Structured, CS-based materials modified by grafting and crosslinking can be used to remove Cu, Pb, Zn, Ni, Hg, Cd, Cr, Pt, Pd, Co, etc. It was shown that modified crosslinked CS possesses increased adsorption capacity and stability in comparison with native CS, not only with respect to heavy metals, but also for organic pollutants, such as phenols, dyes, etc. The authors of [112] noted that the development of CS derivatives with selectivity for substances other than heavy metal ions calls for further exploration. There is also a lack of data on the selectivity of CS-based adsorbents when purified solutions contain several different metals simultaneously [113].

Upadhyay et al. [114] provided a deep analysis on CS-based adsorbents intended for the removal of heavy metals (Cu, Pb, Cr, Ni, Zn, Mn, Fe, Hg, Ag, Cd) from wastewater. Different synthesis techniques were described. Special attention was paid to the problem of regeneration of CS-containing adsorbents and also to the design of experiments in continuous mode. It was stressed that researchers must focus on real industrial problems to develop effective adsorbents that can simultaneously remove multiple pollutants and, at the same time, have good desorption percentages for further reuse. Novel adsorbents should also be pH-independent since pH monitoring in industrial effluents is both time- and money-consuming.

In spite of the fact that crosslinked and grafted CS-based materials have an increased number of adsorption sites and higher pH stability and reusability [115], further improvement of adsorbent characteristics can be achieved via the development of composite organic-inorganic materials, including magnetically separable ones.

3.2. Chitosan-Based Organic/Inorganic Composite Adsorbents

In most cases, composite CS-based materials represent the combination of CS with inorganic compounds such as metal oxides. Such CS oxide composites typically are obtained via preliminarily mixing CS solution with solid inorganic particles and the subsequent gelation of the resulting composite material.

It is noteworthy that the same method can be used for the synthesis of CS-based composites with carbonaceous materials. For example, Zhang et al. [116] synthesized crosslinked CS/graphene nanoplate composite spheres (CS-GNPs) by a simple mixing of GNPs with CS solution followed by syringe dripping and CS crosslinking with GA. The adsorption activities of CS-GNPs were evaluated by the example of two azo acid dyes: MO and acid red 1 (AR 1). For the optimized composite material, the adsorption capacity of MO was 230.91 mg/g and 132.94 mg/g for AR 1, respectively. It was shown that CS-GNPs can be easily separated from the solution and efficiently regenerated after reaching saturated adsorption. After five cycles, its adsorption capacity for MO was about 90%.

Jawad et al. [117] synthesized Schiff's base-crosslinked CS-GA loaded with TiO₂ NPs (Figure 16) for the removal of reactive red 120 (RR120) dye from aqueous solutions in batch mode at various RR120 concentrations, adsorbent dosages, contact times and pHs (3–12). CS-TiO₂ composites were prepared by mixing certain amounts of titania NPs with CS before the dissolution and formation of CS beads and further crosslinking. Different ratios of TiO₂ NPs were used, such as 25% of TiO₂ (CS-GA/TNC-25) and 50% of CS-GA/TNC-50. CS-GA/TNC-25 exhibited the best adsorptive property (103.1 mg/g at 303 K), which was likely due to the perfect balance between the surface area and available aminogroups in this composite. The kinetics and isotherm model results indicated [117] that the adsorption of RR120 was affected by chemisorption and multilayer adsorption. The adsorption mechanism of RR120 on the CS-GA/TNC-25 surface was assigned to various interactions, such as electrostatic attraction, $n-\pi$ stacking and H-bonding.

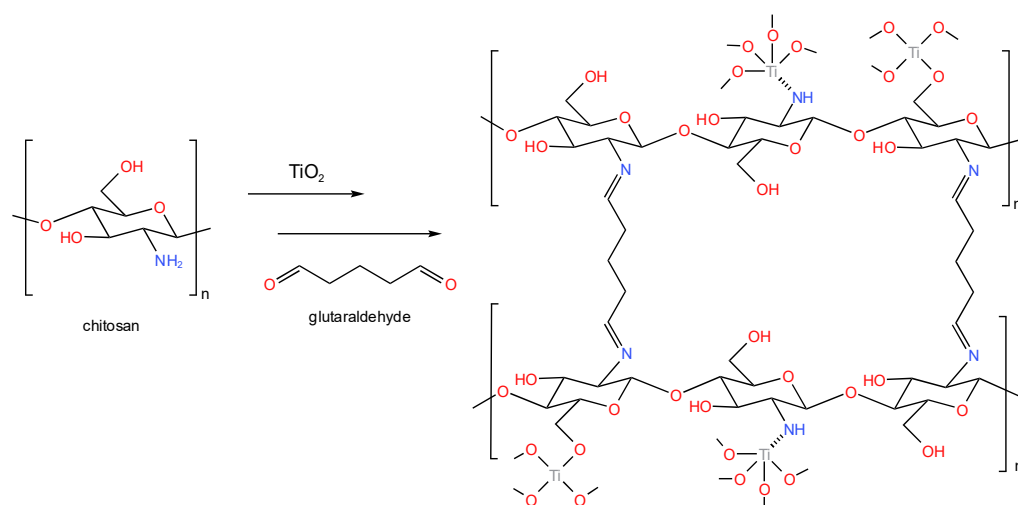


Figure 16. Simplified representation of the synthesis of composite CS-TiO₂ [117].

A novel CS material (ECS@Ca@CTA) was prepared [118] for the adsorption of sodium dodecylbenzene sulfonate (SDBS). CS was complexed with CaCl₂ and crosslinked into hollow spheres with GA (Figure 17). However, a part of the CS' amino groups was depleted. Therefore, the amino groups were reactivated with ethylenediamine; then, the ECS@Ca was quaternized with (3-chloro-2-hydroxypropyl) trimethylammonium chloride (CTA) and prepared as a hollow sphere structure with a wrinkled surface (designated ECS@Ca@CTA) in order to improve the effect of pH on adsorption of SDBS.

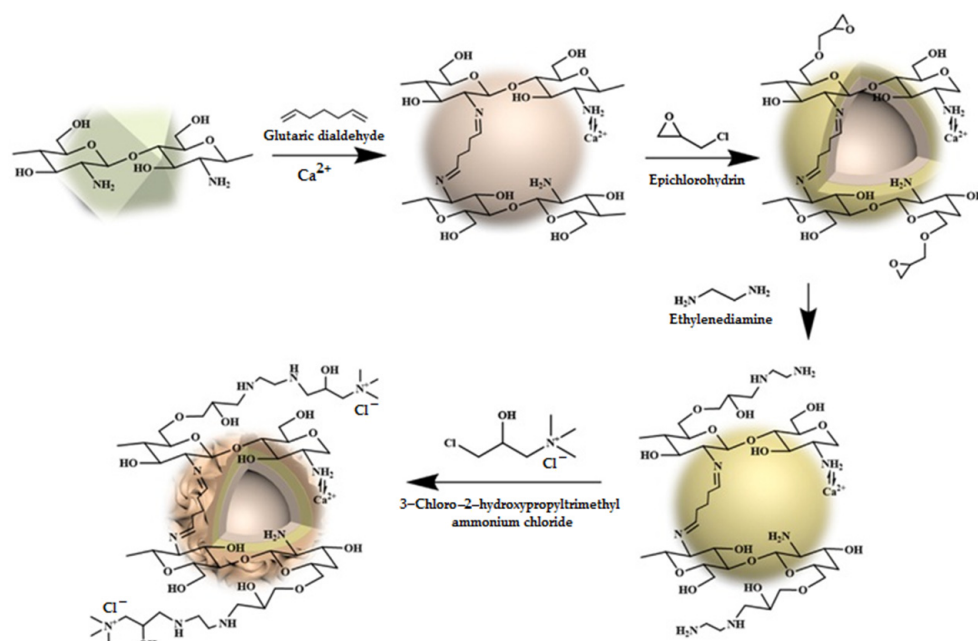


Figure 17. Mechanism of formation of ECS@Ca@CTA. Reproduced with permission from authors of [118], Elsevier, 2019.

pH has a great impact on the adsorption of SDBS. It was shown [118] that the pH dependence of CS-based adsorbents can be improved using CTA. Ca²⁺ and CTA cause CS to be positively charged at different pH levels, while ethylenediamine increases the number of amino groups. Thus, the maximum adsorption capability of ECS@Ca@CTA was 2430, 1967 and 1116 mg/g at pH 3.0, 7.0 and 10.0 for SDBS, respectively. Crosslinking of CS into wrinkled hollow spheres resulted in an increase in the specific surface area, chemical

stability and capability of SDBS capture. The adsorption capacity of ECS@Ca@CTA can still reach over 80% after six repeated adsorption–desorption runs.

A composite adsorbent made of CS and bentonite clay was prepared [119] and used for the adsorption of Cr(VI) ions from aqueous solutions. A composite CS–bentonite clay was obtained by mixing bentonite with CS solution in 2% acetic acid with further dripping in NaOH solution to form composite CS capsules, which underwent crosslinking with GA. The effects of pH, adsorbent dosage, adsorbate concentration, temperature and contact time were studied in batch mode. The experimental data were well-fitted to a Scatchard adsorption isotherm and the adsorption capacity was calculated from the isotherm model. It was found that bentonite clay had a maximum adsorption capacity of 11,076 mg/g, while the composite revealed an almost ten times higher maximum adsorption capacity (106,444 mg/g) for the removal of Cr(VI) ions at 25 °C, pH 2 and a contact time of 60 min. The mechanism of adsorption included ion exchange, electrostatic interaction and complexation.

CS beads modified with FeO and TiO₂ NPs were synthesized by Patiño-Ruiz et al. [120] using an anionic crosslinking procedure, which allowed beads with semispherical shapes to be obtained. FeO and TiO₂ NPs were synthesized by performing coprecipitation and green chemistry methods, respectively, and then mixed with CS solution. The CS–FeO/TiO₂ mixture was then dripped in NaOH solution, washed and dried at room temperature. The resulting CS–FeO/TiO₂ beads showed high BET surface area (27.13 m²/g) and pore size (6.8 nm). These results were attributed to the presence of NPs, which promoted the formation of porosity and increased the surface area. After the incorporation of NPs, the semicrystalline nature of the CS changed into a completely amorphous structure due to the break in intermolecular bonding. The CS–FeO/TiO₂ revealed excellent thermal stability (up to 270 °C) and superparamagnetic response, attributed to the presence of FeO and TiO₂ NPs.

Adsorption experiments were performed using naphthalene as an example of polycyclic aromatic hydrocarbons (PAHs). The pseudo-second-order model properly fitted the adsorption data, indicating that chemisorption was the primary adsorption mechanism. CS–FeO/TiO₂ showed a higher adsorption capacity of 33.1 mg/g compared to the 29.8 mg/g of the unmodified CS beads. A maximum adsorption capacity of 149.3 mg/g for CS–FeO/TiO₂ was found. The high affinity toward PAHs was due to additional non-covalent forces. Strong chemisorption between naphthalene and the functional groups as well as electrostatic interaction with the NPs was found [120].

CS/hematite nanocomposite hydrogel capsules (HC–H) were developed by Ohemeng-Boahen et al. [121] using an anionic surfactant gelation occurring simultaneously with the immobilization and impregnation of α -Fe₂O₃ NPs within the gel matrix. Hematite NPs were mixed with CS solution in 2% acetic acid. The resulting mixtures were dripped into an aqueous solution of sodium dodecyl sulfate, SDS (50 g/L). SDS penetrated the drops, which allowed for the creation of CS hydrogel capsules. Thus, a series of HC–H samples were prepared with different loadings of hematite NPs varying from 10% up to 60% (*v/v*). The HC–H composites were highly stable in acidic media (even at pH 2) and revealed enhanced adsorptive capacity for Congo red (CR). The maximum adsorption capacity of HC–H60 was 4705.6 mg/g (26.7 times more than that of the pristine CS hydrogel capsule (176.5 mg/g)).

Zr–organic frameworks (Uio-66, named Zr@BDC metal–organic frameworks (MOFs)) were prepared using Zr(IV) and 1,4-benzenedicarboxylic acid (BDC) for efficient fluoride removal [122]. Since the Zr@BDC MOFs possessed some limitations such as column blockage and pressure drop during field tests, the Zr@BDC MOFs were modified with CS (Zr@BDC–CS). The Zr@BDC–CS spheres were obtained via the common mixing of Zr@BDC MOFs with CS solution with subsequent dripping in NaOH solution. The synthesized Zr@BDC MOFs and Zr@BDC–CS spheres possessed the highest defluoridation capacities at 4935 and 4982 mgF/kg within 20 min, respectively. The defluoridation capacity of the Zr@BDC–CS was slightly dependent on the pH level and was majorly diminished in the

presence of HCO_3^- . The defluoridation mechanism of the Zr@BDC-CS spheres was mainly dominated by electrostatic attraction and complexation. It was shown that the Zr@BDC-CS spheres had positively charged Zr^{4+} , which attracted negatively charged fluoride ions. Moreover, at the appropriate pH ($\text{pH} < 6.54$), protonated hydroxyl and amino groups of CS can also easily adsorb fluoride via electrostatic interaction. A reusability study indicated that the prepared Zr@BDC-CS spheres are regenerable and reusable for up to six cycles.

Wang et al. [123] developed innovative and multifunctional CS-based hydrogel beads (the diameter of the dried beads was about 600 μm) immobilized with Ag NPs using polydopamine (PDA) coating, which simultaneously enhanced both the antimicrobial and adsorption activity. In contrast to the most recently published research, gelation of CS beads was carried out using oxidized dextran (OD)—a dialdehyde polymer able to form Schiff's bases with polyamines (i.e., CS). Crosslinked CS beads were coated with PDA via polymerization of dopamine (DA) on the surface of the beads (Figure 18). Ag NPs were synthesized via the adsorption of AgNO_3 by PDA-coated CS beads.

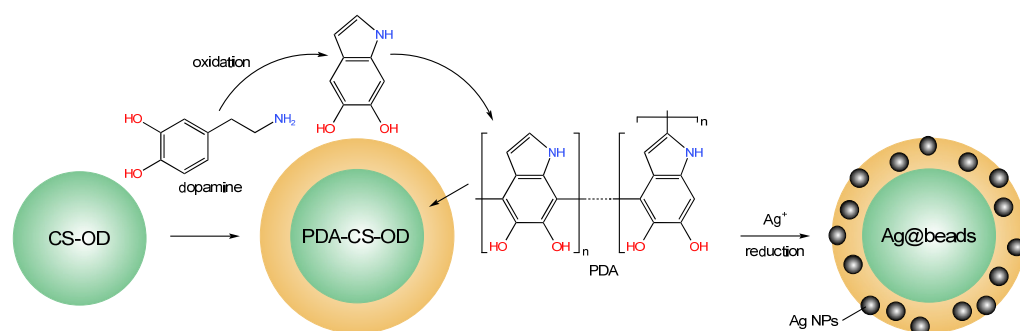


Figure 18. Schematic diagram of the preparation of the Ag@beads (based on Ref. [123]).

It was shown that Ag NPs with sizes ranging from 50 nm to several hundred nanometers were immobilized not only on the surface but also in the interior of the PDA-coated CS beads. The covalent silver–carboxylate linkage along with hydrophobic and van der Waals forces was evidenced using FTIR spectroscopy. The adsorption performance of the Ag@beads was investigated for the removal of an anionic dye (CR) and Cu(II). The adsorption capacity of the Ag@beads at equilibrium state was reached at 7 and 9 mg/g for CR and Cu(II), respectively. Moreover, the antimicrobial activities of the Ag@beads were found against Gram-negative *Escherichia coli* and Gram-positive *Staphylococcus aureus*, showing Ag@beads to be good candidates for an integrative approach to efficiently controlling both the microbial and chemical quality of wastewater [123].

3.3. Magnetically Separable Chitosan Composites

Magnetically separable composites based on various biopolymers are widely used for removal of different heavy metals from aqueous solutions [124]. Incorporating magnetic materials into the CS matrix and shaping CS in various forms such as beads, membranes, hydrogels, etc., greatly boosts the separation problem of CS [115]. In spite of the fact that many magnetic CS materials have been prepared for the adsorption of metal ions, Fan et al. [125] noticed that, to date, there is no standard method for the comprehensive evaluation of material performance. Thus, two methods for evaluation of the overall performance of magnetic materials were established [125], which consider both heavy metal ion adsorption capacity (Q) and magnetic recovery of the material after use:

- (i) Based on calculation of the adsorption recovery index using the values of Q and recovery time (t) needed for achieving 98% material recovery, a higher adsorption recovery index value shows better magnetic material performance;
- (ii) Based on effort vector data visualization, in which the position of a magnetic material is shown on a coordinate depicted using normalized Q and saturation magnetization value, the distance from the data point to the target indicates the performance of the material.

Moreover, Fan et al. [125] used two methods for the preparation of magnetic CS beads. The first method (embedding method) was based on the most widespread approach—preliminarily synthesis of Fe_3O_4 NPs, mixing of magnetic NPs with CS solution, and dripping of Fe_3O_4 -CS solution in NaOH solution with further crosslinking with GA. The second method (chemical coprecipitation method) was based on the dissolution of CS and precursors of magnetic particles (Fe(II) and Fe(III)salts) in 3% acetic acid with subsequent dripping of this mixture in NaOH solution and crosslinking with GA. Thus, two series of magnetic CS beads with different Fe_3O_4 /CS mass ratios were prepared.

Synthesized magnetic CS beads were used for the adsorption of Ag^+ , Cu^{2+} , Hg^{2+} , Cr^{3+} and Cr^{6+} from aqueous solutions and recovery studies. Compared to the adsorption recovery index, the effort vector data visualization was more straightforward and easier to use. While comparing the two magnetic CS bead synthesis methods based on the proposed effort vector data visualization, it was found [125] that both synthesis methods allow for similar efficiency of heavy metal adsorption and data distribution. Independent of the synthesis method, CS beads containing 0.3 g of CS and 0.7 g of Fe_3O_4 NPs revealed best performance for the adsorption of the chosen heavy metal ions.

Though most researchers prefer to synthesize CS-based materials in the form of beads, which possess low flow resistance and are hence convenient for continuous mode operation, for special applications, CS films and coatings can be obtained.

CS nanocomposite films were prepared [126] using in situ precipitation of magnetic particles. The method of synthesis was based on the above-described chemical coprecipitation. The difference was in the shaping of the resulting material: a film was obtained by pouring the mixture (CS and iron salts) into Teflon Petri dishes and subsequently drying and rinsing it with NaOH solution; no crosslinking agents were added.

The magnetic CS film was tested as an adsorbent for arsenic ions, revealing a higher adsorption capacity (10.4 mg/g) compared to common CS film (1.6 mg/g). The higher equilibrium adsorption capacity was explained by the synergic effects of CS and iron oxide particles regarding the adsorption capacities of the phases, film surface morphology (a much more irregular surface in the case of the nanocomposite), polymeric matrix crystallinity and electrostatic forces that prevail in acidic pH [126].

Eivazzadeh-Keihan et al. [127] synthesized a CS-containing magnetic nanobiocomposite. The composite was prepared using the chemical coprecipitation method with several significant differences: (i) before synthesis, the CS was guanidinylated, as shown in Figure 19; (ii) a modified CS was mixed with Fe(II) and Fe(III) salts with the subsequent formation of precipitate by adding ammonia solution. The resulting nanobiocomposite had a core-shell structure, where the core was represented by Fe_3O_4 NPs with average sizes of 30–34 nm, while the shell consisted of the modified CS.

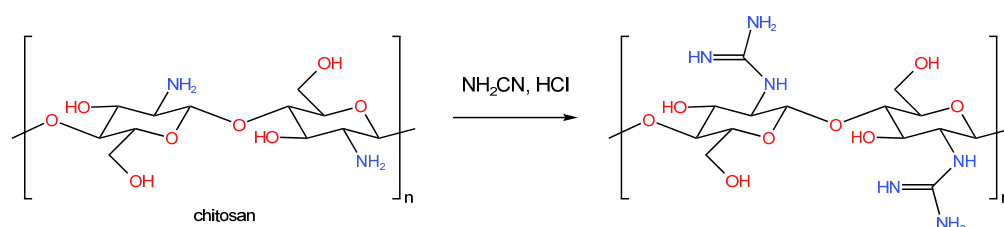


Figure 19. Guanidinylation of CS [127].

The application of this nanobiocomposite was evaluated in two different fields: the adsorption and in vitro hyperthermia procedures [127]. Adsorption capacity was studied with respect to copper (Cu^{+2}), lead (Pb^{+2}) and chromium (Cr^{+6}) ions. Different parameters including time, temperature and amount of biosorbent were optimized for each heavy metal ion. In optimized conditions, the adsorptions of Cu^{+2} , Pb^{+2} and Cr^{+6} were, respectively, 100%, 98.64% and 33.76%. Concerning the in vitro hyperthermia process, the maximum specific absorption rate value (70.59 w/g) was obtained by using 1 mg/mL of the nanobiocomposite, with very promising results.

Another example of a modified CS loaded with magnetic NPs is CS functionalized with an aromatic Schiff's base ligand (3,3-diphenylpropylimine methyl benzaldehyde—PPIMB) (Figure 20). Such a treatment allowed for a high number of binding sites for the effective adsorption of lead ion in the aqueous medium [128]. It is noteworthy that CS was modified with PPIMB directly after the beading procedure. A magnetic CS–PPIMB adsorbent was prepared by dispersion of Fe_3O_4 NPs in acetic acid with the subsequent addition of CS–PPIMB to this solution.

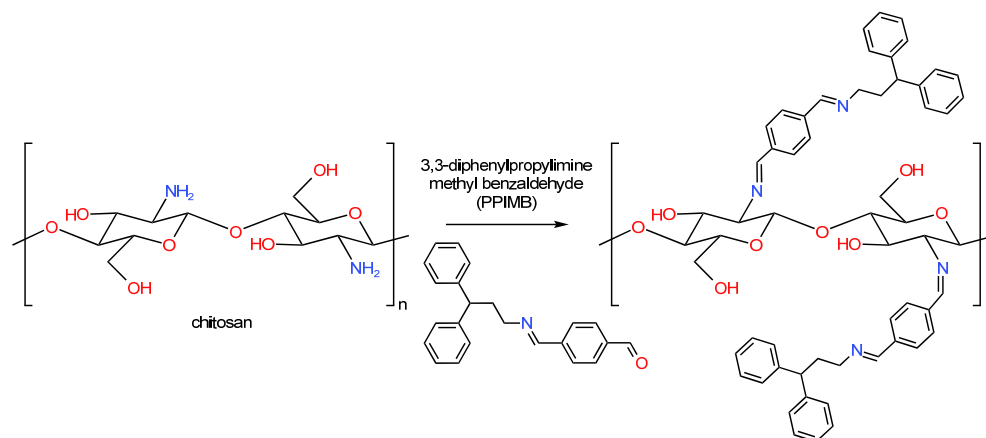


Figure 20. Functionalization of CS with PPIMB [128].

The effect of pH, collision time, adsorbent dosage and initial concentration of Pb(II) was studied. The adsorption capacity of magnetic CS–PPIMB against Pb(II) was 230.48 mg/g, which was higher than that of many similar adsorbents. Moreover, it was shown that magnetic CS–PPIMB adsorbent was highly selective toward Pb(II) compared to other metal ions. The strong binding energy of the Pb atoms with aromatic rings and imine groups of the synthesized adsorbent was confirmed using theoretical computations. The synthesized magnetic CS–PPIMB also revealed good regeneration capacity towards Pb(II) ions after five successive adsorption–desorption cycles [128].

CS-based magnetic composites can be applied not only for the removal of cations, but also for anions from aqueous solutions.

As an example of recent research, PEI-grafted CS core–shell magnetic NPs ($\text{Fe}_3\text{O}_4/\text{CS}/\text{PEI}$) were synthesized and applied for adsorbing phosphate in water [129]. This magnetic composite was obtained by using the embedding method (see above). No shaping of the resulting mixture was carried out. Instead, an aqueous solution of a gelating agent (TPP) was added directly to the mixture containing CS and Fe_3O_4 NPs. Thus, ionotropic gelation of CS occurred directly on the surface of the Fe_3O_4 NPs. Then, PEI was grafted onto the surface of $\text{Fe}_3\text{O}_4/\text{CS}$ preliminarily treated with ECH, which reacted with the hydroxymethyl groups of the CS (the molar ratio of total amino groups of PEI to the hydroxyl groups of the CS was fixed at 2.5).

The composite $\text{Fe}_3\text{O}_4/\text{CS}/\text{PEI}$ had a maximum adsorption capacity of 48.2 mg/g with respect to phosphate ions at an equilibrium pH = 3.0 and 25 °C. The primary mechanism for phosphate adsorption on the $\text{Fe}_3\text{O}_4/\text{CS}/\text{PEI}$ particles was electrostatic attraction. The preferential adsorption of phosphate in the presence of other excess anions including chloride, nitrate, carbonate and sulfate was also shown [129]. Regeneration experiments revealed that more than 90% of the phosphate was desorbed by 0.05 mol/L of the NaOH solution. However, after five consecutive adsorption–desorption cycles, the adsorption capacity of $\text{Fe}_3\text{O}_4/\text{CS}/\text{PEI}$ decreased by 40%.

Elanchezhiyan et al. [130] studied the adsorption of long-chain perfluorinated chemicals (PFCs)—namely, perfluorooctanoate (PFOA) and perfluorooctane sulfonate (PFOS)—from water using reduced graphene oxide (rGO)-modified zinc ferrite (ZnFe_2O_4)-immobilized chitosan beads (rGO–ZF@CB) as an adsorbent.

rGO-ZF@CB was prepared in three steps:

- (i) ZnFe₂O₄ (ZF) NPs were synthesized using the chemical coprecipitation method;
- (ii) rGO nanosheets were synthesized by using a modified Hummer's method with natural graphite;
- (iii) Magnetic rGO-ZF@CB was synthesized by using a crosslinking reaction with GA (2.5%). Before magnetic bead preparation, rGO nanosheets and ZF NPs were added into the ethanol solution. A suspension of rGO and ZF NPs was mixed with CS solution in acetic acid. Then, this reaction mixture (rGO-ZF@CS) was dripped into 1 M NaOH solution using a syringe needle. The resulting wet magnetic beads, washed with water until reaching neutral pH, were treated with GA, which allowed magnetic rGO-ZF@CB to be obtained.

The rGO-ZF@CB possessed a maximum adsorption capacity of 16.07 mg/g for PFOA and 21.64 mg/g for PFOS. Both the electrostatic attractions and hydrophobic interactions drove the removal of PFOA and PFOS using prepared rGO-ZF@CB [130].

Carbon-Fe₃O₄ (C/Fe₃O₄) core-shell NPs modified with CS were synthesized [131] for the removal of MO from aqueous solutions. The C/Fe₃O₄ NPs were prepared using the hydrothermal method, in which glucose served as a carbon source. The resulting C/Fe₃O₄ NPs were covered with CS with a method similar to the one described above [129], using GA as crosslinking agent. Fast adsorption of MO in the wide pH range of 3–11 using CS-covered C/Fe₃O₄ NPs was shown, and the maximum adsorption capacity was found to be 425 mg/g at 45 °C.

A comparison of different adsorbents is presented in Table 1. As can be seen, there is a number of CS-based composite materials. In spite of this variety, the general trend, allowing for the achievement of high adsorption capacity, is the use of crosslinking agents (preferably covalent crosslinking) and grafting of functional groups, resulting in a noticeable increase in number of adsorption sites.

Table 1. Comparison of adsorption performance of some of the recent CS-based materials.

CS-Containing Adsorbent	Crosslinking Agent	Shaping	Contaminant	Absorption Conditions	Absorption Capacity	Ref.
CS/MAH-DVB-3	DVB	No	MB	298 K, pH 10	503 mg/g	[97]
Pyridine-modified CS	No	No	Cu(II)	25 °C, pH 5.5	1.84 mmol/g	[98]
			Cr(VI)	25 °C, pH 3.6	3.86 mmol/g	[98]
CS-DEO	DEO	Beads	RR2	Room temperature, pH 2	788.6 mg/g	[99]
CS-DEO-SP	DEO	Beads	Cr(VI)	25 °C, pH 2	352 mg/g	[100]
CS	GA	Beads	MG	30–40 °C, pH 6	714.29 mg/g	[101]
			IC	30–40 °C, pH 6	11.02 mg/g	[101]
CS	GA	Beads	Diesel oil solution in hexane	Ambient	1.820 mg/g	[102]
	ECH			Ambient	1.642 mg/g	[102]
	No			Ambient	1.065 mg/g	[102]
CS-EGDE	EGDE	Film	RR120	303 K, pH 5	165.3 mg/g	[103]
			MO	303 K, pH 4	131.2 mg/g	[103]
EPCS@PEI	ECH	Beads	DS	308 K, pH 4.2	253.32 mg/g	[104]
PEI-ECH-FA-CS	ECH	Micro spheres	Cr(VI)	298 K, pH 3	331.32 mg/g	[106]
			Pb(II)	298 K, pH 5	302.56 mg/g	[106]
CS	TPP and ECH	Beads	MO	Room temperature, pH 3	79.55 mg/g	[107]
AgCl@CS	GA	Microspheres	Iodide anion	25 °C, pH 2–10	1.5267 mmol/g	[110]
CS-GNPs	GA	Spheres	MO	298 K, pH 3	230.91 mg/g	[116]
			AR 1	298 K, pH 4	132.94 mg/g	[116]
CS-GA/TNC-25	GA	No	RR 120	303 K, pH 3	103.1 mg/g	[117]

Table 1. Cont.

CS-Containing Adsorbent	Crosslinking Agent	Shaping	Contaminant	Absorption Conditions	Absorption Capacity	Ref.
ECS@Ca@CTA	GA	Hollow spheres	SDBS	Room temperature, pH 3	2430 mg/g	[118]
CS-bentonite clay	GA	Capsules	Cr(VI)	25 °C, pH 2	106.444 mg/g	[119]
CS-FeO/TiO ₂	No	Beads	Naphthalene	25 °C, pH Not indicated	149.3 mg/g	[120]
HC-H60	SDS	Capsules	CR	30 °C, pH 4	4705.6 mg/g	[121]
Zr@BDC-CS	No	Spheres	Fluoride ion	Room temperature, pH 6	4982 mg/kg	[122]
Ag@beads	Oxidized dextran	Beads	CR Cu (II)	30 °C, pH 5 30 °C, pH 5	7 mg/g 9 mg/g	[123] [123]
Magnetic composites						
CS-Fe ₃ O ₄	No	Film	As(III)	25 °C, pH 3	10.4 mg/g	[126]
MGC (guanidinylated CS)	No	Core(Fe ₃ O ₄)-shell particles	Pb(II)	60 °C, pH 7	22.64 mg/g	[127]
CS-PPIMB	No	Beads	Pb(II)	303 K, pH 5.5	230.48 mg/g	[128]
Fe ₃ O ₄ /CS/PEI	TPP	Core-shell particles	Phosphate ion	25 °C, pH 3	48.2 mg/g	[129]
rGO-ZF@CB	GA	Beads	PFOA PFOS	25 °C, pH 3 25 °C, pH 3	16.07 mg/g 21.64 mg/g	[130] [130]
CS-covered C/Fe ₃ O ₄	GA	Core-shell particles	MO	45 °C, pH 3–11	425 mg/g	[131]

4. Chitosan as Catalytic Support

Due to the existence of different functional groups (see Figure 2), CS-based materials can be used as supports for catalytically active metals and enzymes.

4.1. Catalytic Metal–Chitosan Composites

The lives of NPs can be divided into three stages: preparation, storage and application. The stabilization of particles' physical and chemical characteristics is critical and must be carefully controlled [132]. Metal deposition on CS is a promising area of research in the field of catalysis, since CS is a source of various functional groups that can effectively bind metal ions or NPs [133,134]. In the resulting catalytic materials, CS can serve as a reducing agent (due to the presence of hydroxymethyl and amino groups) and stabilizer as well, which is able to control the sizes of metal NPs to some extent.

Any modifications to CS influence the concentration of functional groups and contribution of different interactions (hydrogen bonds, electrostatic interactions, π - π stacking interactions, etc.). For example, it was found that the DD and molecular weight of CS influences the sizes of Au NPs. At low CS concentration (0.005% and 0.01% (*w/v*)), individual spherical Au NPs with a mean diameter of about 10 nm were obtained regardless of chitosan DD and Mw, while anisotropic Au NPs were obtained at a concentration above 0.05% (*w/v*) [135].

The growth of larger polygonal Au NPs was promoted as the higher concentration and lower DD CS was used. Chitoooligomers (2.4 kDa, DD 94%) showed the highest reduction ability for Au(III) and the synthesized Au NPs exhibited aggregation. In general, it was concluded that the DD and concentration of CS is more important than Mw [135].

CS and its derivatives can be used as stabilizers of various catalytically active metal ions and NPs (Mn [136], Co [112,137], Cu [138–146], Ag [147–149], Pd [150–155], Pt [156], etc.) and metal oxides [133,157–160].

Since CS-containing materials require relatively mild reaction conditions, their catalytic applications are also limited. In the last years, attention was mainly paid to the hydrogenation of nitro-compounds, catalytic oxidation, cross-coupling reactions, click chemistry and some other processes. The hydrogenation of nitro-compounds is one of the most widespread

catalytic processes in which CS-based systems can be tested [141,144,147,150–152,161]. It is noteworthy that CS-containing materials are known as prospective adsorbents for the removal of heavy metals and dyes from wastewater; thus, in many works, their adsorption ability was successfully combined with catalytic properties. The shaping of such catalytic systems can be varied: films, fibers, beads or capsules.

For example, Cu NPs were stabilized in CS–SiO₂ nanocomposite fibers [141]. CS–SiO₂ fibers were prepared by mixing SiO₂ NPs (5 wt.% of CS) with CS solution in acetic acid with subsequent precipitation of fiber via extrusion of the mixture into NaOH solution using a syringe. Dried CS–SiO₂ composite fibers were then treated with solutions of metal salts (Cu, Co, Ag and Ni) and reducing agent (NaBH₄) that allowed for the formation of metal NPs 20–40 nm in diameter on the fibers' surface. The resulting metal-containing composites were used for the reduction of 4-nitroaniline (4-NA) and decolorization of CR in aqueous medium using NaBH₄ as a hydrogen source. Cu/CS–SiO₂ revealed high catalytic efficiencies in the reduction of 4-NA and CR compared to other metals: the apparent rate constants of $6.17 \times 10^{-3} \text{ s}^{-1}$ and $1.68 \times 10^{-2} \text{ s}^{-1}$ were observed for the reduction of 4-NA and CR, respectively. A percentage of 94.53 of 4-NA was converted in 9 min. The percent reduction of CR in 5 min was found to be 92.7%. The catalytic activity of Cu/CS–SiO₂ was also examined in the reduction of nitrophenols (2-NP, 3-NP and 4-NP), which were successfully converted in a short time of 8–10 min, and other dyes (MO, MB and acridine orange (AO)). More than 90% of MO, MB and AO were decolorized in 6, 9 and 14 min, respectively.

Raza et al. [142] developed CuO NPs embedded in porous CS membranes using a solution-casting approach with sodium TPP as a crosslinker and polyethylene glycol as a porogen. The CuO NPs incorporated in CS membranes exhibited exceptional photocatalytic activities against MO and MB. These dyes were degraded to 62–65% at 30 mg/L. CS-based porous membranes retained about 95% of their photodegradation activity for up to five cycles. It is noteworthy that CS-based adsorbents themselves can possess photocatalytic activity in the absence of any metals. For example, organic nanocomposite based on paddy straw (PS) incorporated with CS and crosslinked with sodium TPP [143] was used for the photocatalytic adsorption of dyes (rhodamine B (RhB) and MG) and allowed for the removal 96.04% of RhB (10 mg/L) and 98.15% of MG (10 mg/L) for 1 h at 3.0 g/L of PS–CS, pH = 6.2 and 60 °C.

Khan et al. [144] prepared a polyurethane sponge (PUS) covered with CS. CS was deposited from acidic solution; no gelating agents were used. CS–PUS samples were treated with aqueous solutions of metal (Ni, Cu, Co, Ag) salts and reduced with NaBH₄. Resulting catalytic materials were tested in a model reaction of 4-NP hydrogenation by NaBH₄. It was found that Cu/CS–PUS outperformed among the other Me/CS–PUS: complete conversion of 4-NP was found for 5 min (the reaction rate constant was 0.7923 min^{-1}). Moreover, Cu/CS–PUS catalyst was used for the reduction of different dyes (MO, AO and CR) and its high performance was observed for the CR.

An electrocatalytic reduction of 4-NA was studied using CS-stabilized Ag NPs on carbon paste [147]. Ag NPs with a mean diameter of about 51 nm were formed by the reduction of silver nitrate with NaBH₄ in the presence of CS as a stabilizing agent. To build a voltammetric sensor (CS–Ag NPs/CPE), a carbon paste electrode (CPE) was immersed in aliquid suspension of CS–Ag NPs. The reduction overpotential of 4-NA shifted from –752.26 mV at CPE to –304 mV in CS–Ag NPs/CPE, and then showed a surface-controlled process with acatalytic rate constant of $0.125 \times 10^{-3} \text{ L}/(\text{mol} \times \text{s})$.

As previously mentioned, CS-containing materials are usually shaped using alkaline solutions and different gelating agents. This process requires a large amount of solvents, acids and alkalines. In the work of Sun et al. [150], CS powder and thermoplastic polyurethane (TPU) were mixed to form a membrane using selective laser sintering. This method has the advantages of simple operation, fast membrane formation and low preparation cost. The shape of the hybrid CS–TPU membrane can be flexibly designed while varying the conditions of sintering. It was shown that the sintered CS–TPU composite

membrane has superhydrophilic properties and can effectively adsorb Cu(II) and Pb(II) in water with maximum adsorption capacities of 19.6 mg/g and 30.4 mg/g, respectively. Pd(II) could also be adsorbed by the membrane to form palladium-loaded composite materials, which could be used as a catalyst for hydrogenation of 4-NP by sodium borohydride, allowing 96% conversion in 20 min.

Zhu et al. [152] synthesized the series of CS-based composite hydrogels doped with Pd NPs by adding graphene oxide (GO), carbon nanotubes (CNTs) and layered double hydroxaltes (LDHs) to CS hydrogel with GA as a crosslinking agent. Pd NPs with sizes of about 2–5 nm were formed in situ during the gelation process. It is noteworthy that palladium precursor (Na_2PdCl_4) was added at the CS solution preparation stage, while GA and other components (GO, CNTs or LDHs) were added later. Obtained catalysts were tested in a modelled reaction of 4-NP hydrogenation and exhibited promising catalytic activity. Highest reaction rate constant (0.218 min^{-1}) was found for CS–CNT–PdNPs.

The green synthesis of magnetically separable hybrid metal nanobiomaterials (Fe_3O_4 @CS–MeNPs; Me = Au and Pd) was reported [161]. The magnetic NPs (about 35 nm in diameter) were synthesized using the biomineralization process and coated with CS, followed by binding and reduction of metal ions. CS-encapsulated magnetic NPs (Fe_3O_4 @CS) were prepared using the water-in-oil emulsion method with span-80 as surfactant. Samples of Fe_3O_4 @CS decorated with Au and Pd NPs were synthesized using a microwave-mediated in situ reduction of Au(III) and Pd(II) ions (Figure 21).

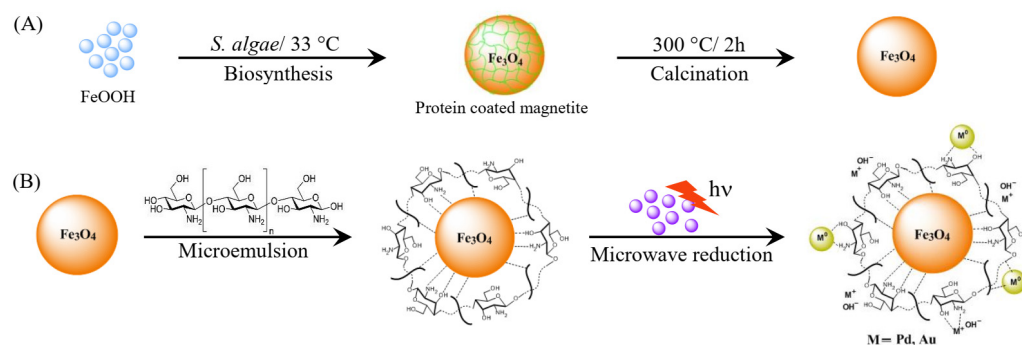


Figure 21. Schematic representation of synthesis of biogenic magnetic NPs (A), encapsulation of magnetic NPs with CS and formation of metal NPs on CS-encapsulated magnetic NPs (B) to form hybrid metal nanobiomaterial (Fe_3O_4 @CS–MeNPs). Reprinted with permission from authors of [161], American Chemical Society, 2017.

The as-synthesized hybrid nanobiomaterials were tested for several model reactions such as photocatalytic reduction of dye (MB), hydrogenation of 4-NP and Suzuki cross-coupling in aqueous solution. At ambient temperature, Fe_3O_4 @CS–AuNPs (5.6 wt.% Au) and Fe_3O_4 @CS–PdNPs (2.6 wt.% Pd) took only 1 min under UV light to complete the reduction of MB with k_{app} of 4.0 min^{-1} and 5.0 min^{-1} . The 4-NP hydrogenation reaction was completed within 3–14 min depending on the MeNPs on the hybrid nano-biomaterial and reaction temperature. The catalytic behavior of Fe_3O_4 @CS–PdNPs in the C–C bond formation (Suzuki reaction) of phenylboronic acid (1.5 mmol) and *p*-iodoacetophenone (1 mmol) in aqueous solution was explored under various conditions. It was found that, when the Suzuki reaction was carried out in the normal laboratory condition at 50°C , 98% yield (TON = 50,256 and TOF = 16,752) was found after 3 h. In addition, the hybrid nanobiomaterials demonstrated excellent recyclability and reusability without significant loss of catalytic activities [161].

Khan et al. [149] reported the formation of Ag NPs in CS hydrogels. Briefly, CS solutions with the addition of crosslinking agent (formaldehyde) were poured into plastic tubes and kept for 24 h, and then the obtained hydrogels were washed with NaOH solution and water. CS hydrogels were immersed in an aqueous solution of AgNO_3 (10 mM) for 3 days at room temperature, allowing for the formation of Ag NPs. No reducing agents

were used. Synthesized Ag–CS samples were tested in a hydrogenation of 2-NP and AO using NaBH_4 as a reducing agent. Both reactions proceeded at high rate constants of 0.260 min^{-1} and 0.253 min^{-1} for 2-NP and AO, respectively.

Ultrafine nitrogen-doped TiO_2 NPs were formed on the surface of hollow quaternized CS by electrostatic self-assembly, providing a unique core–shell structure (QCS@N-TiO_2) [148]. Then, Ag NPs were deposited on the surface of QCS@N-TiO_2 via a simple photodeposition process. Thus, QCS@Ag-TiO_2 multifunctional catalytic materials were fabricated (Figure 22).

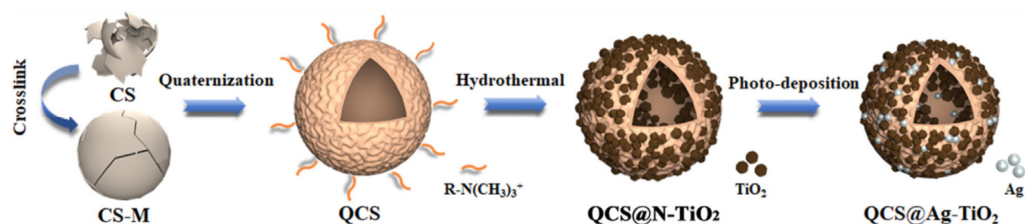


Figure 22. Scheme of QCS@Ag-TiO_2 synthesis. Reproduced with permission from authors of [148], Elsevier, 2020.

QCS@Ag-TiO_2 allowed for the catalytic degradation of SDBS under visible light: 96.4% of SDBS conversion was achieved within 180 min. The excellent degradation characteristic was ascribed to a large number of active sites and adsorption sites on the surface of the quaternized CS, effective separation of electron–holes in N-TiO_2 and surface plasmon resonance and photothermal effect of Ag NPs [148].

As previously mentioned, CS-based materials can be used not only for stabilization of catalytic metal NPs, but also for metal ions.

A CS-based, magnetically recoverable and recyclable catalyst, MCS-GT@Co(II) , was developed for the highly efficient and green synthesis of 2,4,5-trisubstituted and 1,2,4,5-tetrasubstituted imidazoles [137]. The catalyst was prepared by immobilization of CS onto Fe_3O_4 using GA as crosslinker followed by Co(II) ion immobilization (see Figure 23). Fe_3O_4 NPs were prepared using the coprecipitation method and added to CS acid solution. The resulting mixture was crosslinked with GA (designated as MCS-GT NPs). Resulting MCS-GT NPs (with sizes of about 20 nm) were treated with cobalt acetate solution (MCS-GT@Co(II) NPs).

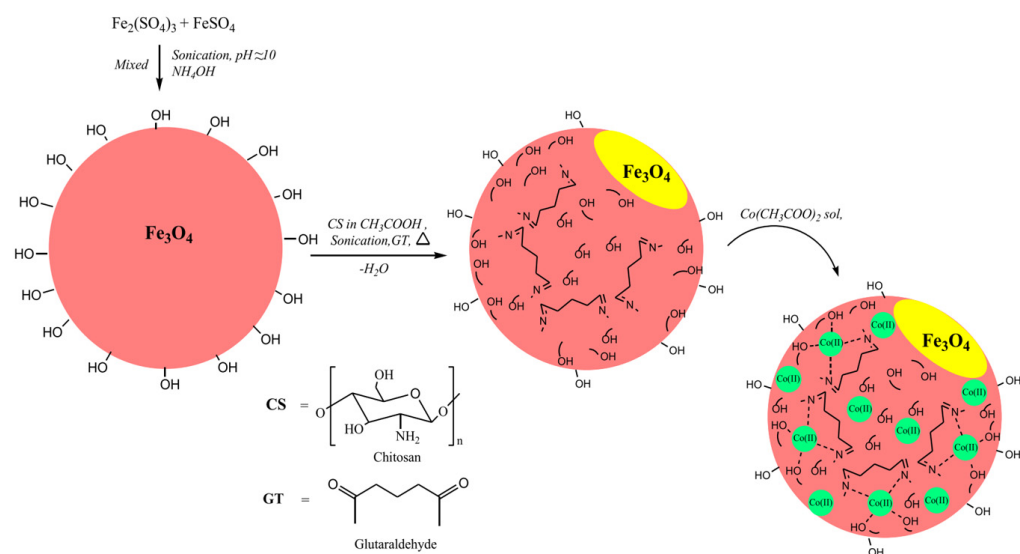


Figure 23. Stepwise synthesis of MCS-GT@Co(II) magnetic NPs. Reproduced with permission from authors of [137], Wiley, 2018.

MCS–GT@Co(II) NPs were tested in one-pot three- and four-component condensation reactions to synthesize 2,4,5-trisubstituted and 1,2,4,5-tetrasubstituted imidazoles of biological and pharmaceutical importance. The MCS–GT@Co(II) catalyst allowed high yields (in most cases 90–99%) and purity of products, short reaction time, atom economy, easy and environmentally benign work-up procedure, clean and mild reaction conditions, use of various substituted aldehydes and amines, easy separation of catalyst by applying an external magnet, recyclability and reusability of the catalyst and no use of column chromatography for the purification of products [137].

Photolabile heterogeneous Cu(II) precatalyst supported by CS powder (CuBP–CS) was developed and tested in copper-catalyzed azide–alkyne cycloaddition [138]. The benzophenone (BP) photosensitizer was employed in catalytic amount, i.e., 10 mol% with respect to the Cu(II) ions, to effectively promote the Cu(II) to Cu(I) photoreduction process (Figure 24). This allowed for the effective synthesis of a range of triazoles, in particular those bearing sugar moieties, under light illumination and sodium ascorbate-free conditions.

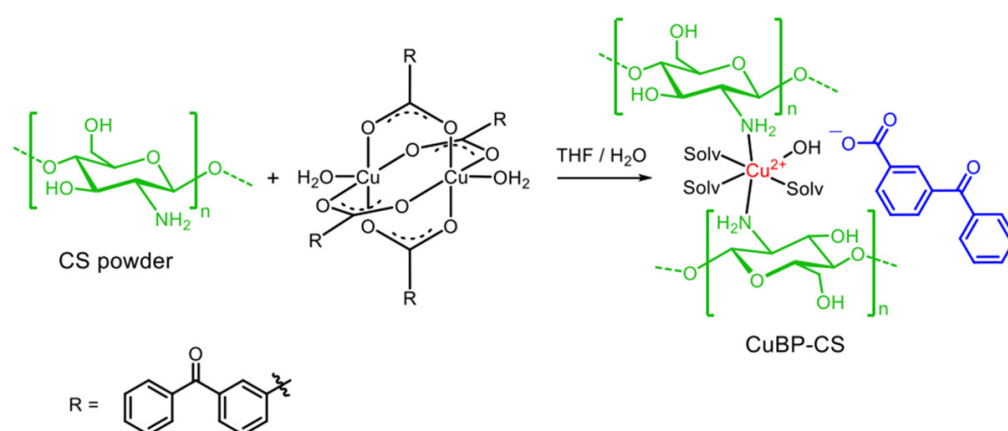


Figure 24. Synthesis of CuBP–CS. Reproduced with permission from authors of [138], Wiley, 2018.

The catalytic activity of CuBP–CS was shown to be effectively switched on when illuminated with a low intensity UVA-emitting lamp. The catalyst could be recovered and reused several times with no appreciable decrease in catalytic activity. As a practical application of the procedure, the anticonvulsant drug rufinamide was isolated at 82% yield on a 10 mmol-scale synthesis [138].

CS-supported copper catalysts were synthesized [139] using a simple procedure: different Cu(II) and Cu(I) salts or Cu powders were added to a CS suspension. Series of CS@copper catalysts were obtained and tested in the synthesis of alkyl/aryl-mixed phosphates by conversion of P–N bonds into P–O bonds through a nucleophilic substitution reaction under aerobic conditions. The deaminated esterification was conducted under relatively mild conditions, generating nitrogen gas as a byproduct. The developed methodology enabled the preparation of mixed phosphates in moderate-to-excellent yields (up to 94%). However, the decreased copper content of the recovered catalyst indicated that active species were leaching during the reaction or workup procedure and might have been responsible for the loss of activity.

CS-supported CuSO_4 (CTS– CuSO_4) and CS-supported Cu NP/ Cu_2O microcrystal (CuNP/ Cu_2OMCs)-heterogeneous catalysts were developed [140] using CS powder without any additional shaping or crosslinking.

Different crystal structures of Cu_2OMCs were obtained in combination with Cu NPs through the chemical reduction of CuSO_4 using ascorbic acid as a reducing agent [140]. These composites were applied for the synthesis of bis(indolyl)methanes under mild solvent-free conditions (80 °C). Depending on the aldehyde, in most cases, a yield of the target products from 15% up to 100% was achieved using the catalyst with the highest CuSO_4 content (78.2 wt.% CTS– CuSO_4). It was also found that CTS–CuNP/ Cu_2OMC catalyst was an effective alternative to CTS– CuSO_4 in the synthesis of bis(indolyl)methanes

when aliphatic aldehydes were used. Reusability of the obtained catalysts was up to five catalysis/recovery cycles.

Cu-containing, CS-based catalysts can be also used for the oxidation of sulfides into sulfoxides, which are versatile synthetic intermediates [145,146]. Naghipour and Fakhri [145,146] reported the synthesis of magnetically separable catalysts via anchoring of a CS–Schiff's base complex (CS was functionalized with 5-bromosalicylaldehyde [145] or picolinaldehyde [146]) to the surface of Fe_3O_4 NPs (with an average size of 20 nm) with subsequent metalation with Cu(II) acetate. Fe_3O_4 –CS–Schiff's base Cu complexes catalyzed the oxidation of sulfides to sulfoxides with 100% selectivity in all cases under green reaction conditions and excellent yields. Moreover, easy recovery and reusability up to four cycles without noticeable loss of catalytic activity was found.

One of the interesting directions is the synthesis of aerogels from CS for different applications (drug delivery, biomedicine, environmental protection (purification of gases and liquids), thermal insulation and catalysis) [153,154,162–164]. Aerogels can be obtained from different CS-containing composites consisting of other natural/synthetic polymers and inorganic materials (metals, oxides, GO, etc.). The procedure of CS-based aerogel synthesis includes several steps: (i) preparation of CS solution; (ii) gelation (a large variety of gelating agents can be used); (iii) pretreatments before drying (solvent exchange or chemical modification); (iv) drying, resulting in the formation of a porous solid (supercritical drying or freeze drying); (v) post-drying treatment (second drying step) [164].

Takeshita et al. [164] classified the catalytic activity of CS aerogels in three categories: (i) direct organocatalysis of NH_2 as a Brønsted base and/or hydrogen bond; (ii) use of NH_2 as a support of organocatalysts through chemical modifications; and (iii) supports of inorganic materials, such as metal NPs and oxides.

Le Goff et al. [153] synthesized secondary amino CS derivatives by reacting CS aerogels with arylaldehydes under heterogeneous conditions. CS aerogels were prepared in the form of beads. CS beads were obtained via common dripping of CS acidic solution into sodium hydroxide solution and then dehydrated using successive immersion in a series of water–ethanol baths of increasing alcohol concentration. Finally, CS beads were dried under supercritical CO_2 conditions to provide aerogel material. CS aerogels were treated with several aldehydes to reach a high degree of substitution during the imineformation process. Then, the reduction of CS–Schiff's base derivatives succeeded using NaBH_3CN , and a high reduction ratio (>80%) was achieved (Figure 25). Textural analyses showed that successive heterogeneous chemical modifications to CS aerogels do not lead to a collapse of the structure and aerogels keep a surface of about $250 \text{ m}^2/\text{g}$ with a distribution of mesopores centered at 23 nm.

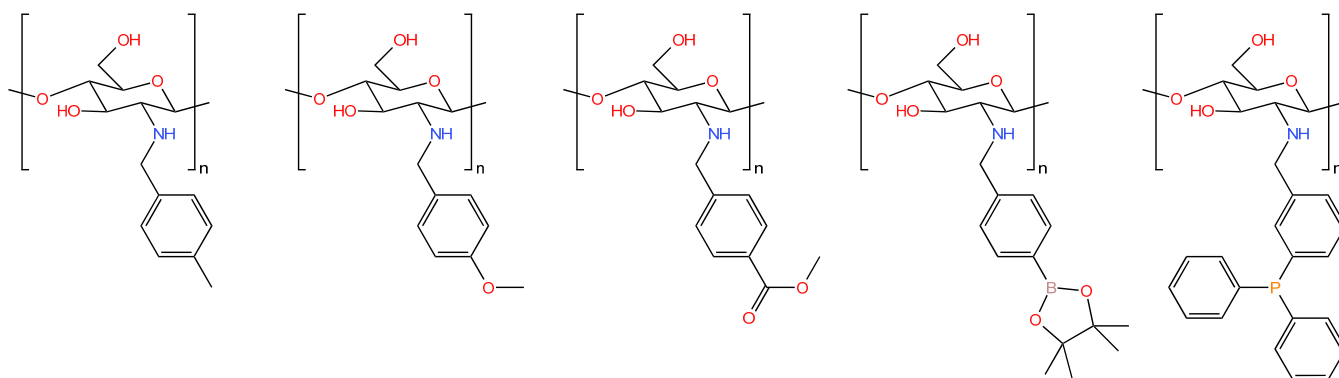


Figure 25. Types of modified CS aerogels [153].

A phosphine-based CS aerogel was used as a phosphorylated ligand in the Pd-catalyzed allylic substitution—one of the most important reactions for carbon–carbon and carbon–heteroatom bond formation. The allylation reaction between (*E*)-1,3-diphenyl-3-acetoxyprop-1-ene and dimethyl malonate using *N,O*-bis(trimethylsilyl)acetamide as

base was selected as a model reaction. The reaction was completed after 24 h at 20 °C, affording the expected allylated malonate in good 76% yield [153].

One of the recent studies on CS-based metallic aerogels was carried out by Shen et al. [154], who applied an unusual approach for the fabrication of metallic aerogels—pyrolysis of xerogels derived from CS–metal (M = Fe, Co, Ni) hydrogels. Metallic aerogels were synthesized using the following steps: (i) CS–metal complexes were formed by the addition of metal salts to acidic CS solutions; (ii) NaOH was added to the resulting mixtures under vigorous stirring that resulted in hydrogel formation; (iii) the metallic hydrogels were freeze-dried; (iv) the dried metallic hydrogels were calcined at a defined temperature (800, 1200 or 1300 °C) for 2 h. Thus, metal NPs were formed and encapsulated in graphite shells. It was shown that the resulting metallic aerogels are highly stable, efficient and selective nanocatalysts towards the hydrogenation of different nitroarenes to amines at low catalyst loading (1.2 mol.%). Using Fe@ΓC-1300, more than 99% yield of target products was achieved in THF–water mixture (1:1) at 130 °C and 5 MPa for 48 h. This catalyst could be reused for more than 30 runs without obvious loss of activity and selectivity. These distinguished performances were attributed to the graphitic shells formed during pyrolysis, which hampered the possible aggregation of metal NPs, prevented metal leaching and increased their stability.

Functionalization of CS with phosphine groups is a promising approach for the development of Pd-containing catalysts intended for cross-coupling reactions, which proceed via a homogeneous mechanism. For example, de Souza et al. [155] developed CS functionalized with diphenylphosphine (PPh₂) and crosslinked with GA (Figure 26). CS–PPh₂ was used to immobilize Pd NPs with a size of about 4 nm, active in Heck cross-coupling (yield of reaction products 80–89%). The CS–PPh₂–Pd catalyst could be recycled up to three times with negligible Pd-leaching. Moreover, Pd-loading was decreased down to 0.1 mol.% with no significant yield losses.

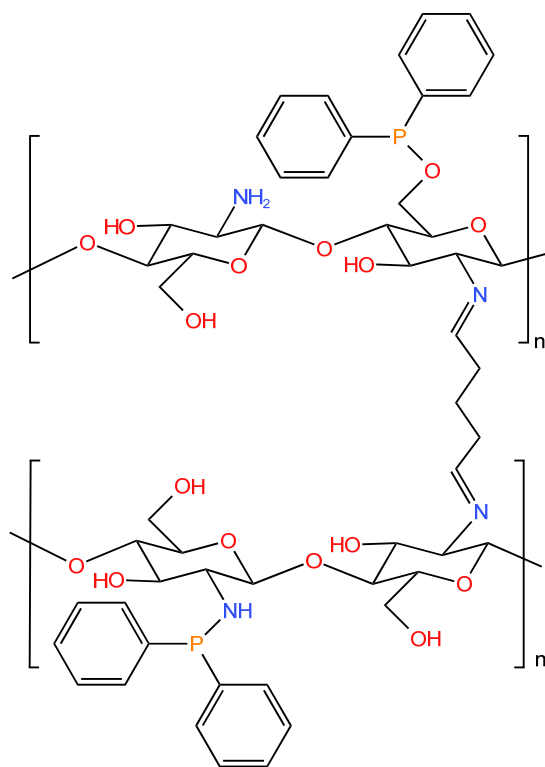


Figure 26. Scheme of CS–PPh₂ (based on Ref. [155]).

Different catalytically active oxides (ZnO, MgO, Cu₂O, CuO, Fe₃O₄) can be stabilized with CS [133,158–160]. For example, Bashal et al. [133] synthesized CS–ZnO composite films containing ZnO NPs (30–32 nm) with a variation in ZnO content (5–25 wt.%). It was

found that CS–ZnO nanocomposite film (20 wt.%) could be a viable, effective, recyclable (for more than three uses) and heterogeneous base catalyst in the synthesis of different thiazoles with high yields (up to 93%). Catalytic systems based on CS functionalized with IC and Cu₂O or CuO NPs were obtained [158] for the click reaction and CO₂ fixation with high efficiency. Riyadh et al. [159] prepared a composite CS–MgO film serving as an efficient and ecofriendly basic catalyst, allowing for the synthesis of two novel series of 5-arylo-2-hydrazonothiazoles and 2-hydrazono [1,3,4] thiadiazoles, incorporating a sulfonamide group, under microwave irradiation. Yields of target products exceeded 80% depending on started compounds. The average size of the MgO particles was found to be approximately 6–11 nm for 10 wt.% and it was found that the particles' size slightly decreased with increasing magnesia content. The CS–MgO nanocatalyst could be easily recovered and reused many times without loss in its catalytic activity. Saba et al. [160] synthesized Schiff's base of Fe₃O₄@CS with 4,4'-diselenobisbenzaldehyde (Fe₃O₄@CSSe) composite and used it as a catalyst for the oxidation of sulfides in the presence of H₂O₂ at room temperature. The yield of sulfoxides was found to depend on the amount of H₂O₂, catalyst loading and solvent nature. For example, oxidation of dibutyl sulfide was observed in asolvent-free condition with a yield of 94% in the presence of 20 mg Fe₃O₄@CSSe and 0.5 mL H₂O₂.

Bimetallic NPs stabilized with CS are rarely reported. One of the recent studies was reported by Puthukkara P et al. [165], who synthesized CS-stabilized bimetallic iron/nickel (CS-Fe/Ni) NPs using a chemical reduction of metal precursors with NaBH₄ in CS solution. No crosslinking agents were used. The average size of the NPs was below 15 nm. CS-Fe/Ni was used for the removal of dyes (MG, MB) at various NP dosages, contact times and the initial concentrations of the dyes. At the chosen conditions (50 mg/L of dye solution (40 mL) and 2 g/L of the adsorbent; contact time 180 min), CS-Fe/Ni NPs revealed high removal efficiency: 99% and 88% of dye removal for cationic dye (MG) and anionic dye (MB), respectively.

Recently, Bumagin et al. [166] reported the synthesis of polymetallic ferromagnetic Pd–Fe–Co–Ni–CS composites for the Heck reaction in aqueous media in the presence of an ionic liquid. Synthesis of the composite was carried out by mechanochemical activation by grinding CS powder with corresponding metal salts with subsequent treatment with reducing agent (NaBH₄). Additionally, the resulting composite was coated with palladium (Pd–Fe–Co–Ni–CS@Pd). The obtained catalysts were tested in Heck cross-coupling between different aryl bromides and iodides, allowing for a high yield of reaction products (93–98%) in the presence of 0.5 mol.% of Pd. Thus, the following intermediate conclusions can be pointed out:

- (i) The ability of CS to effectively adsorb both organic and inorganic compounds can be used for the development of catalytic systems, in which the inorganic part, entrapped by CS, is in catalytically active phase while organic adsorbate is the subject of catalytic transformation;
- (ii) In spite of vast experience in the field of adsorbent development, researchers working in catalysis seem to rarely use all the accessible achievements. For example, crosslinking agents are typically not used, as well as certain shaping at macro-level of the resulting catalytic material that could be useful in continuously operating reactors. Adsorption of metal cations was found to proceed more effectively while using CS grafted with different functional groups (see Section 3); hence, it is surprising that in many reported studies devoted to the use of metal ions as catalysts, native CS without any modifications was applied. Thus, there is room for further improvement;
- (iii) Magnetically separable catalysts obviously have the advantage of easy separation from the reaction mixture, but these catalysts have a limitation—sensitivity to low pH, since CS itself cannot prevent the dissolution of magnetic NPs. Thus, CS crosslinking and coating of magnetic NPs with a protective shell (carbonaceous or oxide), resistant to low pH, is a promising approach.

4.2. Chitosan-Containing Composite Biocatalysts

CS is widely used for the immobilization of enzymes as a part of support for covalent binding or encapsulation [167–172]. The ability of CS to shape beads/microspheres, microcapsules, fibers, membranes, coatings, sponges and gels has expanded its applicability as a support for the immobilization of a wide range of biomolecules and enzymes [173]. However, despite the advantages of using CS as a support for enzyme immobilization, CS beads and fibers are quite fragile and mechanically unstable [174,175].

As previously mentioned, the mechanical properties of CS-based materials can be increased via covalent crosslinking (i.e., with GA or ECH). However, the cytotoxicity of the aforementioned crosslinking agents may hinder the use of CS hydrogels for pharmaceutical and biomedical applications. Thus, in contrast to CS-based adsorbents and metal-containing catalysts, toxic GA is replaced with the safer TPP at the crosslinking stage. For example, Ji et al. [176] used CM prepared by dripping of CS acid solution in the solution of sodium TPP (crosslinking agent) for further co-immobilization of 7 α - and 7 β hydroxysteroid dehydrogenases (HSDH). It is noteworthy that the immobilization of these enzymes was carried out by preliminary activation of CM with GA that is common for enzyme deposition on heterogeneous supports. CM-immobilized HSDHs were used for the conversion of taurochenodeoxycholic acid (a component of chicken bile). The catalytic reaction reached equilibrium within 4 h. The yield of reaction product (tauroursodeoxycholic acid) was about 62% after equilibrium and the content of tauroursodeoxycholic acid in the reaction product was as high as 33.16% [176]. A similar procedure was applied by Singh et al. [177] for the immobilization of extracellular inulinase from *Kluyveromyces marxianus* on CS beads. Under the optimized conditions, a maximum yield 65.5% of immobilized inulinase was obtained. The maximum hydrolysis of inulin—84.5%—was observed at 125 rpm after 4 h using an immobilized enzyme. The developed immobilized biocatalyst was successfully used for the hydrolysis of inulin for 14 batches.

An unusual approach was proposed by Manan et al. [178], who synthesized a hybrid support consisting of CS and chitin nanowhiskers (CNWs). CNWs were introduced into CS solution in 2% acetic acid containing tannic acid as a crosslinking agent, and then the obtained mixture was dripped into NaOH solution. The resulting CS/CNWs beads were treated with 1-ethyl-3-[3-dimethylaminopropyl]carbodiimide (EDAC) hydrochloride and N-hydroxysuccinimide (NHS) for further immobilization of *Rhizomucor miehei* lipase (LIP). The LIP loading of 2 mg/g was achieved, corresponding to the specific and residual activity of 537 U/g and 137%, respectively. Immobilized LIP was used for synthesis of eugenyl benzoate with the highest yield of 56.3% achieved for 5 h using 3 mg/mL of LIP-CS/CNWs with a molar ratio of eugenol:benzoic acid of 3:1.

De Freitas et al. [179] immobilized β -galactosidase produced by the yeast *Kluyveromyces lactis* NRRL Y1564 and delivered an enzymatic activity of 4418.37 U/g_{cell} after 12 h of processing on the CS particles without any crosslinker (CS was dissolved in 2% acetic acid, and then coagulating agent (KOH) was added during stirring). After coagulation, CS particles were activated with GA, ECH or glycidol. GA was chosen as an optimal activating agent. The biocatalyst obtained by immobilization in CS-GA allowed for the effective hydrolyzation lactose of milk (42.8% of conversion) and produced lactulose (17.32 g/L).

Okura et al. [180] prepared GA-activated CS hydrogel (an acidic solution of CS was dripped into NaOH solution), which was further treated with glycine solution (CS-GA-Gly). The obtained CS-GA-Gly was used for the immobilization of the LIP from *Thermomyces lanuginosus* (TLL). CS-GA-Gly-TLL was ~four times more active than CS-GA-TLL in both olive oil emulsion hydrolysis and alkyl palmitate synthesis via esterification. Isoamyl palmitate synthesis in isooctane at 50 °C using CS-GA-Gly-TLL provided a maximum conversion of 85% after 90 min of reaction. After nine consecutive runs, the biocatalyst retained 34% of its initial activity.

Aggerwal et al. [181] immobilized trypsin on the surface of GA-activated ZnO/CS nanocomposite through covalent attachment via Schiffbase linkages. GA-ZnO/CS nanocomposite was synthesized using a relatively simple procedure including the following steps:

(i) synthesis of ZnO NPs; (ii) addition of ZnO NPs to CS solution; (iii) addition of NaOH solution to suspension of ZnO NPs to form ZnO/CS nanocomposite; (iv) activation of ZnO/CS with GA. Optimal immobilization conditions (incubation time (16 h), enzyme concentration (1.8 mg/mL) and pH (7.8)) were investigated to obtain the maximum activity of the immobilized trypsin. The immobilized trypsin exhibited optimum catalytic activity at pH 8.5 and 60 °C. Immobilized trypsin preserved 67% of initial activity at 50 °C during 2 h of incubation and sustained nearly 50% of catalytic activity until the 9th repeated cycle of utilization. Moreover, the immobilized trypsin retained 50% of its enzymatic activity after 90 days of storage at 4 °C.

Aman et al. [182] studied the immobilization of dextranucrase produced by an indigenously isolated strain of *Leuconostoc mesenteroides* AA1 on CS beads, which were crosslinked and activated with GA. Immobilized dextranucrase exhibited higher catalytic performance in a broader range of pH than the soluble form. The immobilized version worked better at lower pH values of 4.0 and 4.5 and exhibited approximately 75.0% and 82.0% of relative activity compared to that of the soluble form, respectively.

Bôa Morte et al. [183] developed a magnetically separable biocatalyst based on amano LIP immobilized on Fe₃O₄ NPs (nanomagnetite (nM)) either modified with 3-aminopropyltriethoxysilane (APTES) or stabilized with oleic acid (OA) (Figure 27) and then modified with CS (nM-OA-CS). For the modification of nM-OA with CS, nM-OA particles were dispersed in acidic solution of CS and then dripped in NaOH solution. The nM-APTES and nM-OA samples disclosed crystal sizes of 8.07 and 8.69 nm, respectively. The nM-OA-CS displayed an average particles size of 918.6 nm. Lip was immobilized by covalent binding with GA on both nM-APTES-GA and nM-OA-CS-GA supports with different surface/volume ratios. The catalytic activity of nM-APTES-GA-LIP (85%) was higher than that of nM-OA-CS-GA-LIP (46%), which reflected the correlation between enzyme loading efficiency on the magnetic nanosupports and their relative activity, essential to potential use in a magnetically stabilized fluidized bed reactor.

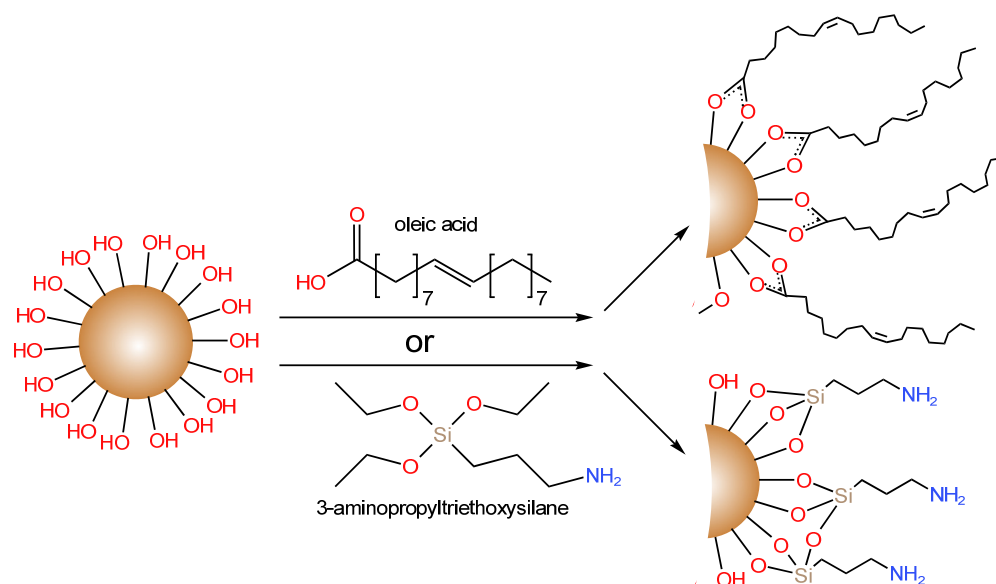


Figure 27. Synthesis of nM-OA or nM-APTES NPs (based on Ref. [183]).

A two-step approach was proposed by Wang et al. [184] for the synthesis of a novel type of bio-friendly composite membrane of poly(methyl acrylate-co-acrylic acid) and CS (PMA-co-PAA@CS), which served as a support for the immobilization of horseradish peroxidases (HRP). A composite membrane was obtained by the following steps:

- (i) The PMA-co-PAA membrane was obtained using the electrospinning method;
- (ii) Carboxyl groups of PMA-co-PAA were activated with EDAC/NHS;
- (iii) The activated membrane was immersed in CS solution in 0.2 M acetic acid.

Then, PMA-co-PAA@CS was treated with GA and HRP was immobilized.

Immobilized HRP (about 110 mg/g) revealed noticeably higher thermal (25–60 °C), pH (4–10) and storage stabilities compared to native HRP. Moreover, the PMA-co-PAA@CS–HRP was demonstrated to be an active and recyclable biocatalyst for the catalytic oxidation of 4-NP over 10 cycles. The activity of PMA-co-PAA@CS–HRP reached maximum at a concentration of 4-NP of 100 mg/L, allowing 86% removal efficiency. The improved performance of the immobilized HRP was attributed to CS, which provided not only a hydrophilic environment but also multiple binding sites for the HRP [184].

Costa-Silva et al. immobilized LIP of *Cercospora kikuchii* [185] on CS beads, which were prepared using a generally accepted method and were activated with sodium metaperiodate, ECH or GA. Among the chosen activating agents, GA allowed the best immobilized enzyme for all the analyzed parameters, mainly LIP activity retention, which represented an improvement of 46.5% on the free LIP. It is noteworthy that CS beads underwent fluidized bed drying that provided excellent features (low moisture content (3.84% *w/w*) and water activity (~0.10)) for LIP application in organic media for the esterification/transesterification process. The obtained immobilized LIP system was used [185] to catalyze the synthesis of butyl butyrate with high yield (98.96%).

A further improvement of the biocatalyst preparation procedure was the application of the magnetic separation principle and spray drying method [186]. Fe₃O₄–CS–LIP microparticles were prepared by mixing magnetic NPs (Fe₃O₄/CS ratio was 1/4 *w/w*) and enzyme solution (LIP of *Candida rugosa*) with CS solution in acetic acid. Optionally, activating agents (e.g., GA) were added. The resulting mixture was either dripped to the solution of sodium TPP or, alternatively, underwent spray drying. It was found that all the immobilized derivatives retained between 73.6% and 84.6% of initial enzyme activity in the reaction of isoamyl caprylate synthesis. Long-term storage (6 months) at 5 °C revealed that the immobilized derivatives retained more than 70% of their activity. For comparison, free LIP retained only 18.3% of its activity. The immobilization process also made LIP reuse possible: composite materials retained between 40% and about 60% of their initial activity after ten reuse cycles.

Apriceno et al. studied the immobilization of laccase (LAC) from *Trametes versicolor* on CS-based supports [187,188]. CS beads were prepared and crosslinked with GA or ECH and used for LAC immobilization (CS–GA–LAC or CS–ECH–LAC). Moreover, for the immobilization of LAC, for the first time, the direct conjugation of the enzyme was applied through the interaction between the carbonyl group, formed after the periodate oxidation of the LAC carbohydrate portion, and the amino groups of CS (CS–LAC). All the three methods were reliable for the immobilization of LAC. However, the CS–LAC system revealed higher storage stability: it retained initial activity for 30 days in the oxidation reaction of 2,2'-azino-bis-(3-ethyl-benzothiazoline-6-sulfonic acid) (ABTS) to its cation radical ABTS⁺. On the contrary, CS–GA–LAC and CS–ECH–LAC showed a decrease in activity of 50 and 40%, respectively [187]. Another catalytic system used for LAC immobilization was based on manganese iron oxide (MnFe₂O₄) magnetic NPs coated with CS using two methods: (i) after the formation of magnetic NPs; (ii) during the synthesis of magnetic NPs (*in situ*). Both methods, in general, followed the well-known procedures described in previous sections of this review. LAC was covalently bonded to the resulting composites with GA. It was found that both CS-based supports possessed more specific activity against ABTS than the naked magnetic NPs, which exhibited not-Fenton-type intrinsic activity, attributed to the Fe³⁺ surface ions. The potential oxidant activity of the developed biocatalytic systems was tested for the degradation of diclofenac at room temperature in the presence of ABTS as a mediator. It was shown that in contrast to the free LAC, the enzyme immobilized on magnetic supports possessed both good resistance to temperature denaturation and storage stability for 30 days. The most promising system, based on the *in situ*-formed magnetic NPs covered with CS, showed diclofenac removal efficiency of 78%, higher than that of the free enzyme (70%). Almost no decrease in catalytic

activity was found for this system due to the active conformation assumed by the covalently immobilized enzyme and to the contribution to the activity of the CS-coated support [188].

A magnetically separable, CS-based material was applied for immobilization of LIP from *Candida antarctica* by Ariffin et al. [189]. For the synthesis of composite support, maghemite NPs (2–3 nm) were placed into CS solution in 1.5% acetic acid. Then, the excess CS was removed by washing the solution with deionized water and separated with an external magnet. The resulting material was dispersed into a solution of sodium TPP to form a maghemite/CS/TPP composite. For the immobilization of LIP, GA was applied. Optimization of the conditions for LIP immobilization allowed for the selection of the process variables: 9 h incubation time, 55 °C incubation temperature and 12% (v/v) GA content. The optimized immobilized LIP activity was 1.8 U for the *p*-nitrophenyl palmitate hydrolysis reaction.

Carli et al. [190] immobilized β -glucosidase from *Humicola insolens* (Bglhi) and endoglucanase from *Scytalidium thermophilum* (Egst) on Fe₃O₄ NPs derivatized with CS/GA/N-(5-amino-1-carboxy-pentyl) iminodiacetic acid (AB-NTA) and functionalized with NiCl₂ using the procedure developed by Carneiro et al. [191]. Briefly, CS solution in acetic acid was added to a suspension of Fe₃O₄ NPs and then CS-covered magnetic NPs were treated with crosslinking agent (GA). After removing the excess of GA, composite NPs were treated with AB-NTA and NiCl₂. Immobilization of Bglhi and Egst proceeded with the coordination of the imidazole group of a 6-histidine tag added to either the N-terminal (in the case of Bglhi) or C-terminal (in the case of Egst) of the protein with the Ni²⁺ coordinated with NTA group of NPs. The immobilization yields were about 20% for Bglhi and Egst with efficiencies of 132% and 115%, respectively. The two enzymes were also co-immobilized with a yield of about 49%. The optimal temperatures of the immobilized enzymes were 70 °C and 55 °C for Egst and Bglhi, respectively. The individually immobilized enzymes, when combined, showed a synergistic effect on the substrates tested (*p*-nitrophenyl- β -D-glucopyranoside for Bglhi and carboxymethylcellulose for Egst) and similar action when compared to the co-immobilized enzymes.

Core-shell CS beads (CSBs) and dried CS beads were synthesized by Charoenwongpaiboon et al. [192]. DBs were obtained using the typical procedure with slight modifications: CS was dissolved in a mixed acid solution containing acetic acid, lactic acid and citric acid and then dripped into NaOH solution, washed and dried at 60 °C. For CSB preparation, dried CS beads were soaked in a 0.5% acetic acid solution for 60 s and then neutralized by the addition of an equimolar amount of NaOH. CSBs were found to be an effective support for immobilization of recombinant inulosucrase (INU) from *Lactobacillus reuteri* 121 (GA was used as an activating agent). INU-CSBs were used for the synthesis of inulin-type fructooligosaccharide and revealed a higher optimum temperature (60 °C) compared to free INU (50 °C). Moreover, the pH stability and thermostability of the INU-CSBs improved significantly. After being reused for 12 cycles, the INU-CSBs retained about 45% of their initial activity. The inulin-type fructooligosaccharide was also continuously synthesized in a fixed-bed bioreactor for at least 30 h using INU-CSBs.

Crosslinked enzyme aggregates (CLEAs) are an alternative to carrier-bound enzymes, allowing for the immobilization of enzymes in their own macromolecular matrix. Several enzymes were crosslinked using a bifunctional reagent (e.g., GA) and exhibited 10 to 1000 times higher specific activity (IU/g_{catalyst}) than their carrier-bound enzyme counterparts [193]. Co-immobilization of different enzymes (combi-CLEAs) allows cascade reactions to be carried out; however, the small and variable particle size of combi-CLEAs (5–50 μ m) remains as a problem. Thus, Tavernini et al. [193] entrapped combi-CLEAs of β -D-glucosidase (β G) and α -L-arabinofuranosidase (ARA) in CS beads. The beads were obtained by dripping the mixture of solutions of combi-CLEAs and CS into sodium TPP solution. The resulting biocatalyst beads (average diameter 1.24 mm) retained full activity after 91 days of incubation under winemaking conditions, having specific activities of 0.91 and 0.88 IU/g β G and ARA, respectively. Such characteristics make them suitable for aroma enhancement in wines.

Some researchers proposed the use of genipin (GP) extracted from the fruits *Genipa americana* and *Gardenia jasminoides* Ellis as a crosslinking reagent (Figure 28) [194–197]. GP is 5000–10,000 times less cytotoxic than GA. Hyun et al. [198] suggested a new anodic catalyst consisting of CNTs, 4-nitrobenzoic acid (4-NBA), CS, GP and glucose oxidase (GOx) to promote glucose oxidation and the performance of an enzymatic biofuel cell. The new CNT/4-NBA/[CS/GOx/GP] catalyst contained a large amount of GOx (17.8 mg/mL) and produced a high anodic current ($331 \mu\text{A}/\text{cm}^2$ at 0.3 V vs. Ag/AgCl) with low onset potential (0.05 V vs. Ag/AgCl).

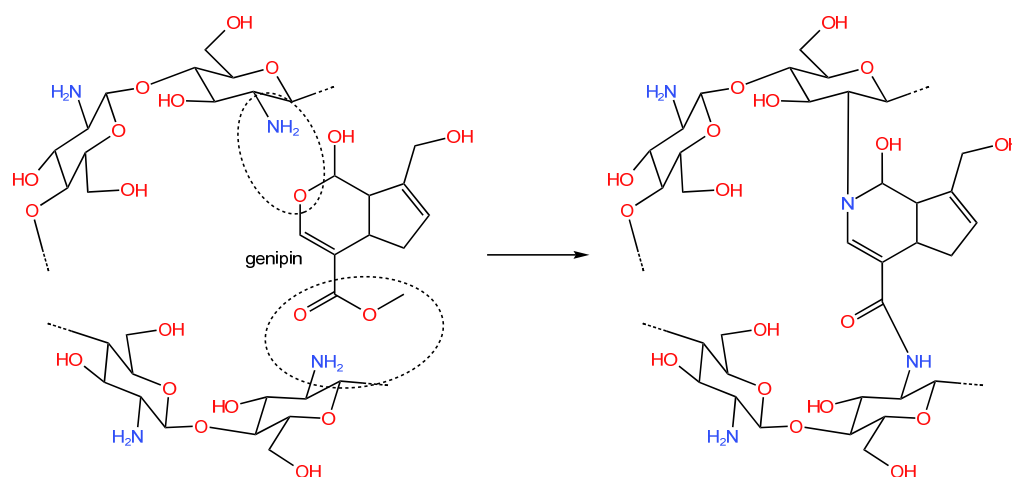


Figure 28. Crosslinking of CS with GP [198].

Ma et al. [199] used GP for the activation of CS beads prepared using typical dripping of CS acidic solution into NaOH solution and immobilization of LAC (Figure 29) from white rot fungus *Trametes pubescens* for removal of different dyes including CR, MB, etc. Maximum immobilization was obtained with 0.10% (*v/v*) GP and 4.0 U mL^{-1} of enzyme solution after activation and contact for 14 h and 6 h, respectively. Improved pH, thermal and storage stabilities of the immobilized LAC were obtained when compared with the free counterpart. The CS–LAC system exhibited a residual activity of >55% after 11 cycles, demonstrating better durability than the free LAC. The activity loss of CS–LAC after 30 days of storage at 4°C was 42.86%.

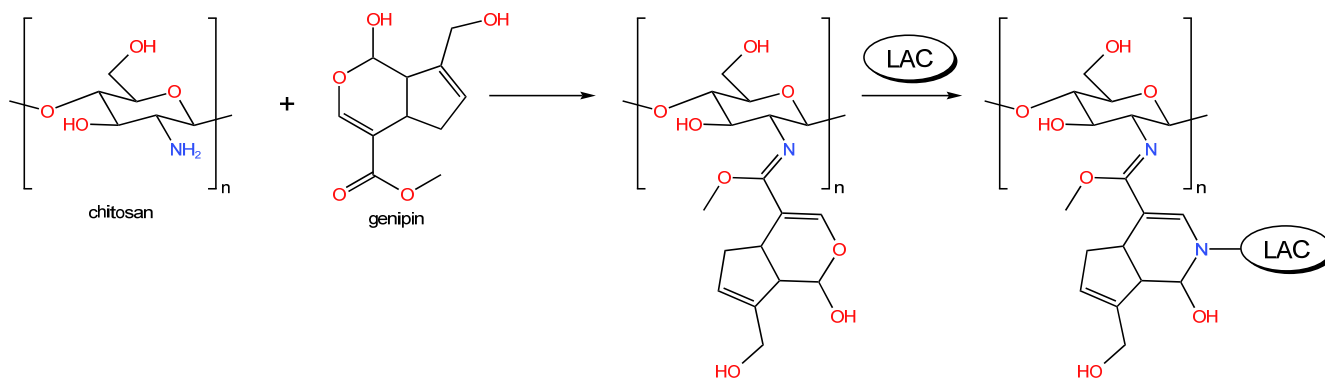


Figure 29. Activation of CS with GP and further immobilization of LAC [199].

Klein et al. [200] immobilized β -D-galactosidase from *Aspergillus oryzae* on CS particles, which were obtained by dissolution of CS in acidic medium with subsequent dripping into NaOH solution. After the enzyme adsorption, GP was applied as crosslinking agent. β -D-galactosidase–CS–GP particles were applied for the synthesis of galactooligosaccharides at a different variation of the initial lactose concentration, pH and temperature, and yields of 30% were achieved. β -D-galactosidase immobilized using GP had higher activity than

the biocatalyst prepared using GA. The immobilized enzyme maintained 100% of its initial activity after 25 batches of lactose hydrolysis.

The biotechnological route of utilizing *Rhizomucor miehei* LIP conjugated to a magnetite support was proposed by Rahman et al. [201] to produce pentyl valerate—a fuel additive. Magnetic Fe₃O₄ NPs were added to a suspension of chitin in CS solution in the presence of mineral oil and Tween 80. This mixture was treated with GA and then the pH was adjusted to 10 with NaOH solution. The resulting magnetically separable composite material was separated using an external magnetic field, washed and dried, and, after activation with EDAC/NHS, used for immobilization of LIP. The highest yield of pentyl valerate (96%) was reached under an optimized condition (50 °C, using a valeric acid/pentanol molar ratio of 1:2, with a LIP loading of 1.5 mg/mL and incubation time of 3 h). The immobilized LIP retained 90% activity after 40 days of storage and leached an initial 3.5% of the LIP, likely due to insufficient rinsing during preparation.

Saikia et al. [202] immobilized inulinase from *Aspergillus niger* on CS-coated magnetic NPs. Magnetite NPs were prepared using the co-precipitation method and placed into CS acidic solution. Further addition of NaOH solution allowed for the formation of CS gel with the entrapped Fe₃O₄ NPs. CS-based magnetic composite was activated with EDAC/NHS for immobilization of inulinase. Hydrolysis of 5% inulin using immobilized inulinase (2.5 U/mg) led to a fructose release of 35.8 g/L at pH 6.0 and a temperature of 60 °C in 3 h. Obtained fructose was further used to produce hydroxymethylfurfural over TiO₂ magnetic silica spheres. The immobilized inulinase was recycled with up to 10 cycles of inulin hydrolysis with 9.2 g/L of fructose released at the 10th cycle.

Medium-chain, oleic (18:1n-9) and medium-chain fatty acid structured lipids were produced by Akil et al. [203] via acidolysis reaction in solvent-free medium with capric (10:0) and lauric (12:0) free fatty acids and triolein or olive oil using *Yarrowia lipolytica* LIP as a biocatalyst. This LIP was immobilized by microencapsulation in CS–alginate beads, which were produced by ionotropic gelation of CS with SA. Prior to gelation, SA was solubilized in the enzyme extract. The resulting mixture was dripped into a solution of calcium chloride and CS, resulting in the formation of microcapsules. The immobilized LIP resulted in a similar incorporation efficiency for lauric acid with olive oil triacylglycerols and this reaction could be performed for five cycles without catalytic activity loss.

Co-immobilization of LAC and ABTS was carried out [204] for removal of 2,4-dichlorophenol, bisphenol A, indole and anthracene. LAC was immobilized on magnetic CS NPs modified with amino-functionalized ionic liquid containing ABTS (MACS–NIL) based on Cu ion chelation (MACS–NIL–Cu–LAC). First, CS was modified with NIL, and then the obtained CS–NIL was dissolved in acetic acid and added dropwise to the suspension of Fe₃O₄ NPs containing ABTS. After that, a solution of NaOH was added, resulting in the formation of MACS–NIL. The MACS–NIL NPs were activated with Cu(II) and then the LAC was immobilized (Figure 30).

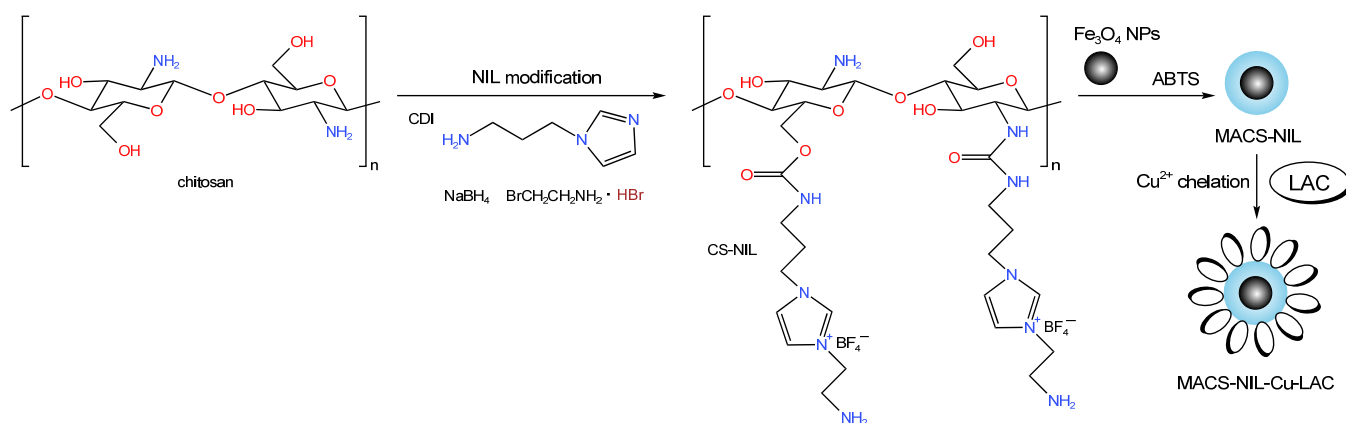


Figure 30. Simplified representation of MACS–NIL–Cu–LAC synthesis (based on Ref. [204]).

MACS–NIL–Cu–LAC revealed enhanced activity (1.7-fold more than of free LAC), improved pH and temperature adaptability, and increased thermal and storage stability. The MACS–NIL–Cu–LAC had good removal efficiency with 100% for 2,4-dichlorophenol in water at 25 °C, even when the concentration reached 50 mg/L. The reusability study showed that after six catalytic runs, the removal efficiency of 2,4-dichlorophenol using MACS–NIL–Cu–LAC could still reach 93.2%. Moreover, the MACS–NIL–Cu–LAC exhibited higher catalytic efficiencies with 100%, 70.5% and 93.3% for bisphenol A, indole and anthracene, respectively [204].

Ospina et al. [205] carried out a one-pot immobilization of β -galactosidase using the silica sol–gel encapsulation process combined with metal chelation using CS and Ca(II), Zn(II) or Cu(II). Briefly, sodium silicate and CS solutions in acetic acid were mixed (pH = 6), salt solution (500 mM CaCl₂, ZnCl₂ or CuCl₂) was added and then the enzyme was added (100 IU/mL). No additional crosslinking agents were used. Metal chelation was proposed to play an important role in the encapsulation process. It was found that the presence of cations does not affect encapsulation efficiency (81%) and has positive effects on the maximum catalytic potential. However, depending on the metal type, at 60 °C, different thermal behavior was observed: Ca(II)—hyperactivating (1.6 times higher activity compared to the soluble enzyme)/stabilizing; Zn(II)—hyperactivating/non-stabilizing; and Cu(II)—non-hyperactivating/non-stabilizing effects. As a result, hydrolytic and transgalactosylation activities of the enzyme (33.6–57.4% total lactose conversion) were higher than those reported with analogue biocatalysts.

Cai et al. [206] developed a promising strategy for LIP immobilization based on the magnetic microspheres functionalized with hyaluronic acid (HA) and CS (Fe₃O₄@SiO₂@{CS/HA}₃). First, Fe₃O₄ magnetic microspheres and the core–shell were synthesized using a hydrothermal reaction and the sol–gel method, respectively. Then, a layer-by-layer assembly of HA and CS on the surface of the Fe₃O₄@SiO₂ microspheres was carried out. LIP was covalently bonded on the surface of the resulting microspheres using EDAC/NHS to produce Fe₃O₄@SiO₂@{CS/HA}₃@LIP. Fe₃O₄@SiO₂@{CS/HA}₃@LIP showed good thermal and long-term stability (after storage for 30 days at 4 °C Fe₃O₄@SiO₂@{CS/HA}₃@LIP retained 78% of the initial activity), reusability (85% of initial activity was retained after nine consecutive cycles) and catalytic activity for the synthesis of the structured lipid of 1,3-dioleoyl-2-palmitoylglycerol—healthy component of food, oil and pharmaceutical intermediates.

Olshannikova et al. [36] synthesized CS modified with 4-acetylsulfanylchloride (see Figure 2) for the immobilization of proteases (ficin, papain and bromelain). Enzyme immobilization was carried out by complexation via the addition of modified CS to an enzyme solution having pH = 9 or 10. No additional shaping or crosslinking was applied. It was found that the hydroxy, thionyl and amino groups of 2-(4-acetamido-2-sulfanylamine)CS were involved in the complexation process. The immobilized papain (protein content was about 12 mg/g_{support}) was more active compared to other immobilized proteases. Moreover, the total and specific proteolytic activities of immobilized papain were higher (122% and 102%, respectively) compared to the native enzyme due to hyperactivation.

Moreover, Olshannikova et al. [207] and Red'ko et al. [208] synthesized a series of nano- and microparticles of CS with the addition of ascorbic acid for further immobilization of papain and bromelain. CS particles were prepared by dissolving CS in acetic acid solution with the subsequent addition of NaOH under constant stirring. Ascorbic acid was added to the CS solution before gelation. The immobilized papain exhibited 40% of its catalytic activity after incubation for 168 h in Tris–HCl buffer (0.05 M, pH 7.5) at 37 °C, while the free enzyme retained only 15% of its activity [207]. The free bromelain retained 13% of its activity after incubation for 168 h, while the immobilized enzyme exhibited between 33% and 39% of its activity depending on the molecular weight of the CS and its particle sizes [208].

A novel organic–inorganic hybrid nanoflower was obtained by Xu et al. [209] via the CS-regulated biomimetic mineralization of calcium phosphate (CaP) to immobilize sucrose phosphorylase (SPase) via self-assembly (CS–CaP@SPase). CS was dissolved in acetic acid

with a subsequent addition of TPP aqueous solution during stirring. Then, CaP and SPase were added. The obtained CS–CaP@SPase exhibited excellent pH, byproduct and organic solvent (acetonitrile) tolerance, and storage stability. CS–CaP@SPase maintained about 70% of relative activity, while free SPase retained only 5% at 60 °C. The CS–CaP@SPase activity reached its maximum at pH = 8; at pH = 7 it retained 90% of relative activity, while the free SPase retained 65% of relative activity. It was proposed that the active groups on the CS–CaP surface could interact with H⁺, which could reduce the effects of H⁺ on the activity of SPase. Moreover, the relative activity of CS–CaP@SPase was still retained at about 80% after 10 cycles and maintained 75% after 15 days.

Gu et al. [210] developed bienzyme biocatalysts by co-immobilization of HRP and GOx on DA-modified cellulose–CS composite beads via covalent binding (cellulose–CS@DA/HRP–GOx) (Figure 31). To produce cellulose–CS@DA/HRP–GOx, cellulose and CS were dissolved in the ionic liquid ([Emim][OAc]); then, the resulting solution was added dropwise into ultrapure water to obtain cellulose–CS composite beads. The cellulose–CS composite beads and a certain amount of DA were placed in Tris–HCl buffer solution (pH 8.5) and left to react. Then, cellulose–CS@DA beads were used as a support for the co-immobilization of HRP and GOx at different ratios (3:1, 2:1, 1:1, 1:2 and 1:3).

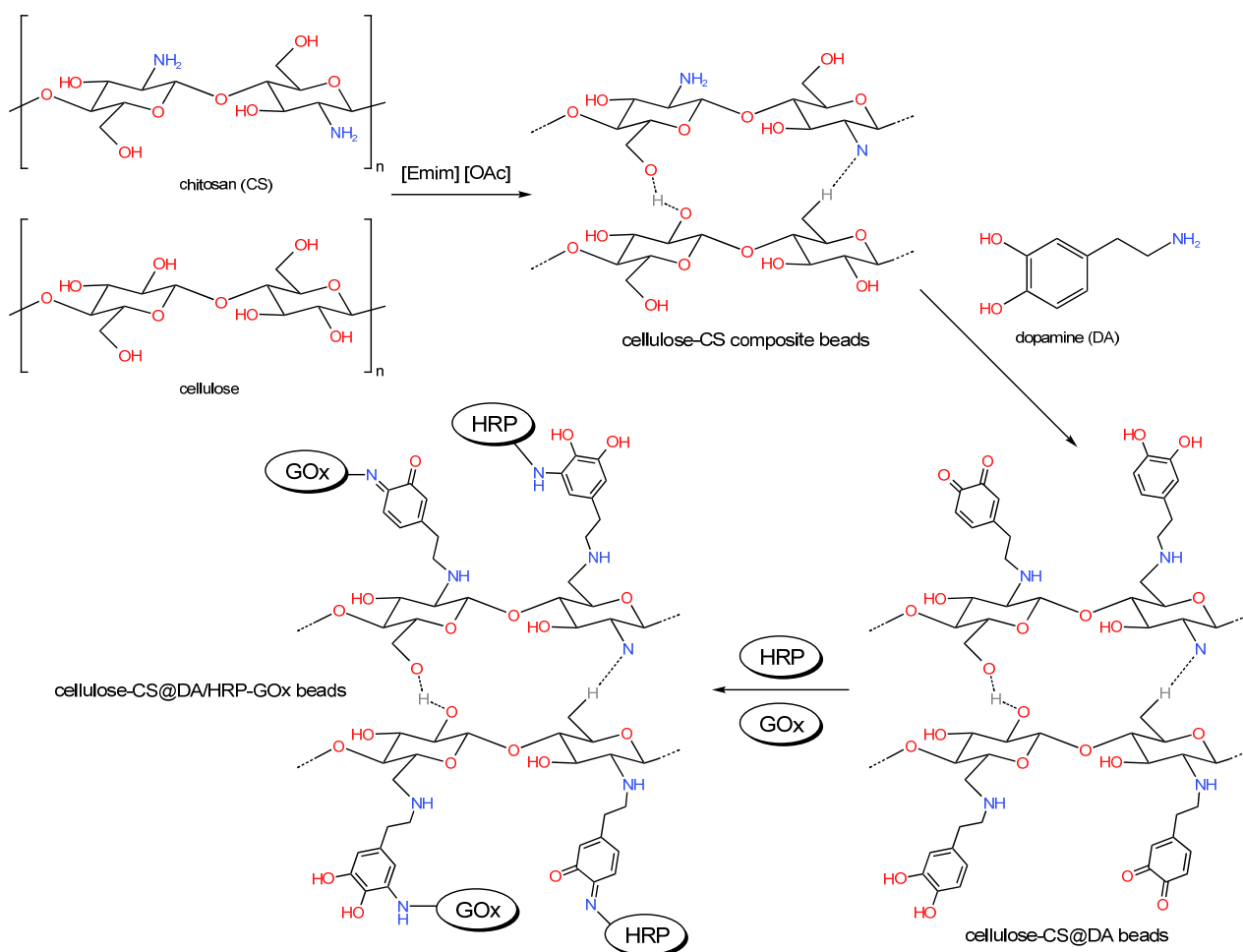


Figure 31. Simplified representation of synthesis of cellulose–CS@DA/HRP–GOx composite beads (based on Ref. [210]).

Cellulose–CS@DA/HRP–GOx beads showed good ability to catalytically degrade acridine in wastewater. The highest degradation rate of acridine (99.5%, 8 h) was found at an HRP-to-GOx ratio of 2:1. For comparison, the degradation rate of acridine in the case of cellulose–CS@DA/HRP and cellulose–CS@DA/GOx was 93.8% and 15.8%, respectively,

for 8 h. Additionally, the developed bienzyme biocatalyst maintained a degradation rate of 61.2% after six cycles of acridine degradation [210].

HRP was immobilized with 90% efficiency on the agarose–CS hydrogel (ACS–HRP) using NHS as a mild chemical crosslinker [211] and used for degradation of reactive blue 19. CS was dissolved in 1% acetic acid and then added to agarose aqueous solution under continuous mixing. After that, freshly prepared NHS solution was added to the agarose–CS solution. This mixture was used to incorporate HRP; the resulting suspension was poured in sterile glass plates and placed at 4 °C for 1 h to solidify the gel matrix completely. ACS–HRP preserved higher activity under acidic environments with a pH of 4.0 (38 vs. 5.9%), and well stabilized under alkaline conditions, retaining 3.9-fold greater activity than free HRP at pH 10. Using ACS–HRP, 1.6- and 4-fold greater activity was achieved at 50 and 70 °C, respectively, compared to the free enzyme. After 5 and 10 cycles of use, the ACS–HRP retained above 90% and 60% of original activity, respectively.

Pereira et al. [212] reported the microencapsulation of LIP from *Yarrowia lipolytica* IMUFRJ 50,682 with ionotropic gelation of CS with SA. Briefly, SA was dissolved in LIP enzymatic extract, and then microcapsules were formed by dripping in calcium chloride and CS solution (CS was preliminarily dissolved in acetic acid). Microcapsules remained in the CaCl₂ solution for a determined time at pH = 7 and were then lyophilized. The catalytic activity of the immobilized LIP was estimated using p-nitrophenyl laurate as a substrate. The optimum parameters of immobilization were found (3.1% (w/v) SA, 0.2% (w/v) CS, 0.14 M CaCl₂ and 1 min complexation time) allowing for high immobilization yield (99.8%) and 150.7 U/g of LIP activity. Microcapsules containing LIP from *Y. lipolytica* were more stable at 37 °C than the free enzyme and retained 50% of activity after the second reaction cycle and could be used for five reactions with 20% of initial activity.

A biocatalyst for the continuous production of gluten-reduced beer was developed by Benucci et al. [213] based on immobilized prolyl endopeptidase from *Aspergillus niger* (AN–PEP). AN–PEP was immobilized on CS beads, which we obtained by common dripping CS acidic solution into NaOH solution and then functionalized with a polydialdehyde starch crosslinker. The maximum specific activity of the immobilized enzyme was 0.016 IU/mg_{BSAeq}. (BSA (bovine serum albumin) was used as standard protein). The immobilization increased the thermal stability of AN–PEP, which showed similar catalytic properties in synthetic beer (toward the synthetic substrate Z-Gly–Pro–pNA) when it was applied at 20 °C or at 50 °C. The continuous treatment in a fluidized bed reactor allowed for the reduction of the initial gluten content (65 mg/kg) in commercial beer from barley malt, reaching 19 mg/kg after 9 h and 15 mg/kg after 10 h of treatment.

Chen et al. [214] reported the synthesis of a biocatalyst using co-encapsulation of LAC and a natural redox mediator soybean meal extract (SBE) on Ca-modified CS–alginate beads (CA–Ca–SBE–LAC). SA was dissolved in SBE solution and then mixed with certain amount of LAC. Then, an alginate–SBE–LAC mixture was slowly dripped into CS–CaCl₂ solution in acetic acid. The obtained CA–Ca–SBE–LAC beads were hardened at room temperature for 6 h and applied for degradation of phenanthrene. A high degradation efficiency of 94.4% was achieved for 0.5 ppm phenanthrene aqueous solution for 20 min, which was 20–30% higher than that of free LAC. The CA–Ca–SBE–LAC maintained high catalytic activities over a wide range of pH values (from 4 up to 9) and remained stable during 10 cyclic runs (the degradation efficiency of phenanthrene was 83.1%) and after 50 days of storage at 4 °C (the degradation efficiency of phenanthrene was 92%). The contributions of the free radical pathway and nonradical pathway to phenanthrene were 12.5% and 87.5%, respectively, and achieved the maximum double synergy of the mediator and LAC.

Metal oxide NPs can benefit not only from the activity of inorganic catalysts, but also biocatalysts. El-Shishtawy et al. [215] synthesized crosslinked CS/ZnO nanocomposite, which was additionally improved by Fe₂O₃ NPs. ZnO NPs were suspended in CS acidic solution followed by mixing different concentrations of Fe₂O₃ NPs. A CS/ZnO/Fe₂O₃ nanocomposite was washed with distilled water and dried at 80 °C. No shaping, crosslinking or activation of CS/ZnO/Fe₂O₃ was carried out. The immobilization of catalase was

provided by adsorption at room temperature overnight. The CS/ZnO/Fe₂O₃ achieved an immobilization yield of 84.32%. After 10 repeated cycles, the remaining immobilized catalase activity was 45%. After 60 days of storage at 4 °C, the remaining activity of the immobilized enzyme was found to be 47%. Maximum activity immobilized catalase was 19.92 μmol/mL, which is nearly double compared to the free enzyme (10.45 μmol/mL).

Girelli et al. [216] developed a hybrid support using calcium ion as a linking agent that coordinated the silanol and hydroxyl groups of CS. Silica was treated with Ca(NO₃)₂ and added to the CS solution. Then, the aqueous phase was removed with evaporation under vacuum, while the solid phase was treated with methanol and KOH. The obtained SiO₂-Ca-CS (Figure 32) was used to immobilize LAC, which was preliminarily oxidized with periodate (see also Ref. [187]).

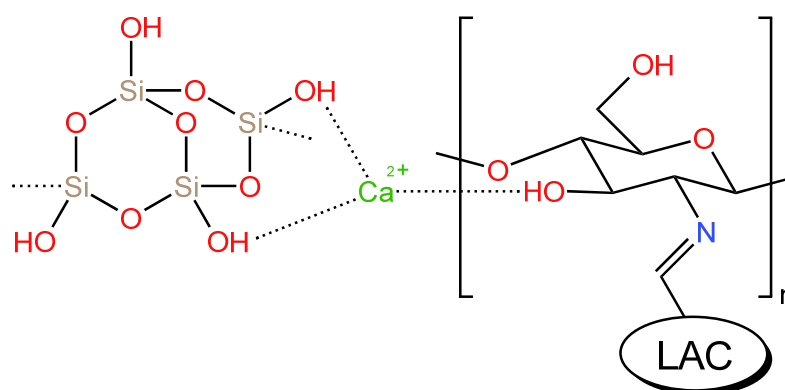


Figure 32. Scheme of SiO₂-Ca-CS-LAC [216].

SiO₂-Ca-CS-LAC was then packed in a column and used in a flow system for phenol removal. Seven different phenolic compounds (catechol, 4-methylcatechol, tyrosol, phenol, caffeic acid, vanillic acid, syringic acid, *p*-coumaric acid) were oxidized in a continuous mode for 21 h. The SiO₂-Ca-CS-LAC for allowed 90% of the phenols' removal, showed good storage stability (70% of activity in 70 days) and good reusability (90–50% of catalytic activity at the 4th reuse depending on the CS type). The best performance was obtained with the low molecular weight CS (50–190 kDa) at pH = 5 and with a flow rate of 0.7 mL/min. In addition, when all the phenols were together, a general increase in the phenols' removal was obtained in contrast to when they were alone [216].

Khan et al. [217] synthesized a biocatalyst based on β-galactosidase physically adsorbed on PANI-CS or PANI-CS-Ag nanocomposites. PANI-CS was prepared by using the copolymerization technique, according to which CS was added to aniline solution at 0–5 °C, and then ammonium persulfate (APS) was added (typical conditions for PANI synthesis via oxidative polymerization of aniline). Ag NPs were obtained separately and added to the CS-containing aniline solution prior PANI synthesis. The resulting PANI-CS and PANI-CS-Ag nanocomposites were used for deposition of β-galactosidase. The enhancement in catalytic activity of the enzyme in the presence of silver by a factor of 1.23 was found for the reaction of lactose hydrolysis. Both immobilized enzyme preparations exhibited remarkably high stability against pH (2–9) and temperature (20–80 °C) compared to the free form. PANI-CS-Ag-bound β-galactosidase was able to retain 94% of its initial activity after ten repeated uses. It was underlined that both PANI-CS and PANI-CS-Ag-bound β-galactosidase can serve as powerful recognition probes in biosensor applications for lactose detection.

LIP from *Mucor miehei* was immobilized on CS hydrogels by Vassiliadi et al. [218] without using any crosslinking or activating agents. CS was dissolved in acidic solution (pH = 3), and then LIP solution was added. The obtained biocatalytic material was tested in a model esterification reaction of propyl laurate synthesis. The immobilized LIP showed an optimum operation temperature of 30 °C and maintained high catalytic activity in various nonpolar organic solvents. The biocatalyst presented excellent reusability, with only 10%

loss of activity after 12 uses, which was higher than that obtained from LIP-containing CS beads prepared with a crosslinker. The residual activity decreased to 62% of the initial one after one day of storage, and to 42% after 4 days, remaining at the same level for about month under freeze ($-20\text{ }^{\circ}\text{C}$).

Some comparative characteristics of biocatalysts are presented in Table 2.

Table 2. Comparison of some recent biocatalysts based on CS-containing supports.

Enzyme	Support	Shape	Crosslinking Agent	Additional Activating Agent	Recycling Stability	Storage Stability	Ref.
LIP	CS/CNWs	Beads	Tannic acid	EDAC/NHS	Not indicated	Not indicated	[178]
	CS-GA-Gly	Beads	No	GA	34% of activity after nine reuses	Not indicated	[180]
	nM-OA-CS-GA	NPs	No	GA	Not indicated	Not indicated	[183]
	CS	Beads	No	GA	75.2% of activity after 10 reuses	85.5% of activity after 6 months at $5\text{ }^{\circ}\text{C}$	[185]
	Fe ₃ O ₄ -CS-GA	Microparticles	No	GA	60% of activity after 10 reuses	80% of activity after 6 months at $5\text{ }^{\circ}\text{C}$	[186]
	Maghemite/CS/TPP	NPs	TPP	GA	Not indicated	Not indicated	[189]
	Chitin/CS/Fe ₃ O ₄	NPs	GA	EDAC/NHS	Not indicated	90% of activity after 40 days at $30\text{ }^{\circ}\text{C}$	[201]
	CS-alginate	Microcapsules	No	No	No loss of activity after five reuses	Not indicated	[203]
	Fe ₃ O ₄ @SiO ₂ @(CS/HA) ₃	NPs	No	EDAC/NHS	85% of activity after 9 reuses	78% of activity after 30 days at $4\text{ }^{\circ}\text{C}$	[206]
	CS-SA	Microcapsules	No	No	20% of activity after five reuses	Not indicated	[212]
CS	-	No	No	90% of activity after 12 reuses	42% of activity after 4 days and more at $-20\text{ }^{\circ}\text{C}$	[218]	
LAC	CS	Beads	No	No	40% of activity after five reuses	100% of activity after 30 days at $4\text{ }^{\circ}\text{C}$	[187]
	CS-GA	Beads	GA	No	20% of activity after five reuses	50% of activity after 30 days at $4\text{ }^{\circ}\text{C}$	[187]
	MnFe ₂ O ₄ -CS	NPs	No	GA	no loss of activity after five reuses	No loss of activity after 30 days at $4\text{ }^{\circ}\text{C}$	[188]
	CS	Beads	No	GP	>55% of activity after 11 reuses	57% of activity after 30 days at $4\text{ }^{\circ}\text{C}$	[199]
	MACS-NIL-Cu	NPs	-	-	93.2% of activity after five reuses	95% of activity after 30 days at $4\text{ }^{\circ}\text{C}$	[204]
	CA-Ca-SBE	Beads	No	No	83.1% of activity after 10 reuses	92% of activity after 50 days at $4\text{ }^{\circ}\text{C}$	[214]
	SiO ₂ -Ca-CS	-	No	No	90–50% of activity after four reuses depending on CS	70% of activity after 70 days at $4\text{ }^{\circ}\text{C}$	[216]
β-galactosidase	CS	Microspheres	No	GA	Not indicated	100% of activity after 105 days at $4\text{ }^{\circ}\text{C}$	[179]
	CS-GP	Beads	GP	GP	No loss of activity after 25 reuses	Not indicated	[200]
	SiO ₂ -Me-CS	-	No	No	Not indicated	Not indicated	[205]
	PANI-CS-Ag	-	No	No	94% of activity after 10 reuses	94% of activity after 60 days at $4\text{ }^{\circ}\text{C}$	[217]
β-glucosidase	Fe ₃ O ₄ -CS/GA/AB-NTA-Ni ²⁺	NPs	GA	6-His tags of enzymes interacted with Ni ²⁺	40% of activity after five reuses	Not indicated	[190]
Endoglucanase		NPs	GA		10% of activity after five reuses	Not indicated	[190]
Catalase	CS/ZnO/Fe ₂ O ₃	-	No	No	45% of activity after 10 reuses	47% of activity after 60 days at $4\text{ }^{\circ}\text{C}$	[215]
HRP	PMA-co-PAA@CS fibers	Membrane	EDAC/NHS	GA	70% of activity after 10 reuses	80% of activity after 35 days at $30\text{ }^{\circ}\text{C}$	[184]
	ACS	Membrane	no	NHS	>60% of activity after 10 reuses	Not indicated	[211]
HRP&GOx	Cellulose-CS@DA	Beads	no	DA	61.2% of activity after six reuses	88.8% of activity after 60 days at $4\text{ }^{\circ}\text{C}$	[210]
SPase	CS-CaP	Nano-flower	TPP	no	80% of activity after 10 reuses	75% of activity after 15 days at $4\text{ }^{\circ}\text{C}$	[209]
7α-HSDH and 7β-HSDH	CM	Microspheres	TPP	GA	>85% of activity after six reuses	Not indicated	[176]

Table 2. Cont.

Enzyme	Support	Shape	Crosslinking Agent	Additional Activating Agent	Recycling Stability	Storage Stability	Ref.
Inulinase	CS	Beads	TPP	GA	78.2% of activity after nine reuses	Not indicated	[177]
	CS/Fe ₃ O ₄	NPs	no	EDAC/NHS	50% of activity after 10 reuses	Not indicated	[202]
INU	CSB	Beads	no	GA	45% of activity after 12 reuses	Not indicated	[192]
Trypsin	GA-ZnO/CS	NPs	no	GA	50% of activity after nine reuses	50% of activity after 90 days at 4 °C	[181]
Dextran-sucrase	CS	Beads	GA	GA	22% of activity after 10 reuses	60% of activity after 28 days at 4 °C	[182]
βG and ARA (combi-CLEA)	CS	Beads	TPP	No	Not indicated	100% activity after 91 days at 16 °C	[193]

Based on the presented data, the following trends can be noticed, and brief conclusions made:

- (i) There are four main approaches to the preparation of CS-based supports for the immobilization of enzymes: CS beads optionally crosslinked with different agents; CS capsules typically formed by ionotropic gelation with SA; core-shell NPs consisting of an inorganic core (usually magnetic) covered with CS; membranes;
- (ii) Enzymes can be immobilized using the following general approaches: encapsulation into CS-containing gel; covalent binding to the surface of a CS-based support; physical adsorption on the support surface. Among the mentioned approaches, covalent binding seems to be more promising for the development of sustainable biocatalysts, allowing high reusability and storage stability. Though, at the same, it should be noted that catalytic behavior strongly depends on the used substrate and the choice of solvent that makes data comparison difficult;
- (iii) In contrast to adsorbents, crosslinking of CS is rarely applied (typically in the case of CS beads), though it can benefit the properties of the resulting biocatalytic system. Among crosslinking agents, TPP and GP are prospective since they have low toxicity compared to GA. However, GA is still the most widespread activating agent for the covalent binding of enzymes;
- (iv) Metal ions, while presented in catalyst composition, can increase the pH stability of the biocatalyst and, in some cases, result in enzyme hyperactivation. Magnetic NPs incorporated in a polymeric environment do not always have an obvious positive impact on catalyst stability; however, they allow for an important advantage—the simplicity of biocatalyst separation from the reaction mixture.

5. Conclusions

CS provides a number of opportunities for the production of environmentally friendly adsorbents and catalytic supports due to the existence of functional groups and the ability to form different shapes (fibers, membranes, beads, NPs, etc.).

For adsorption purposes, the general trend is the use of crosslinking agents (preferably covalent crosslinking) and grafting of functional groups, resulting in a noticeable increase in the number of adsorption sites. However, this approach (CS modification) is rarely used in catalysis, especially in the development of biocatalysts, since the high adsorption ability of CS with respect to both inorganic and organic components may have a negative influence on the biocatalysts' efficiency. Thus, in the case of biocatalysts, CS can be used as a surface modifier of solid supports in an amount of less than 1 wt.%. This also contributes to the maximum availability of active centers of the immobilized enzymes.

At the same time, in the case of metal-catalyzed catalytic reactions, the high adsorption ability of CS can be used for the development of catalytic systems, in which the inorganic part entrapped by CS is a catalytically active phase while organic adsorbate is the subject of catalytic transformation. Thus, modified (grafted), CS-based materials are promising catalytic supports. In the composition of catalytic supports, crosslinking agents are typically not used, as well as certain shaping at a macro-level of the resulting catalytic materials.

The use of CS in biocatalytic processes is based primarily on its excellent gel-forming ability and the presence of amino groups available for interactions in its composition. Thanks to gelation, it is possible to synthesize various stable forms of solid supports for the immobilization of enzymes. Amino groups of CS are used for the covalent crosslinking of enzymes via activating agents due to the formation of Schiff's bases (GA) or amide bonds (carbodiimides), as well as the crosslinking of CS itself in order to form particles of a certain shape. The combination of these properties allows for the achievement of high activity and the operational stability of synthesized biocatalytic systems. CS is most widely used for the immobilization of oxidoreductases (peroxidases, LACs and GOxs) and hydrolases (e.g., LIPs).

Magnetically separable catalysts/biocatalysts obviously have the advantage of easy separation from the reaction mixture, but most of these catalysts have the limitation of sensitivity to low pH. Thus, the further improvement of magnetically separable CS-based composites is a promising area of research.

Author Contributions: Conceptualization, L.Z.N., B.B.T. and V.G.M.; methodology, L.Z.N.; software, L.Z.N.; validation, V.G.M.; formal analysis, B.B.T.; investigation, P.E.I. and P.Y.S.; resources, L.Z.N.; data curation, P.E.I. and P.Y.S.; writing—original draft preparation, L.Z.N. and B.B.T.; writing—review and editing, L.Z.N., B.B.T. and V.G.M.; visualization, L.Z.N.; supervision, M.G.S.; project administration, V.G.M.; funding acquisition, V.G.M. All authors have read and agreed to the published version of the manuscript.

Funding: This research was funded by the Ministry of Science and Higher Education of the Russian Federation, grant number 075-15-2022-1232.

Data Availability Statement: Not applicable.

Conflicts of Interest: The authors declare no conflict of interest.

Abbreviations

ABTS: 2,2'-azino-bis-(3-ethyl-benzothiazoline-6-sulfonic acid); AO: acridine orange; AR: acid red; ARA: α -L-arabinofuranosidase; BDC: 1,4-benzenedicarboxylic acid; BglIi: β -glucosidase from *Humicola insolens*; CB: chitosan beads; CLEAs: crosslinked enzyme aggregates; CMS: chitosan-based minispheres; CNTs: carbon nanotubes; CR: Congo red; CS: chitosan; CSBs: core-shell CS beads; DA: dopamine; DD: deacetylation degree; DEO: 1,2,7,8-diepoxyoctane; DS: diclofenac sodium; DVB: divinylbenzene; ECH: epichlorohydrin; EDAC: 1-ethyl-3-[3-dimethylaminopropyl]carbodiimide; Egs: endoglucanase from *Scytalidium thermophilum*; FA: formaldehyde; β G: β -D-glucosidase; GA: glutaraldehyde; GNPs: graphene nanoplates; GO: graphene oxide; GOx: glucose oxidase; GP: genipin; GTMA: glycidyl trimethylammonium chloride; HA: hyaluronic acid; HRP: horseradish peroxidase; HSDH: hydroxysteroid dehydrogenases; IC: indigo carmine; INU: inulosucrase; LAC: laccase; LIP: lipase; MAH: maleic anhydride; MB: methylene blue; MCs: microcrystals; MG: malachite green; MOFs: metal-organic frameworks; MPs: microparticles; NA: nitroaniline; 4-NBA: 4-nitrobenzoic acid; NHS: N-hydroxysuccinimide; NIL: amino-functionalized ionic liquid; nM: nanomagnetite; NPs: nanoparticles; 2(3,4)-NP, 2(3,4)-nitrophenol; OA: oleic acid; OD: oxidized dextran; PAA: poly(acrylic acid); PAHs: polycyclic aromatic hydrocarbons; PANI: polyaniline; PDA: polydopamine; PE: polyelectrolyte; PEI: polyethylenimine; PFCs: perfluorinated chemicals; PFOA: perfluorooctanoate; PFOS: perfluorooctane sulfonate; PMA: poly(methyl acrylate); PPIMB: 3,3-diphenylpropylimine methyl benzaldehyde; RR: reactive red; SDBS: sodium dodecylbenzene sulfonate; SDS: sodium dodecyl sulfate; SP: spermine; SPase: sucrose phosphorylase; TCS: thiolated CS; TPP: triphosphosphate; ZF: zinc ferrite.

References

1. Aranaz, I.; Alcántara, A.R.; Civera, M.C.; Arias, C.; Elorza, B.; Heras Caballero, A.; Acosta, N. Chitosan: An Overview of Its Properties and Applications. *Polymers* **2021**, *13*, 3256. [[CrossRef](#)] [[PubMed](#)]
2. Boominathan, T.; Sivaramakrishna, A. Recent Advances in the Synthesis, Properties, and Applications of Modified Chitosan Derivatives: Challenges and Opportunities. *Top. Curr. Chem.* **2021**, *379*, 19. [[CrossRef](#)] [[PubMed](#)]
3. Crini, G. Historical Review on Chitin and Chitosan Biopolymers. *Environ. Chem. Lett.* **2019**, *17*, 1623–1643. [[CrossRef](#)]

4. Sivashankari, P.R.; Prabakaran, M. 5-Deacetylation Modification Techniques of Chitin and Chitosan. In *Chitosan Based Biomaterials*; Jennings, J.A., Bumgardner, J.D., Eds.; Woodhead Publishing: Sawston, UK, 2017; Volume 1, pp. 117–133. [CrossRef]
5. Di Nardo, T.; Hadad, C.; Nguyen Van Nhien, A.; Moores, A. Synthesis of High Molecular Weight Chitosan from Chitin by Mechanochemistry and Aging. *Green Chem.* **2019**, *21*, 3276–3285. [CrossRef]
6. Pillai, C.K.S.; Paul, W.; Sharma, C.P. Chitin and Chitosan Polymers: Chemistry, Solubility and Fiber Formation. *Prog. Polym. Sci.* **2009**, *34*, 641–678. [CrossRef]
7. Pérez-Álvarez, L.; Ruiz-Rubio, L.; Vilas-Vilela, J.L. Determining the Deacetylation Degree of Chitosan: Opportunities to Learn Instrumental Techniques. *J. Chem. Educ.* **2018**, *95*, 1022–1028. [CrossRef]
8. Yeul, P.; Shrivastava, S. Chitosan: An Overview. *Int. J. Curr. Res.* **2012**, *4*, 176–182. [CrossRef]
9. Zhang, M.; Zhang, F.; Li, C.; An, H.; Wan, T.; Zhang, P. Application of Chitosan and Its Derivative Polymers in Clinical Medicine and Agriculture. *Polymers* **2022**, *14*, 958. [CrossRef]
10. *Chitosan Market Size, Share & Trends Analysis Report by Application (Pharmaceutical & Biomedical, Water Treatment, Cosmetics, Food & Beverage), by Region (APAC, North America, Europe, MEA), and Segment Forecasts, 2020–2027*; Report ID: 978-1-68038-798-8; Grand View Research: San Francisco, CA, USA, 2020; Available online: <https://www.grandviewresearch.com/industry-analysis/global-chitosan-market> (accessed on 1 February 2023).
11. Kumar, N.; Joshi, N.C. Adsorption Applications of Synthetically Prepared PANI-CuO Based Nanocomposite Material. *J. Ind. Chem. Soc.* **2022**, *99*, 100551. [CrossRef]
12. Toumi, I.; Djelad, H.; Chouli, F.; Benyoucef, A. Synthesis of PANI@ZnO Hybrid Material and Evaluations in Adsorption of Congo Red and Methylene Blue Dyes: Structural Characterization and Adsorption Performance. *J. Inorg. Organomet. Polym.* **2022**, *32*, 112–121. [CrossRef]
13. El-Shazly, A.H.; Elkady, M.; Abdelraheem, A. Investigating the Adsorption Behavior of Polyaniline and Its Clay Nanocomposite towards Ammonia Gas. *Polymers* **2022**, *14*, 4533. [CrossRef]
14. Hajjaoui, H.; Soufi, A.; Boumya, W.; Abdennouri, M.; Barka, N. Polyaniline/Nanomaterial Composites for the Removal of Heavy Metals by Adsorption: A Review. *J. Compos. Sci.* **2021**, *5*, 233. [CrossRef]
15. Peñas-Sanjuán, A.; López-Garzón, R.; López-Garzón, J.; Pérez-Mendoza, M.; Melguizo, M. Preparation of a Poly-alkylamine Surface-functionalized Carbon with Excellent Performance as a Pd(II) Scavenger. *Carbon* **2012**, *50*, 2350–2352. [CrossRef]
16. Choi, W.; Min, K.; Kim, C.; Ko, Y.S.; Jeon, J.W.; Seo, H.; Park, Y.-K.; Choi, M. Epoxide-functionalization of Polyethyleneimine for Synthesis of Stable Carbon Dioxide Adsorbent in Temperature Swing Adsorption. *Nat. Commun.* **2016**, *7*, 12640. [CrossRef]
17. Huang, X.; Wang, L.; Zhang, J.; Du, X.; Wu, S.; Wang, H.; Wei, X. A Novel ϵ -Polylysine-modified Microcrystalline Cellulose Based Antibacterial Hydrogel for Removal of Heavy Metal. *Int. J. Biol. Macromol.* **2020**, *163*, 1915–1925. [CrossRef] [PubMed]
18. Rivas, B.L.; Maureira, A.; Guzmán, C. Poly(L-lysine) as a Polychelator to Remove Toxic Metals Using Ultrafiltration and Bactericide Properties of Poly(L-lysine)-Cu²⁺ Complexes. *Polym. Bull.* **2011**, *67*, 763–774. [CrossRef]
19. Xue, W.; Liu, B.; Zhang, H.; Ryu, S.; Kuss, M.; Shukla, D.; Hu, G.; Shi, W.; Jiang, X.; Lei, Y.; et al. Controllable Fabrication of Alginate/poly-L-ornithine Polyelectrolyte Complex Hydrogel Networks as Therapeutic Drug and Cell Carriers. *Acta Biomater.* **2022**, *138*, 182–192. [CrossRef] [PubMed]
20. Kaczmarek, M.B.; Struszczyk-Swita, K.; Li, X.; Szczesna-Antczak, M.; Daroch, M. Enzymatic Modifications of Chitin, Chitosan, and Chito oligosaccharides. *Front. Bioeng. Biotechnol.* **2019**, *7*, 243. [CrossRef] [PubMed]
21. Huang, K.-S.; Sheu, Y.-R.; Chao, I.-C. Preparation and Properties of Nanochitosan. *Polym. Plast. Technol. Eng.* **2009**, *48*, 1239–1243. [CrossRef]
22. Ma, F.; Wang, Z.; Zhao, H.; Tian, S. Plasma Depolymerization of Chitosan in the Presence of Hydrogen Peroxide. *Int. J. Mol. Sci.* **2012**, *13*, 7788–7797. [CrossRef]
23. Prasertsung, I.; Damrongsakkul, S.; Saito, N. Degradation of β -Chitosan by Solution Plasma Process (SPP). *Polym. Degrad. Stab.* **2013**, *98*, 2089–2093. [CrossRef]
24. Li, J.; Cai, J.; Fan, L. Effect of Sonolysis on Kinetics and Physicochemical Properties of Treated Chitosan. *J. Appl. Polym. Sci.* **2008**, *109*, 2417–2425. [CrossRef]
25. Tsao, C.T.; Chang, C.H.; Lin, Y.Y.; Wu, M.F.; Han, J.L.; Hsieh, K.H. Kinetic Study of Acid Depolymerization of Chitosan and Effects of Low Molecular Weight Chitosan on Erythrocyte Rouleaux Formation. *Carbohydr. Res.* **2011**, *346*, 94–102. [CrossRef] [PubMed]
26. Pierre, G.; Salah, R.; Gardarin, C.; Traikia, M.; Petit, E.; Delort, A.-M.; Mameri, N.; Moulti-Mati, F.; Michaud, P. Enzymatic Degradation and Bioactivity Evaluation of C-6 Oxidized Chitosan. *Int. J. Biol. Macromol.* **2013**, *60*, 383–392. [CrossRef] [PubMed]
27. Thadathil, N.; Velappan, S.P. Recent Developments in Chitosanase Research and Its Biotechnological Applications: A Review. *Food Chem.* **2014**, *150*, 392–399. [CrossRef] [PubMed]
28. Kumar, M.N.V.R.; Muzzarelli, R.A.A.; Muzzarelli, C.; Sashiwa, H.; Domb, A.J. Chitosan Chemistry and Pharmaceutical Perspectives. *Chem. Rev.* **2004**, *104*, 6017–6084. [CrossRef]
29. Berth, G.; Dautzenberg, H. The Degree of Acetylation of Chitosans and Its Effect on the Chain Conformation in Aqueous Solution. *Carbohydr. Polym.* **2002**, *47*, 39–51. [CrossRef]
30. Balan, V.; Verestiuc, L. Strategies to Improve Chitosan Hemocompatibility: A Review. *Eur. Polym. J.* **2014**, *53*, 171–188. [CrossRef]
31. Kahya, N. Water Soluble Chitosan Derivatives and Their Biological Activities: A Review. *Polym. Sci.* **2019**, *5*, 1–11. [CrossRef]

32. Ayati, A.; Heravi, M.M.; Daraie, M.; Tanhaei, B.; Bamoharram, F.F.; Sillanpaa, M. H₃PMo₁₂O₄₀ Immobilized Chitosan/Fe₃O₄ as a Novel Efficient, Green and Recyclable Nanocatalyst in the Synthesis of Pyrano-pyrazole Derivatives. *J. Iran Chem. Soc.* **2016**, *13*, 2301–2308. [[CrossRef](#)]
33. Kong, A.; Wang, P.; Zhang, H.; Yang, F.; Huang, S.P.; Shan, Y. One-pot fabrication of magnetically recoverable acid nanocatalyst, heteropolyacids/chitosan/Fe₃O₄, and its catalytic performance. *Appl. Catal. A Gen.* **2012**, *417–418*, 183–189. [[CrossRef](#)]
34. Nurunnabi, M.; Revuri, V.; Huh, K.M.; Lee, Y.-K. Chapter 14—Polysaccharide Based Nano/microformulation: An Effective and Versatile Oral Drug Delivery System. In *Nanostructures for Oral Medicine. Micro and Nano Technologies*; Andronesco, E., Grumezescu, A., Eds.; Elsevier: Amsterdam, The Netherlands, 2017; pp. 409–433. [[CrossRef](#)]
35. Coquery, C.; Negrell, C.; Caussé, N.; Pébère, N.; David, G. Synthesis of New High Molecular Weight Phosphorylated Chitosans for Improving Corrosion Protection. *Pure Appl. Chem.* **2019**, *91*, 509–521. [[CrossRef](#)]
36. Olshannikova, S.S.; Malykhina, N.V.; Lavlinskaya, M.S.; Sorokin, A.V.; Yudin, N.E.; Vyshkvorkina, Y.M.; Lukin, A.N.; Holyavka, M.G.; Artyukhov, V.G. Novel Immobilized Biocatalysts Based on Cysteine Proteases Bound to 2-(4-Acetamido-2-sulfanilamide) Chitosan and Research on Their Structural Features. *Polymers* **2022**, *14*, 3223. [[CrossRef](#)]
37. Suresh, R.; Deepa, M.; Sudha, P.N.; Gomathi, T.; Pavithra, S.; Moganavally, P. Synthesis, Characterization, Biological and Catalytic Activity of Carboxymethyl Chitosan Schiff Base Metal Complexes. *IJMS* **2022**, *51*, 423–431. [[CrossRef](#)]
38. Rostami, N.; Dekamin, M.G.; Valiey, E.; Fanimoghadam, H. Chitosan-EDTA-Cellulose Network as a Green, Recyclable and Multifunctional Biopolymeric Organocatalyst for the One-pot Synthesis of 2-Amino-4H-pyran Derivatives. *Sci. Rep.* **2022**, *12*, 8642. [[CrossRef](#)] [[PubMed](#)]
39. Federer, C.; Kurpiers, M.; Bernkop-Schnürch, A. Thiolated Chitosans: A Multi-talented Class of Polymers for Various Applications. *Biomacromolecules* **2021**, *22*, 24–56. [[CrossRef](#)]
40. Raghavendra Naveen, N.; Gopinath, C.; Subba Rao, D. A Spotlight on Thiolated natural Polymers and Their Relevance in Mucoadhesive Drug Delivery System. *Future J. Pharm. Sci.* **2018**, *4*, 47–52. [[CrossRef](#)]
41. Grosso, R.; de-Paz, M.-V. Thiolated-Polymer-Based Nanoparticles as an Avant-Garde Approach for Anticancer Therapies—Reviewing Thiomers from Chitosan and Hyaluronic Acid. *Pharmaceutics* **2021**, *13*, 854. [[CrossRef](#)]
42. Bernkop-Schnürch, A.; Krauland, A.H.; Leitner, V.M.; Palmberger, T. Thiomers: Potential Excipients for Non-Invasive Peptide Delivery Systems. *Eur. J. Pharm. Biopharm.* **2004**, *58*, 253–263. [[CrossRef](#)] [[PubMed](#)]
43. Schmitz, T.; Grabovac, V.; Palmberger, T.F.; Hoffer, M.H.; Bernkop-Schnürch, A. Synthesis and Characterization of a Chitosan-N-acetyl Cysteine Conjugate. *Int. J. Pharm.* **2008**, *347*, 79–85. [[CrossRef](#)]
44. ALSamman, M.T.; Sánchez, J. Recent Advances on Hydrogels Based on Chitosan and Alginate for the Adsorption of Dyes and Metal Ions from Water. *Arab. J. Chem.* **2021**, *14*, 103455. [[CrossRef](#)]
45. Dragan, E.S.; Dinu, M.V. Advances in Porous Chitosan Based Composite Hydrogels: Synthesis and Applications. *React. Funct. Polym.* **2020**, *146*, 104372. [[CrossRef](#)]
46. Ahmad, Z.; Salman, S.; Khan, S.A.; Amin, A.; Rahman, Z.U.; Al-Ghamdi, Y.O.; Akhtar, K.; Bakhsh, E.M.; Khan, S.B. Versatility of Hydrogels: From Synthetic Strategies, Classification, and Properties to Biomedical Applications. *Gels* **2022**, *8*, 167. [[CrossRef](#)] [[PubMed](#)]
47. Berger, J.; Reist, M.; Mayer, J.M.; Felt, O.; Gurny, R. Structure and Interactions in Chitosan Hydrogels Formed by Complexation or Aggregation for Biomedical Applications. *Eur. J. Pharm. Biopharm.* **2004**, *57*, 35–52. [[CrossRef](#)]
48. Boucard, N.; Viton, C.; Domard, A. New Aspects of the Formation of Physical Hydrogels of Chitosan in a Hydroalcoholic Medium. *Biomacromolecules* **2005**, *6*, 3227–3237. [[CrossRef](#)] [[PubMed](#)]
49. Sánchez-Cid, P.; Jiménez-Rosado, M.; Romero, A.; Pérez-Puyana, V. Novel Trends in Hydrogel Development for Biomedical Applications: A Review. *Polymers* **2022**, *14*, 3023. [[CrossRef](#)]
50. Shoueir, K.R.; El-Desouky, N.; Rashad, M.M.; Ahmed, M.K.; Janowska, I.; El-Kemary, M. Chitosan Based-Nanoparticles and Nanocapsules: Overview, Physicochemical Features, Applications of a Nanofibrous Scaffold, and Bioprinting. *Int. J. Biol. Macromol.* **2021**, *167*, 1176–1197. [[CrossRef](#)]
51. Nasef, S.M.; Khozemy, E.E.; Kamoun, E.A.; El-Gendi, H. Gamma Radiation-Induced Crosslinked Composite Membranes Based on Polyvinyl Alcohol/chitosan/AgNO₃/vitamin E for Biomedical Applications. *Int. J. Biol. Macromol.* **2019**, *137*, 878–885. [[CrossRef](#)] [[PubMed](#)]
52. Mndlovu, H.; du Toit, L.C.; Kumar, P.; Choonara, Y.E.; Marimuthu, T.; Kondiah, P.P.D.; Pillay, V. Bioplatfrom Fabrication Approaches Affecting Chitosan-Based Interpolymer Complex Properties and Performance as Wound Dressings. *Molecules* **2020**, *25*, 222. [[CrossRef](#)]
53. Chamkouri, H.; Chamkouri, M. A Review of Hydrogels, Their Properties and Applications in Medicine. *Am. J. Biomed. Sci. Res.* **2021**, *11*, 485–493. [[CrossRef](#)]
54. Rasool, A.; Rizwan, M.; Islam, A.; Abdullah, H.; Shafqat, S.S.; Azeem, M.K.; Rasheed, T.; Bilal, M. Chitosan-Based Smart Polymeric Hydrogels and Their Prospective Applications in Biomedicine. *Starch* **2021**, 2100150. [[CrossRef](#)]
55. Bashir, S.; Teo, Y.Y.; Ramesh, S.; Ramesh, K.; Rizwan, M. Synthesis and Characterization of pH-Sensitive N-Succinyl Chitosan Hydrogel and Its Properties for Biomedical Applications. *J. Chil. Chem. Soc.* **2019**, *64*, 4571–4574. [[CrossRef](#)]
56. Ghauri, Z.H.; Islam, A.; Qadir, M.A.; Gull, N.; Haider, B.; Khan, R.U.; Riaz, T. Development and Evaluation of pH-Sensitive Biodegradable Ternary Blended Hydrogel Films (chitosan/guar gum/PVP) for Drug Delivery Application. *Sci. Rep.* **2021**, *11*, 21255. [[CrossRef](#)] [[PubMed](#)]

57. Lei, M.; Huang, W.; Sun, J.; Shao, Z.; Zhao, L.; Zheng, K.; Fang, Y. Synthesis and Characterization of Thermo-Responsive Polymer Based on Carboxymethyl Chitosan and Its Potential Application in Water-based Drilling Fluid. *Colloids Surf. A Physicochem. Eng. Asp.* **2021**, *629*, 127478. [CrossRef]
58. Sarwan, T.; Kumar, P.; Choonara, Y.E.; Pillay, V. Hybrid Thermo-Responsive Polymer Systems and Their Biomedical Applications. *Front. Mater.* **2020**, *7*, 73. [CrossRef]
59. Ahsan, A.; Farooq, M.A.; Parveen, A. Thermosensitive Chitosan-Based Injectable Hydrogel as an Efficient Anticancer Drug Carrier. *ACS Omega* **2020**, *5*, 20450–20460. [CrossRef] [PubMed]
60. Shin, B.; Kim, J.; Vales, T.P.; Yang, S.K.; Kim, J.-K.; Sohn, H.; Kim, H.-J. Thermoresponsive Drug Controlled Release from Chitosan-Based Hydrogel Embedded with Poly(N-isopropylacrylamide) Nanogels. *J. Polym. Sci. Part A Polym. Chem.* **2018**, *56*, 1907–1914. [CrossRef]
61. Dash, M.; Chiellini, F.; Ottenbrite, R.M.; Chiellini, E. Chitosan—A versatile semi-synthetic polymer in biomedical applications. *Prog. Polym. Sci.* **2011**, *36*, 981–1014. [CrossRef]
62. Ranjha, N.M.; Khan, S. Chitosan/Poly (vinyl alcohol) Based Hydrogels for Biomedical Applications: A Review. *J. Pharm. Altern. Med.* **2013**, *2*, 30–41. Available online: <https://iiste.org/Journals/index.php/JPAM/article/view/4379> (accessed on 1 February 2023).
63. Babicheva, T.S.; Konduktorova, A.A.; Shmakov, S.L.; Shipovskaya, A.B. Formation of Liesegang Structures under the Conditions of the Spatiotemporal Reaction of Polymer-Analogous Transformation (Salt→Base) of Chitosan. *J. Phys. Chem. B* **2020**, *124*, 9255–9266. [CrossRef]
64. Zohuriaan-Mehr, M.J. Advances in Chitin and Chitosan Modification through Graft Copolymerization: A Comprehensive Review. *Iran. Polym. J.* **2005**, *14*, 235–265.
65. Jenkins, D.W.; Hudson, S.M. Review of Vinyl Graft Copolymerization Featuring Recent Advances toward Controlled Radical Based Reactions and Illustrated with Chitin/Chitosan Trunk Polymers. *Chem. Rev.* **2001**, *101*, 3245–3274. [CrossRef] [PubMed]
66. Zakharova, N.V.; Simonova, M.A.; Zelinskii, S.N.; Annenkov, V.V.; Filippov, A.P. Synthesis, Molecular Characteristics, and Stimulus-Sensitivity of Graft Copolymer of Chitosan and Poly (N, N-diethylacrylamide). *J. Mol. Liq.* **2019**, *292*, 111355. [CrossRef]
67. Erdodi, G.; Kennedy, J.P. Amphiphilic Conetworks: Definition, Synthesis, Applications. *Prog. Polym. Sci.* **2006**, *31*, 1–18. [CrossRef]
68. Naskar, S.; Sharma, S.; Kuotsu, K. Chitosan-Based Nanoparticles: An Overview of Biomedical Applications and Its Preparation. *J. Drug Deliv. Sci. Technol.* **2019**, *49*, 66–81. [CrossRef]
69. Ohya, Y.; Shiratani, M.; Kobayashi, H.; Ouchi, T. Release Behavior of 5-Fluorouracil from Chitosan-Gel Nanospheres Immobilizing 5-Fluorouracil Coated with Polysaccharides and Their Cell Specific Cytotoxicity. *J. Macromol. Sci. Pure Appl. Chem.* **1994**, *31*, 629–642. [CrossRef]
70. Grabnar, P.A.; Kristl, J. The Manufacturing Techniques of Drug-Loaded Polymeric Nanoparticles from Preformed Polymers. *J. Microencapsul.* **2011**, *28*, 323–335. [CrossRef]
71. Patiño-Ruiz, D.; Marrugo, L.; Reyes, N.; Acevedo-Morantes, M.; Herrera, A. Ionotropic Gelation Synthesis of Chitosan-Alginate Nanodisks for Delivery System and In Vitro Assessment of Prostate Cancer Cytotoxicity. *Int. J. Polym. Sci.* **2020**, *2020*, 5329747. [CrossRef]
72. de Carvalho, F.G.; Magalhães, T.C.; Teixeira, N.M.; Gondim, B.L.C.; Carlo, H.L.; Dos Santos, R.L.; de Oliveira, A.R.; Denadai, Á.M.L. Synthesis and Characterization of TPP/Chitosan Nanoparticles: Colloidal Mechanism of Reaction and Antifungal Effect on *C. albicans* Biofilm Formation. *Mater. Sci. Eng. C* **2019**, *104*, 109885. [CrossRef]
73. Nemati, Y.; Zahedi, P.; Baghdadi, M.; Ramezani, S. Microfluidics Combined with Ionic Gelation Method for Production of Nanoparticles Based on Thiol-Functionalized Chitosan to Adsorb Hg (II) from Aqueous Solutions. *J. Environ. Manage.* **2019**, *238*, 166–177. [CrossRef]
74. Pati, F.; Adhikari, B.; Dhara, S. Development of Chitosan-Tripolyphosphate Fibers through pH Dependent Ionotropic Gelation. *Carbohydr. Res.* **2011**, *346*, 2582–2588. [CrossRef] [PubMed]
75. Divya, K.; Jisha, M.S. Chitosan Nanoparticles Preparation and Applications. *Environ. Chem. Lett.* **2018**, *16*, 101–112. [CrossRef]
76. Pessoa, A.C.S.N.; Sipoli, C.C.; de la Torre, L.G. Effects of Diffusion and Mixing Pattern on Microfluidic-Assisted Synthesis of Chitosan/ATP Nanoparticles. *Lab. Chip.* **2017**, *17*, 2281–2293. [CrossRef] [PubMed]
77. Wang, X.; Shi, J.; Li, Z.; Zhang, S.; Wu, H.; Jiang, Z.; Yang, C.; Tian, C. Facile One-Pot Preparation of Chitosan/Calcium Pyrophosphate Hybrid Microflowers. *ACS Appl. Mater. Interfaces* **2014**, *6*, 14522–14532. [CrossRef] [PubMed]
78. Komoto, D.; Furuike, T.; Tamura, H. Preparation of Polyelectrolyte Complex Gel of Sodium Alginate with Chitosan Using Basic Solution of Chitosan. *Int. J. Biol. Macromol.* **2019**, *126*, 54–59. [CrossRef] [PubMed]
79. Boudoukhani, M.; Yahoum, M.M.; Lefnaoui, S.; Moulai-Mostefa, N.; Banhobre, M. Synthesis, Characterization and Evaluation of Deacetylated Xanthan Derivatives as New Excipients in the Formulation of Chitosan-Based Polyelectrolytes for the Sustained Release of Tramadol. *Saudi Pharm. J.* **2019**, *27*, 1127–1137. [CrossRef]
80. Livanovich, K.; Shutava, T. Influence of Chitosan/Dextran Sulfate Layer-by-Layer Shell on Colloidal Properties of Silver Nanoparticles. *Int. J. Nanosci.* **2019**, *18*, 1940077. [CrossRef]
81. Karim, H.M.; Melike, D.G.; Seda, T.S.; Neslihan, G.R.; Emirhan, N.; Kezban, U.; Levent, Ö.; Hakan, E. Atorvastatin-Loaded Nanosprayed Chitosan Nanoparticles for Peripheral Nerve Injury. *Bioinspired Biomim. Nanobiomater.* **2020**, *9*, 74–84. [CrossRef]
82. Ahmed, T.A.; Aljaeid, B.M. Preparation, Characterization, and Potential Application of Chitosan, Chitosan Derivatives, and Chitosan Metal Nanoparticles in Pharmaceutical Drug Delivery. *Drug Des. Devel. Ther.* **2016**, *28*, 483–507. [CrossRef]

83. Lucas, J.; Ralaivao, M.; Estevinho, B.N.; Rocha, F. A New Approach for the Microencapsulation of Curcumin by a Spray Drying Method, in Order to Value Food Products. *Powder Technol.* **2020**, *362*, 428–435. [[CrossRef](#)]
84. Crua, C.; Li, C.; Vogiatzaki, K. Effect of the Scale Resolution on the Two Phase Coupling Characteristics of High Speed Evaporating Sprays Using LES/Eulerian-Lagrangian Methodologies. *Int. J. Multiph. Flow* **2019**, *120*, 103060. [[CrossRef](#)]
85. Luesakul, U.; Puthong, S.; Sansanaphongpricha, K.; Muangsin, N. Quaternized Chitosan-Coated Nanoemulsions: A Novel Platform for Improving the Stability, Anti-Inflammatory, Anti-Cancer and Transdermal Properties of Plai Extract. *Carbohydr. Polym.* **2020**, *230*, 115625. [[CrossRef](#)] [[PubMed](#)]
86. Chaudhary, S.; Kumar, S.; Kumar, V.; Sharma, R. Chitosan Nanoemulsions as Advanced Edible Coatings for Fruits and Vegetables: Composition, Fabrication and Developments in Last Decade. *Int. J. Biol. Macromol.* **2020**, *152*, 154–170. [[CrossRef](#)] [[PubMed](#)]
87. Yu, A.; Shi, H.; Liu, H.; Bao, Z.; Dai, M.; Lin, D.; Lin, D.; Xu, X.; Li, X.; Wang, Y. Mucoadhesive Dexamethasone-Glycol Chitosan Nanoparticles for Ophthalmic Drug Delivery. *Int. J. Pharm.* **2020**, *575*, 118943. [[CrossRef](#)]
88. Liu, L.; Yang, H.; Lou, Y.; Wu, J.-Y.; Miao, J.; Lu, X.-Y.; Gao, J.-Q. Enhancement of Oral Bioavailability of Salmon Calcitonin through Chitosan-Modified, Dual Drug-Loaded Nanoparticles. *Int. J. Pharm.* **2019**, *557*, 170–177. [[CrossRef](#)]
89. Zhang, H.; Li, X.; Kang, H. Chitosan Coatings Incorporated with Free or Nano-Encapsulated Paulownia Tomentosa Essential Oil to Improve shelf-Life of Ready-to-Cook Pork Chops. *LWT* **2019**, *116*, 108580. [[CrossRef](#)]
90. Xu, T.; Ma, Y.; Huang, J.; Lai, H.; Yuan, D.; Tang, X.; Yang, L. Self-Organized Thermo-Responsive Poly (lactic-co-glycolic acid)-graft-pullulan Nanoparticles for Synergistic Thermo-Chemotherapy of Tumor. *Carbohydr. Polym.* **2020**, *237*, 116104. [[CrossRef](#)]
91. Quiñones, J.P.; Peniche, H.; Peniche, C. Chitosan Based Self-Assembled Nanoparticles in Drug Delivery. *Polymers* **2018**, *10*, 235. [[CrossRef](#)]
92. Khan, M.M.; Madni, A.; Torchilin, V.; Filipczak, N.; Pan, J.; Tahir, N.; Shah, H. Lipid-Chitosan Hybrid Nanoparticles for Controlled Delivery of Cisplatin. *Drug Deliv.* **2019**, *26*, 765–772. [[CrossRef](#)]
93. Roy, H.; Nayak, B.S.; Nandi, S. Chitosan Anchored Nanoparticles in Current Drug Development Utilizing Computer-Aided Pharmacokinetic Modeling: Case Studies for Target Specific Cancer Treatment and Future Prospective. *Curr. Pharm. Des.* **2020**, *26*, 1666–1675. [[CrossRef](#)]
94. Pathak, K.; Misra, S.K.; Sehgal, A.; Singh, S.; Bungau, S.; Najda, A.; Gruszecki, R.; Behl, T. Biomedical Applications of Quaternized Chitosan. *Polymers* **2021**, *13*, 2514. [[CrossRef](#)] [[PubMed](#)]
95. Frigaard, J.; Jensen, J.L.; Galtung, H.K.; Hiorth, M. The Potential of Chitosan in Nanomedicine: An Overview of the Cytotoxicity of Chitosan Based Nanoparticles. *Front. Pharmacol.* **2022**, *13*, 880377. [[CrossRef](#)] [[PubMed](#)]
96. Sriwidodo; Umar, A.K.; Wathoni, N.; Zothantluanga, J.H.; Das, S.; Luckanagul, J.A. Liposome-Polymer Complex for Drug Delivery System and Vaccine Stabilization. *Heliyon* **2022**, *8*, e08934. [[CrossRef](#)] [[PubMed](#)]
97. Liu, X.; Zhang, Y.; Ju, H.; Yang, F.; Luo, X.; Zhang, L. Uptake of Methylene Blue on Divinylbenzene Cross-Linked Chitosan/Maleic Anhydride Polymer by Adsorption Process. *Colloids Surf. A Physicochem. Eng. Asp.* **2021**, *629*, 127424. [[CrossRef](#)]
98. Gonçalves, F.J.; Gurgel, L.V.A.; Soares, L.C.; Teodoro, F.S.; Ferreira, G.M.D.; Coelho, Y.L.; da Silva, L.H.M.; Prim, D.; Gil, L.F. Application of pyridine-modified chitosan Derivative for Simultaneous Adsorption of Cu(II) and Oxyanions of Cr(VI) from Aqueous Solution. *J. Environ. Manag.* **2021**, *282*, 111939. [[CrossRef](#)]
99. Vakili, M.; Mojiri, A.; Zwain, H.M.; Yuan, J.; Giwa, A.S.; Wang, W.; Gholami, F.; Guo, X.; Cagnetta, G.; Yu, G. Effect of Beading Parameters on Cross-Linked Chitosan Adsorptive Properties. *React. Funct. Polym.* **2019**, *144*, 104354. [[CrossRef](#)]
100. Vakili, M.; Deng, S.; Liu, D.; Li, T.; Yu, G. Preparation of Aminated Cross-Linked Chitosan Beads for Efficient Adsorption of Hexavalent Chromium. *Int. J. Biol. Macromol.* **2019**, *139*, 352–360. [[CrossRef](#)]
101. Chanajaree, R.; Sriuttha, M.; Lee, V.S.; Wittayanarakul, K. Thermodynamics and Kinetics of Cationic/Anionic Dyes Adsorption on Cross-Linked Chitosan. *J. Mol. Liq.* **2021**, *322*, 114507. [[CrossRef](#)]
102. Farias, P.V.S.; Aragão, D.C.; Farias, M.V.; Correia, L.M.; Carvalho, T.V.; Aguiar, J.E.; Vieira, R.S. Natural and Cross-Linked Chitosan Spheres as Adsorbents for Diesel Oil Removal. *Adsorp. Sci. Technol.* **2015**, *33*, 783–792. [[CrossRef](#)]
103. Jawad, A.H.; Mamat, N.F.H.; Hameed, B.H.; Ismail, K. Biofilm of Cross-Linked Chitosan-Ethylene Glycol Diglycidyl Ether for removal of Reactive Red 120 and Methyl Orange: Adsorption and Mechanism Studies. *J. Environ. Chem. Eng.* **2019**, *7*, 102965. [[CrossRef](#)]
104. Lu, Y.; Wang, Z.; Ouyang, X.-K.; Ji, C.; Liu, Y.; Huang, F.; Yang, L.-Y. Fabrication of Cross-Linked Chitosan Beads Grafted by Polyethylenimine for Efficient Adsorption of Diclofenac Sodium from Water. *Int. J. Biol. Macromol.* **2020**, *145*, 1180–1188. [[CrossRef](#)]
105. Dos Santos, J.M.N.; Pereira, C.R.; Foletto, E.L.; Dotto, G.L. Alternative Synthesis for ZnFe₂O₄/Chitosan Magnetic Particles to Remove Diclofenac from Water by Adsorption. *Int. J. Biol. Macromol.* **2019**, *131*, 301–308. [[CrossRef](#)] [[PubMed](#)]
106. Zhu, W.; Dang, Q.; Liu, C.; Yu, D.; Chang, G.; Pu, X.; Wang, Q.; Sun, H.; Zhang, B.; Cha, D. Cr(VI) and Pb(II) Capture on pH-Responsive Polyethyleneimine and Chloroacetic Acid Functionalized Chitosan Microspheres. *Carbohydr. Polym.* **2019**, *219*, 353–367. [[CrossRef](#)]
107. Sabarudin, A.; Madjid, A.D.R. Preparation and Kinetic Studies of Cross-Linked Chitosan Beads Using Dual Crosslinkers of Tripolyphosphate and Epichlorohydrin for Adsorption of Methyl Orange. *Sci. World J.* **2021**, *11*, 6648457. [[CrossRef](#)]

108. Urtasun, N.; Mignon, A.; Martínez-Alvarez, L.M.; Baieli, M.F.; Hirsch, D.B.; Cascone, O.; Dubruel, P.; Wolman, F.J. Synthesis and Characterization of Chitosan Mini-Spheres with Immobilized Dye as Affinity Ligand for the Purification of Lactoperoxidase and Lactoferrin from Dairy Whey. *Sep. Purif. Technol.* **2021**, *255*, 117700. [[CrossRef](#)]
109. Hirsch, D.B.; Martínez Álvarez, L.M.; Urtasun, N.; Baieli, M.F.; Lázaro-Martínez, J.M.; Glisoni, R.J.; Miranda, M.V.; Cascone, O.; Wolman, F.J. Lactoferrin Purification and Whey Protein Isolate Recovery from Cheese Whey Using Chitosan Mini-Spheres. *Int. Dairy J.* **2020**, *109*, 104764. [[CrossRef](#)]
110. Li, Q.; Mao, Q.; Li, M.; Zhang, S.; He, G.; Zhang, W. Cross-Linked Chitosan Microspheres Entrapping Silver Chloride via the Improved Emulsion Technology for Iodide Ion Adsorption. *Carbohydr. Polym.* **2020**, *234*, 115926. [[CrossRef](#)] [[PubMed](#)]
111. Zhang, Y.; Zhao, M.; Cheng, Q.; Wang, C.; Li, H.; Han, X.; Fan, Z.; Su, G.; Pan, D.; Li, Z. Research Progress of Adsorption and Removal of Heavy Metals by Chitosan and Its Derivatives: A Review. *Chemosphere* **2021**, *279*, 130927. [[CrossRef](#)]
112. Khan, N.; Khan, I.; Zada, N.; Sadiq, M.; Saeed, K. Utilization of Cross-Linked Chitosan for Cobalt Adsorption and Its Reutilization as a Photocatalyst for the Photodegradation of Methyl Violet Dye in Aqueous Medium. *Appl. Water Sci.* **2022**, *12*, 107. [[CrossRef](#)]
113. Begum, S.; Yuhana, N.Y.; Saleh, N.M.; Kamarudin, N.H.N.; Sulong, A.B. Review of Chitosan Composite as a Heavy Metal Adsorbent: Material Preparation and Properties. *Carbohydr. Polym.* **2021**, *259*, 117613. [[CrossRef](#)]
114. Upadhyay, U.; Sreedhar, I.; Singh, S.A.; Patel, C.M.; Anitha, K.L. Recent Advances in Heavy Metal Removal by Chitosan Based Adsorbents. *Carbohydr. Polym.* **2021**, *251*, 117000. [[CrossRef](#)] [[PubMed](#)]
115. Omer, A.M.; Dey, R.; Eltaweil, A.S.; El-Monaem, E.M.A.; Ziara, Z.M. Insights into Recent Advances of Chitosan-Based Adsorbents for Sustainable Removal of Heavy Metals and Anions. *Arab. J. Chem.* **2022**, *15*, 103543. [[CrossRef](#)]
116. Zhang, C.; Chen, Z.; Guo, W.; Zhu, C.; Zou, Y. Simple Fabrication of Chitosan/Graphene Nanoplates Composite Spheres for Efficient Adsorption of Acid Dyes from Aqueous Solution. *Int. J. Biol. Macromol.* **2018**, *112*, 1048–1054. [[CrossRef](#)] [[PubMed](#)]
117. Jawad, A.H.; Mubarak, N.S.A.; Abdulhameed, A.S. Tunable Schiff's Base-Cross-Linked Chitosan Composite for the Removal of Reactive Red 120 Dye: Adsorption and Mechanism Study. *Int. J. Biol. Macromol.* **2020**, *142*, 732–741. [[CrossRef](#)] [[PubMed](#)]
118. Wang, A.; Zhu, Q.; Xing, Z. A Functionalized Chitosan Wrinkled Hollow Sphere Containing Calcium Ions: Efficient Adsorption of Sodium Dodecylbenzenesulfonate (SDBS) from Aqueous Solutions. *J. Colloid Interface Sci.* **2019**, *555*, 203–213. [[CrossRef](#)]
119. Altun, T. Preparation and Application of Glutaraldehyde Cross-Linked Chitosan Coated Bentonite Clay Capsules: Chromium(VI) Removal from Aqueous Solution. *J. Chil. Chem. Soc.* **2020**, *65*, 4790–4797. [[CrossRef](#)]
120. Patiño-Ruiz, D.A.; De Ávila, G.; Alarcón-Suesca, C.; González-Delgado, Á.D.; Herrera, A. Ionic Cross-Linking Fabrication of Chitosan-Based Beads Modified with FeO and TiO₂ Nanoparticles: Adsorption Mechanism toward Naphthalene Removal in Seawater from Cartagena Bay Area. *ACS Omega* **2020**, *5*, 26463–26475. [[CrossRef](#)]
121. Ohemeng-Boahen, G.; Sewu, D.D.; Tran, H.N.; Woo, S.H. Enhanced Adsorption of Congo Red from Aqueous Solution Using Chitosan/Hematite Nanocomposite Hydrogel Capsule Fabricated via Anionic Surfactant Gelation. *Colloids Surf. A Physicochem. Eng. Asp.* **2021**, *625*, 126911. [[CrossRef](#)]
122. Jeyaseelan, A.; Viswanathan, N. Facile Fabrication of Zirconium-Organic Framework-Embedded Chitosan Hybrid Spheres for Efficient Fluoride Adsorption. *ACS ES&T Water* **2022**, *2*, 52–62. [[CrossRef](#)]
123. Wang, T.; Wusigale; Kuttappan, D.; Amalaradjou, M.A.; Luo, Y.; Luo, Y. Polydopamine-Coated Chitosan Hydrogel Beads for Synthesis and Immobilization of Silver Nanoparticles to Simultaneously Enhance Antimicrobial Activity and Adsorption Kinetics. *Adv. Compos. Hybrid. Mater.* **2021**, *4*, 696–706. [[CrossRef](#)]
124. Warkara, S.G.; Meena, J. Synthesis and Applications of Biopolymer/FeO Nanocomposites: A Review. *JNMES* **2022**, *25*, 7–16. [[CrossRef](#)]
125. Fan, C.; Li, K.; He, Y.; Wang, Y.; Qian, X.; Jia, J. Evaluation of Magnetic Chitosan Beads for Adsorption of Heavy Metal Ions. *Sci. Total Environ.* **2018**, *627*, 1396–1403. [[CrossRef](#)] [[PubMed](#)]
126. Kloster, G.A.; Valiente, M.; Marcovich, N.E.; Mosiewicki, M.A. Adsorption of Arsenic onto Films Based on Chitosan and Chitosan/Nano-Iron Oxide. *Int. J. Biol. Macromol.* **2020**, *165*, 1286–1295. [[CrossRef](#)] [[PubMed](#)]
127. Eivazzadeh-Keihan, R.; Radinekiyan, F.; Asgharnasl, S.; Maleki, A.; Bahreinizad, H. A Natural and Eco-Friendly Magnetic Nanobiocomposite Based on Activated Chitosan for Heavy Metals Adsorption and the In-vitro Hyperthermia of Cancer Therapy. *J. Mater. Res. Technol.* **2020**, *9*, 12244–12259. [[CrossRef](#)]
128. Shahraki, S.; Delarami, H.S.; Khosravi, F.; Nejat, R. Improving the Adsorption Potential of Chitosan for Heavy Metal Ions Using Aromatic Ring-Rich Derivatives. *J. Colloid Interface Sci.* **2020**, *576*, 79–89. [[CrossRef](#)]
129. Fu, C.-C.; Tran, H.N.; Chen, X.-H.; Juang, R.-S. Preparation of Polyaminated Fe₃O₄@Chitosan Core-Shell Magnetic Nanoparticles for Efficient Adsorption of Phosphate in Aqueous Solutions. *J. Ind. Eng. Chem.* **2020**, *83*, 235–246. [[CrossRef](#)]
130. Elanchezhian, S.S.D.; Preethi, J.; Rathinam, K.; Njaramba, L.K.; Park, C.M. Synthesis of Magnetic Chitosan Biopolymeric Spheres and Their Adsorption Performances for PFOA and PFOS from Aqueous Environment. *Carbohydr. Polym.* **2021**, *267*, 118165. [[CrossRef](#)]
131. Tanhaei, B.; Ayati, A.; Iakovleva, E.; Sillanpää, M. Efficient Carbon Interlayered Magnetic Chitosan Adsorbent for Anionic Dye Removal: Synthesis, Characterization and Adsorption Study. *Int. J. Biol. Macromol.* **2020**, *164*, 3621–3631. [[CrossRef](#)]
132. Kang, H.; Buchman, J.T.; Rodriguez, R.S.; Ring, H.L.; He, J.; Bantz, K.C.; Haynes, C.L. Stabilization of Silver and Gold Nanoparticles: Preservation and Improvement of Plasmonic Functionalities. *Chem. Rev.* **2019**, *119*, 664–699. [[CrossRef](#)]

133. Bashal, A.H.; Riyadh, S.M.; Alharbi, W.; Alharbi, K.H.; Farghaly, T.A.; Khalil, K.D. Bio-Based (Chitosan-ZnO) Nanocomposite: Synthesis, Characterization, and Its Use as Recyclable, Ecofriendly Biocatalyst for Synthesis of Thiazoles Tethered Azo Groups. *Polymer* **2022**, *14*, 386. [[CrossRef](#)]
134. Verma, D.K.; Malik, R.; Meena, J.; Rameshwari, R. Synthesis, Characterization and Applications of Chitosan Based Metallic Nanoparticles: A Review. *J. Appl. Nat. Sci.* **2021**, *13*, 544–551. [[CrossRef](#)]
135. Sun, L.; Li, J.; Cai, J.; Zhong, L.; Ren, G.; Ma, Q. One Pot Synthesis of Gold Nanoparticles Using Chitosan with Varying Degree of Deacetylation and Molecular Weight. *Carbohydr. Polym.* **2017**, *178*, 105–114. [[CrossRef](#)] [[PubMed](#)]
136. Tong, J.; Li, Y.; Bo, L.; Wang, W.; Li, T.; Zhang, Q. Core-Shell Fe₃O₄@NCS-Mn Derived from Chitosan-Schiff Based Mn Complex with Enhanced Catalytic Activity for Oxygen Reduction Reaction. *Catalysts* **2019**, *9*, 692. [[CrossRef](#)]
137. Singh, H.; Rajput, J.K. Co(II) Anchored Glutaraldehyde Crosslinked Magnetic Chitosan Nanoparticles (MCS) for Synthesis of 2,4,5-Trisubstituted and 1,2,4,5-Tetrasubstituted Imidazoles. *Appl. Organometal. Chem.* **2018**, *32*, e3989. [[CrossRef](#)]
138. Jennah, O.; Beniazza, R.; Lozach, C.; Jardel, D.; Molton, F.; Duboc, C.; Buffeteau, T.; El Kadib, A.; Lastécouères, D.; Lahcini, M.; et al. Photoredox Catalysis at Copper(II) on Chitosan: Application to Photolabile CuAAC. *Adv. Synth. Catal.* **2018**, *360*, 4615. [[CrossRef](#)]
139. Jiao, L.-Y.; Zhang, Z.; Hong, Q.; Ning, Z.-H.; Liu, S.; Sun, M.; Hao, Q.; Xu, L.; Li, Z.; Ma, X.-X. Recyclable Copper Catalyst on Chitosan for Facile Preparation of Alkyl/Aryl Mixed Phosphates via Deaminated Esterification between DiphenylphosphorylAzides and Aliphatic Alcohols. *Mol. Catal.* **2020**, *494*, 111120. [[CrossRef](#)]
140. Reyes-Mercado, E.; Rivas-Loaiza, J.A.; García-Merinos, J.P.; López, Y.; González-Campos, J.B. Chitosan-supported copper salt and copper metal nanoparticles/copper (I) oxide Microcrystals: Efficient and Recyclable Heterogeneous Catalysts for the Synthesis of Bis(indolyl)methanes. *Chem. Eng. Process.* **2021**, *159*, 108201. [[CrossRef](#)]
141. Ali, F.; Khan, S.B.; Kamal, T.; Alamry, K.A.; Bakhsh, E.M.; Asiri, A.M.; Sobahi, T.R.A. Synthesis and Characterization of Metal Nanoparticles Templated Chitosan-SiO₂ Catalyst for the Reduction of Nitrophenols and Dyes. *Carbohydr. Polym.* **2018**, *192*, 217–230. [[CrossRef](#)]
142. Raza, Z.A.; Mobeen, A.; Rehman, M.S.U.; Majeed, M.I. Synthesis of Copper Oxide Nanoparticles Embedded in Porous Chitosan Membrane for Photodegradation of Organic Dyes. *Polym. Bull.* **2022**. [[CrossRef](#)]
143. Sakthivel, S.; Periakaruppan, R.; Vallinayagam, S.; Gandhi, S.; Tappa, M.M.; Sharma, V.K.; Sivaramkrishnan, R.; Suresh, S.; Gurusamy, A. Synthesis and Characterization of Paddy Straw Chitosan Nanocomposite as an Efficient Photocatalytic Bio-adsorbent for the Removal of Rhodamine B and Malachite Green Dye from Aqueous Solution. *Appl. Nanosci.* **2022**. [[CrossRef](#)]
144. Khan, M.S.J.; Kamal, T.; Ali, F.; Asiri, A.M.; Khan, S.B. Chitosan-Coated Polyurethane Sponge Supported Metal Nanoparticles for Catalytic Reduction of Organic Pollutants. *Int. J. Biol. Macromol.* **2019**, *132*, 772–783. [[CrossRef](#)] [[PubMed](#)]
145. Naghipour, A.; Fakhri, A. Efficient Oxidation of Sulfides into Sulfoxides Catalyzed by a Chitosan-Schiff Base Complex of Cu(II) Supported on Supramagnetic Fe₃O₄ Nanoparticles. *Environ. Chem. Lett.* **2016**, *14*, 207–213. [[CrossRef](#)]
146. Fakhri, A.; Naghipour, A. Fe₃O₄@Chitosan-Bound Picolinaldehyde Cu Complex as the Magnetically Reusable Nanocatalyst for Adjustable Oxidation of Sulfides. *Environ. Prog. Sustain. Energy* **2018**, *37*, 1626–1631. [[CrossRef](#)]
147. Laghrib, F.; Ajermoun, N.; Bakasse, M.; Lahrich, S.; El Mhammedi, M.A. Synthesis of Silver Nanoparticles Assisted by Chitosan and Its Application to Catalyze the Reduction of 4-Nitroaniline. *Int. J. Biol. Macromol.* **2019**, *135*, 752–759. [[CrossRef](#)] [[PubMed](#)]
148. Wang, A.; Zhu, Q.; Xing, Z. Multifunctional Quaternized Chitosan@surface Plasmon Resonance Ag/N-TiO₂ Core-Shell Microsphere for Synergistic Adsorption-Photothermal Catalysis Degradation of Low-Temperature Wastewater and Bacteriostasis under visible light. *Chem. Eng. J.* **2020**, *393*, 124781. [[CrossRef](#)]
149. Khan, M.S.J.; Khan, S.B.; Kamal, T.; Asiri, A.M. Catalytic Application of Silver Nanoparticles in Chitosan Hydrogel Prepared by a Facile Method. *J. Polym. Environ.* **2020**, *28*, 962–972. [[CrossRef](#)]
150. Sun, P.; Zhang, L.; Tao, S. Preparation of Hybrid Chitosan Membranes by Selective Laser Sintering for Adsorption and Catalysis. *Mater. Des.* **2019**, *173*, 107780. [[CrossRef](#)]
151. Vedula, S.S.; Yadav, G.D. Chitosan-Based Membranes Preparation and Applications: Challenges and Opportunities. *J. Indian Chem. Soc.* **2021**, *98*, 100017. [[CrossRef](#)]
152. Zhu, J.; Zhang, X.; Qin, Z.; Zhang, L.; Ye, Y.; Cao, M.; Gao, L.; Jiao, T. Preparation of PdNPs Doped Chitosan-Based Composite Hydrogels as Highly Efficient Catalysts for Reduction of 4-Nitrophenol. *Colloids Surf. A Physicochem. Eng. Asp.* **2021**, *611*, 125889. [[CrossRef](#)]
153. Le Goff, R.; Mahé, O.; Le Coz-Botrel, R.; Malo, S.; Goupil, J.-M.; Brière, J.-F.; Dez, I. Insight in Chitosan Aerogels Derivatives—Application in Catalysis. *React. Funct. Polym.* **2020**, *146*, 104393. [[CrossRef](#)]
154. Shen, Y.; Zheng, Q.; Liu, J.; Tu, T. Metallo-aerogels Derived from Chitosan with Encapsulated Metal Nanoparticles as Robust, Efficient and Selective Nanocatalysts Towards Reduction of Nitroarenes. *Nano Res.* **2021**, *14*, 59–65. [[CrossRef](#)]
155. de Souza, J.F.; Lemos, T.S.A.; Biajoli, A.F.P.; Fajardo, A.R. Phosphine-Functionalized Chitosan Microparticles as Support Materials for Palladium Nanoparticles in Heck Reactions. *Catal. Lett.* **2022**, *152*, 2933–2946. [[CrossRef](#)]
156. Khamarnia, S.; Akbari, A.; Ekrami-Kakhki, M.-S.; Saffari, J. Enhanced Catalytic Activity of Pt-NdFeO₃ Nanoparticles Supported on Polyaniline-Chitosan Composite Towards Methanol Electro-Oxidation Reaction. *J. Nanostruct.* **2020**, *10*, 239–257. [[CrossRef](#)]
157. Khodkari, V.; Nazeri, M.T.; Javanbakht, S.; Shaabani, A. In Situ Copper Nanoparticle Immobilization on the Indigo Carmine-Functionalized Chitosan: A Versatile Biocatalyst towards CO₂ Fixation and Click Reactions in Water. *React. Chem. Eng.* **2023**, *8*, 152–163. [[CrossRef](#)]

158. Riyadh, S.M.; Khalil, K.D.; Aljuhani, A. Chitosan-MgO Nanocomposite: One Pot Preparation and Its Utility as an Ecofriendly Biocatalyst in the Synthesis of Thiazoles and [1,3,4]thiadiazoles. *Nanomaterials* **2018**, *8*, 928. [CrossRef]
159. Alayli, A.; Nadaroglu, H.; Turgut, E. Nanobiocatalyst Beds with Fenton Process for Removal of Methylene Blue. *Appl. Water Sci.* **2021**, *11*, 32. [CrossRef]
160. Saba, R.; Aziz, M.K.; Mustafa, G.; Srivastava, A.; Srivastava, S. Schiff's Base of Fe₃O₄@chitosan with 4,4'-Diselenobisbenzaldehyde: Preparation, Characterization and its Catalytic Activity for Oxidation of Sulphides. *J. Polym. Mater.* **2021**, *38*, 153–166. [CrossRef]
161. Parandhaman, T.; Pentela, N.; Ramalingam, B.; Samanta, D.; Das, S.K. Metal Nanoparticle Loaded Magnetic-Chitosan Microsphere: Water Dispersible and Easily Separable Hybrid Metal Nano-biomaterial for Catalytic Applications. *ACS Sustain. Chem. Eng.* **2017**, *5*, 489–501. [CrossRef]
162. Rinki, K.; Dutta, P.K.; Hunt, A.J.; Macquarrie, D.J.; Clark, J.H. Chitosan Aerogels Exhibiting High Surface Area for Biomedical Application: Preparation, Characterization, and Antibacterial Study. *Int. J. Polym. Mater.* **2011**, *60*, 988–999. [CrossRef]
163. Wei, S.; Ching, Y.C.; Chuah, C.H. Synthesis of Chitosan Aerogels as Promising Carriers for Drug Delivery: A Review. *Carbohydr. Polym.* **2020**, *231*, 115744. [CrossRef]
164. Takeshita, S.; Zhao, S.; Malfait, W.J.; Koebel, M.M. Chemistry of Chitosan Aerogels: Three-Dimensional Pore Control for Tailored Applications. *Angew. Chem. Int. Ed.* **2021**, *60*, 9828–9851. [CrossRef] [PubMed]
165. Anju, R.P.P.; Sunil, J.T.; Dinoop, I.S. Chitosan Stabilized Fe/Ni Bimetallic Nanoparticles for the Removal of Cationic and Anionic Triphenylmethane Dyes from Water. *Environ. Nanotechnol. Monit. Manag.* **2020**, *14*, 100295. [CrossRef]
166. Bumagin, N.A. Chitosan-Based Magnetic Polymetallic Pd-Catalysts for Heck Reaction in Aqueous Media. *Russ. J. Gen. Chem.* **2022**, *92*, 63–68. [CrossRef]
167. Krajewska, B. Application of Chitin- and Chitosan-based Materials for Enzyme Immobilizations: A Review. *Enzyme Microb. Technol.* **2004**, *35*, 126–139. [CrossRef]
168. Biró, E.; Németh, Á.S.; Sisak, C.; Feczko, T.; Gyenis, J. Preparation of Chitosan Particles Suitable for Enzyme Immobilization. *J. Biochem. Biophys. Methods* **2008**, *70*, 1240–1246. [CrossRef] [PubMed]
169. Malmiri, H.J.; Jahanian, M.A.G.; Berenjian, A. Potential Applications of Chitosan Nanoparticles as Novel Support in Enzyme Immobilization. *Am. J. Biochem. Biotechnol.* **2012**, *8*, 203–219. [CrossRef]
170. Wang, D.; Jiang, W. Preparation of Chitosan-based Nanoparticles for Enzyme Immobilization. *Int. J. Biol. Macromol.* **2019**, *126*, 1125–1132. [CrossRef]
171. Verma, M.L.; Kumar, S.; Das, A.; Randhawa, J.S.; Chamundeeswari, M. Chitin and Chitosan-based Support Materials for Enzyme Immobilization and Biotechnological Applications. *Environ. Chem. Lett.* **2020**, *18*, 315–323. [CrossRef]
172. Nunes, Y.L.; de Menezes, F.L.; de Sousa, I.G.; Cavalcante, A.L.G.; Cavalcante, F.T.T.; da Silva Moreira, K.; de Oliveira, A.L.B.; Mota, G.F.; da Silva Souza, J.E.; de Aguiar Falcão, I.R.; et al. Chemical and Physical Chitosan Modification for Designing Enzymatic Industrial Biocatalysts: How to Choose the Best Strategy? *Int. J. Biol. Macromol.* **2021**, *181*, 1124–1170. [CrossRef]
173. Bilal, M.; Iqbal, H.M.N. Naturally-derived Biopolymers: Potential Platforms for Enzyme Immobilization. *Int. J. Biol. Macromol.* **2019**, *130*, 462–482. [CrossRef]
174. Chatterjee, S.; Lee, M.W.; Woo, S.H. Enhanced Mechanical Strength of Chitosan Hydrogel Beads by Impregnation with Carbon Nanotubes. *Carbon* **2009**, *47*, 2933–2936. [CrossRef]
175. Wahba, M.I. Porous Chitosan Beads of Superior Mechanical Properties for the Covalent Immobilization of Enzymes. *Int. J. Biol. Macromol.* **2017**, *105*, 894–904. [CrossRef] [PubMed]
176. Ji, Q.; Wang, B.; Li, C.; Hao, J.; Feng, W. Co-Immobilised 7a- and 7b-HSDH as Recyclable Biocatalyst: High-Performance Production of TUDCA from Waste Chicken Bile. *RSC Adv.* **2018**, *8*, 34192–34201. [CrossRef] [PubMed]
177. Singh, R.S.; Singh, R.P.; Kennedy, J.F. Immobilization of yeast inulinase on chitosan beads for the hydrolysis of inulin in a batch system. *Int. J. Biol. Macromol.* **2017**, *95*, 87–93. [CrossRef]
178. Manan, F.M.A.; Attan, N.; Zakaria, Z.; Mahat, N.A.; Wahab, R.A. Insight into the *Rhizomucor miehei* Lipase Supported on Chitosan-Chitin Nanowhiskers Assisted Esterification of Eugenol to Eugenyl Benzoate. *J. Biotechnol.* **2018**, *280*, 19–30. [CrossRef]
179. de Freitas, M.F.M.; Hortencio, L.C.; de Albuquerque, T.L.; Rocha, M.V.P.; Goncalves, L.R.B. Simultaneous Hydrolysis of Cheese Whey and Lactulose Production Catalyzed by β -Galactosidase from *Kluyveromyces lactis* NRRL Y1564. *Bioprocess Biosyst. Eng.* **2020**, *43*, 711–722. [CrossRef]
180. Okura, N.S.; Sabi, G.J.; Crivellenti, M.C.; Gomes, R.A.B.; Fernandez-Lafuente, R.; Mendes, A.A. Improved Immobilization of Lipase from *Thermomyces lanuginosus* on a New Chitosan-Based Heterofunctional Support: Mixed Ion Exchange Plus Hydrophobic Interactions. *Int. J. Biol. Macromol.* **2020**, *163*, 550–561. [CrossRef]
181. Aggarwal, S.; Ikram, S. Zinc Oxide Nanoparticles-Impregnated Chitosan Surfaces for Covalent Immobilization of Trypsin: Stability & Kinetic Studies. *Int. J. Biol. Macromol.* **2022**, *207*, 205–221. [CrossRef]
182. Aman, A.; Shahid, F.; Pervez, S. Exploration of a Three-Dimensional Matrix as Micro-Reactor in the Form of Reactive Polyaminosaccharide Hydrogel Beads Using Multipoint Covalent Interaction Approach. *Biotechnol. Lett.* **2022**, *44*, 299–319. [CrossRef]
183. BôaMorte, E.F.; Marum, D.S.; Saitovitch, E.B.; Alzamora, M.; Monteiro, S.N.; Sanchez Rodriguez, R.J. Modified Magnetite Nanoparticle as Biocatalytic Support for Magnetically Stabilized Fluidized Bed Reactors. *J. Mater. Res. Technol.* **2021**, *14*, 1112–1125. [CrossRef]
184. Wang, C.; Liu, X. Synthesis of Chitosan-Functionalized Fibrous Membrane for Immobilization of Horseradish Peroxidase: Interfacial Property and Application for Catalytic Oxidation of P-Nitrophenol. *J. Eng. Fibers Fabr.* **2018**, *13*, 66–73. [CrossRef]

185. Costa-Silva, T.A.; Carvalho, A.K.F.; Souza, C.R.F.; De Castro, H.F.; Bachmann, L.; Said, S.; Oliveira, W.P. Enhancement Lipase Activity via Immobilization onto Chitosan Beads Used as Seed Particles During Fluidized Bed Drying: Application in butyl Butyrate production. *Appl. Catal. A Gen.* **2021**, *622*, 118217. [CrossRef]
186. Costa-Silva, T.A.; Carvalho, A.K.F.; Souza, C.R.F.; Freitas, L.; De Castro, H.F.; Oliveira, W.P. Highly Effective *Candida rugosa* Lipase Immobilization on Renewable Carriers: Integrated Drying and Immobilization Process to Improve Enzyme Performance. *Chem. Eng. Res. Des.* **2022**, *183*, 41–55. [CrossRef]
187. Apriceno, A.; Girelli, A.M.; Scuto, F.R. Design of a Heterogeneous Enzymatic Catalyst on Chitosan: Investigation on the Role of Conjugation Chemistry in the Catalytic Activity of a Laccase from *Trametes versicolor*. *J. Chem. Technol. Biotechnol.* **2018**, *93*, 1413–1420. [CrossRef]
188. Apriceno, A.; Silvestro, I.; Girelli, A.; Francolini, I.; Pietrelli, L.; Piozzi, A. Preparation and Characterization of Chitosan-Coated Manganese-Ferrite Nanoparticles Conjugated with Laccase for Environmental Bioremediation. *Polymers* **2021**, *13*, 1453. [CrossRef]
189. Ariffin, M.F.K.; Idris, A.; Ngadiman, N.H.A. Optimization of Lipase Immobilization on Maghemite and Its Physico-Chemical Properties. *Braz. J. Chem. Eng.* **2019**, *36*, 171–179. [CrossRef]
190. Carli, S.; Carneiro, L.A.B.C.; Ward, R.J.; Meleiro, L.P. Immobilization of a β -glucosidase and an endoglucanase in ferromagnetic-nanoparticles: A study of synergistic effects. *Protein Expr. Purif.* **2019**, *160*, 28–35. [CrossRef]
191. Carneiro, L.A.B.C.; Ward, R.J. Functionalization of Paramagnetic Nanoparticles for Protein Immobilization and Purification. *Anal. Biochem.* **2018**, *540–541*, 45–51. [CrossRef]
192. Charoenwongpaiboon, T.; Wangpaiboon, K.; Pichyangkura, R.; Prousoontorn, M.H. Highly Porous Core-Shell Chitosan Beads with Superb Immobilization Efficiency for *Lactobacillus reuteri* 121 Inulosucrase and Production of Inulin-Type Fructooligosaccharides. *RSC Adv.* **2018**, *8*, 17008–17016. [CrossRef]
193. Tavernini, L.; Ottone, C.; Illanes, A.; Wilson, L. Entrapment of Enzyme Aggregates in Chitosan Beads for Aroma Release in White Wines. *Int. J. Biol. Macromol.* **2020**, *154*, 1082–1090. [CrossRef]
194. Cui, L.; Xiong, Z.; Guo, Y.; Liu, Y.; Zhao, J.; Zhang, C.; Zhu, P. Fabrication of Interpenetrating Polymer Network Chitosan/Gelatin Porous Materials and Study on Dye Adsorption Properties. *Carbohydr. Polym.* **2015**, *132*, 330–337. [CrossRef] [PubMed]
195. Li, Q.; Wang, X.; Lou, X.; Yuan, H.; Tu, H.; Li, B.; Zhang, Y. Genipin-Crosslinked Electrospun Chitosan Nanofibers: Determination of Crosslinking Conditions and Evaluation of Cytocompatibility. *Carbohydr. Polym.* **2015**, *130*, 166–174. [CrossRef] [PubMed]
196. Mekhail, M.; Jahan, K.; Tabrizian, M. Genipin-Crosslinked Chitosan/Poly-L-lysine Gels Promote Fibroblast Adhesion and Proliferation. *Carbohydr. Polym.* **2014**, *108*, 91–98. [CrossRef]
197. Tacias-Pascacio, V.G.; García-Parra, E.; Vela-Gutiérrez, G.; Virgen-Ortiz, J.J.; Berenguer-Murcia, Á.; Alcántara, A.R.; Fernandez-Lafuente, R. Genipin as An Emergent Tool in the Design of Biocatalysts: Mechanism of Reaction and Applications. *Catalysts* **2019**, *9*, 1035. [CrossRef]
198. Hyun, K.; Kang, S.; Kim, J.; Kwon, Y. New Biocatalyst Including a 4-Nitrobenzoic Acid Mediator Embedded by the Cross-Linking of Chitosan and Genipin and Its Use in an Energy Device. *ACS Appl. Mater. Interfaces* **2020**, *12*, 23635–23643. [CrossRef] [PubMed]
199. Ma, H.-F.; Meng, G.; Cui, B.-K.; Si, J.; Dai, Y.-C. Chitosan Crosslinked with Genipin as Supporting Matrix for Biodegradation of Synthetic Dyes: Laccase Immobilization and Characterization. *Chem. Eng. Res. Des.* **2018**, *132*, 664–676. [CrossRef]
200. Klein, M.P.; Hackenhaar, C.R.; Lorenzoni, A.S.; Rodrigues, R.C.; Costa, T.M.; Ninow, J.L.; Hertz, P.F. Chitosan Crosslinked with Genipin as Support Matrix for Application in Food Process: Support Characterization and β -D-Galactosidase Immobilization. *Carbohydr. Polym.* **2016**, *137*, 184–190. [CrossRef] [PubMed]
201. Rahman, I.N.A.; Wahab, R.A.; Mahat, N.A.; Jamalis, J.; Huri, M.A.M.; Kurniawan, C. Ternary Blended Chitosan/Chitin/Fe₃O₄ Nanosupport for Lipase Activation and Stabilization. *Arab. J. Sci. Eng.* **2019**, *44*, 6327–6337. [CrossRef]
202. Saikia, K.; Rathankumar, A.K.; Varghese, B.A.; Kalita, S.; Subramanian, S.; Somasundaram, S.; Kumar, V.V. Magnetically Assisted Commercially Attractive Chemo-Enzymatic Route for the Production of 5-Hydroxymethylfurfural from Inulin. *Biomass Convers. Biorefinery* **2021**, *11*, 2557–2567. [CrossRef]
203. Akil, E.; Pereira, A.D.S.; El-Bacha, T.; Amaral, P.F.F.; Torres, A.G. Efficient Production of Bioactive Structured Lipids by Fast Acidolysis Catalyzed by *Yarrowia polytica* Lipase, Free and Immobilized in Chitosan-Alginate Beads, in Solvent-Free Medium. *Int. J. Biol. Macromol.* **2020**, *163*, 910–918. [CrossRef]
204. Qiu, X.; Wang, S.; Miao, S.; Suo, H.; Xu, H.; Hu, Y. Co-Immobilization of Laccase and ABTS onto Amino-Functionalized Ionic Liquid-Modified Magnetic Chitosan Nanoparticles for Pollutants Removal. *J. Hazard. Mater.* **2021**, *401*, 123353. [CrossRef] [PubMed]
205. Ospina, V.; Bernal, C.; Mesa, M. Thermal Hyperactivation and Stabilization of β -Galactosidase from *Bacillus circulans* through a Silica Sol–Gel Process Mediated by Chitosan–Metal Chelates. *ACS Appl. Bio Mater.* **2019**, *2*, 3380–3392. [CrossRef] [PubMed]
206. Cai, Z.; Wei, Y.; Wu, M.; Guo, Y.; Xie, Y.; Tao, R.; Li, R.; Wang, P.; Ma, A.; Zhang, H. Lipase Immobilized on Layer-by-layer Polysaccharide-coated Fe₃O₄@SiO₂ Microspheres as a Reusable Biocatalyst for the Production of Structured Lipids. *ACS Sustain. Chem. Eng.* **2019**, *7*, 6685–6695. [CrossRef]
207. Ol'shannikova, S.S.; Red'ko, Y.A.; Lavlinskaya, M.S.; Sorokin, A.V.; Holyavka, M.G.; Artyukhov, V.G. Preparation of Papain Complexes with Chitosan Microparticles and Evaluation of Their Stability Using the Enzyme Activity Level. *Pharm. Chem. J.* **2022**, *55*, 1240–1244. [CrossRef]
208. Red'ko, Y.A.; Ol'shannikova, S.S.; Holyavka, M.G.; Lavlinskaya, M.S.; Sorokin, A.V.; Artyukhov, V.G. Development of a Method for Obtaining Bromelain Associates with Chitosan Micro- and Nanoparticles. *Pharm. Chem. J.* **2022**, *56*, 984–988. [CrossRef]

209. Xu, H.; Liang, H. Chitosan-Regulated Biomimetic Hybrid Nanoflower for Efficiently Immobilizing Enzymes to Enhance Stability and By-Product Tolerance. *Int. J. Biol. Macromol.* **2022**, *220*, 124–134. [[CrossRef](#)]
210. Gu, Y.; Yuan, L.; Li, M.; Wang, X.; Rao, D.; Bai, X.; Shi, K.; Xu, H.; Hou, S.; Yao, H. Co-Immobilized Bienenzyme of Horseradish Peroxidase and Glucose Oxidase on Dopamine modified Cellulose-Chitosan Composite Beads as a High-Efficiency Biocatalyst for Degradation of Acridine. *RSC Adv.* **2022**, *12*, 4290. [[CrossRef](#)]
211. Bilal, M.; Rasheed, T.; Zhao, Y.; Iqbal, H.M.N. Agarose-Chitosan Hydrogel-Immobilized Horseradish Peroxidase with Sustainable Bio-Catalytic and Dye Degradation Properties. *Int. J. Biol. Macromol.* **2019**, *124*, 742–749. [[CrossRef](#)]
212. Pereira, A.D.S.; Fraga, J.L.; Diniz, M.M.; Fontes-Sant'Ana, G.C.; Amaral, P.F.F. High Catalytic Activity of Lipase from *Yarrowia polytica* Immobilized by Microencapsulation. *Int. J. Mol. Sci.* **2018**, *19*, 3393. [[CrossRef](#)]
213. Benucci, I.; Caso, M.C.; Bavaro, T.; Masci, S.; Keršienė, M.; Esti, M. Prolyl Endopeptidase from *Aspergillus niger* Immobilized on a Food-Grade Carrier for the Production of Gluten-Reduced Beer. *Food Control* **2020**, *110*, 106987. [[CrossRef](#)]
214. Chen, X.; Hu, Z.; Xie, H.; Ngo, H.H.; Guo, W.; Zhang, J. Enhanced Biocatalysis of Phenanthrene in Aqueous Phase by Novel CA-Ca-SBE-Laccase Biocatalyst: Performance and Mechanism. *Colloids Surf. A Physicochem. Eng. Asp.* **2021**, *611*, 125884. [[CrossRef](#)]
215. El-Shishtawy, R.M.; Ahmed, N.S.E.; Almulaiky, Y.Q. Immobilization of Catalase on Chitosan/ZnO and Chitosan/ZnO/Fe₂O₃ Nanocomposites: A Comparative Study. *Catalysts* **2021**, *11*, 820. [[CrossRef](#)]
216. Girelli, A.M.; Quattrocchi, L.; Scuto, F.R. Design of Bioreactor Based on Immobilized Laccase on Silica-Chitosan Support for Phenol Removal in Continuous Mode. *J. Biotech.* **2021**, *337*, 8–17. [[CrossRef](#)]
217. Khan, M.; Husain, Q.; Ahmad, N. Elucidating the Binding Efficacy of β -Galactosidase on Polyaniline Chitosan Nanocomposite and Polyaniline Chitosan Silver Nanocomposite: Activity and Molecular Model. *J. Chem. Technol. Biotechnol.* **2019**, *94*, 837–849. [[CrossRef](#)]
218. Vassiliadi, E.; Xenakis, A.; Zoumpantioti, M. Chitosan Hydrogels: A New and Simple Matrix for Lipase Catalyzed Biosyntheses. *Mol. Catal.* **2018**, *445*, 206–212. [[CrossRef](#)]

Disclaimer/Publisher's Note: The statements, opinions and data contained in all publications are solely those of the individual author(s) and contributor(s) and not of MDPI and/or the editor(s). MDPI and/or the editor(s) disclaim responsibility for any injury to people or property resulting from any ideas, methods, instructions or products referred to in the content.